University of Strathclyde

Department of Bioengineering

Modelling of Ions and Small Molecules Through Human Skin *In vivo*

By

Sergio Rico Arias

A thesis presented in fulfilment of the requirements for the degree of Master of Science

2011

Abstract

Skin is the largest organ in the body and one of its most important roles is to act as a barrier between the body and the outside world. This barrier function seeks to impede chemical or biological attack by preventing unwanted molecules entering the body through the skin, as well as preventing desired molecules exiting the body, for example, the regulation of water loss across the skin.

Skin barrier function is also important in the field of transdermal monitoring. This method extracts analytes such as glucose through the skin into a sensor chamber for external measurement. This measurement must then be related to a patient's blood analyte concentration in order to provide a continuous or less invasive method of patient monitoring. Due to a high degree of variation of skin permeability observed in humans a method of calibrating for this variation is required. Present calibration difficulties could be addressed with a greater understanding of the skin barrier function.

The aim of this project is to model the flow of ions (potassium) and small molecules (glucose) through human skin *in vivo*. To achieve this, experiments were performed *in vitro* (on an artificial membrane) as a control and *in vivo* with healthy volunteers (under ethics). These experiments used reverse iontophoresis (RI) to extract ions and small molecules through the skin and into a gel where the extracted concentration was measured. Skin impedance measurements were taken before and after extraction. These results were used to construct an electrical equivalent circuit model to describe the flow of ions and small molecules across skin during extraction by reverse iontophoresis and by passive diffusion.

The structure of both the skin and membrane were successfully modelled with an electrical equivalent circuit model representing the skin structure and deeper tissue. Results show that RI causes a significant reduction in the barrier function of both the membrane and the skin within the first 10 minutes of application. Following this, the extraction of potassium and glucose by reverse iontophoresis was shown to be very predictable and can be approximated by a linear function with time. The results also

demonstrated that skin resistance may be a good measure of skin permeability and can be related to the quantity of analyte extraction in a given time. This ability to relate and model analyte extraction as a function of time and as a function of skin impedance is an important step forward in establishing a calibration algorithm for ion extraction across human skin *in vivo*.

Disclaimer

This thesis is the result of the author's original research. It has been composed by the author and has not been previously submitted for examination which has led to the award of a degree.

Signed: Sergio Rico Arias Date: 15/09/2011

Acknowledgements

First of all, I would like to thank Prof. Mary Helen Grant for giving me the opportunity of studying the MSc in Bioengineering at University of Strathclyde with a grant for the fees without which I couldn't have studied. I would also like to thank Prof. Patricia Connolly for giving me the opportunity to study on this project.

I would like to thank enormously to my supervisor Dr. David Heath, for his support from the very beginning, even before starting with the project; for encouraging me while I was developing the hardest parts of this project; for teaching me the lab practices and providing me with knowledge as to appreciate the research field much more.

I would like to thank my family for their devotedly believe in my eagerness to learn and improve myself daily; for their financial support to have a much better and relaxed life and for their love, even from the distance, from the charming country of Spain.

Also I can't forget thanking to all my classmates for their help during the process of learning the language with the endless number of words, the English language.

Contents

List of figures

Page

List of equations

Page

List of tables

Page

Chapter 1: Introduction

The skin is the largest and outermost organ of the body. One of the most important functions of the skin is to act as a protective barrier that separates two different environments. To achieve this effectively the skin acts as a permselective membrane, i.e., the skin seeks to retain desired molecules and compounds within the body while preventing unwanted or dangerous molecules entering the body. The degree to which the skin prevents the passage of molecules and compounds across its barrier, depends on many factors including skin characteristics as well as the nature, size and charge of the molecules present (Curdy, Kalia et al. 2001; Hadgraft 2004; Martini, Nath et al. 2009).

The movement of molecules and compounds across the skin is of particular interest in transdermal monitoring and topical drug delivery. Here, the permselectivity function of the skin plays an important role. It is important to understand how a given molecule or compound crosses the skin in order to predict its behaviour. To achieve this, various methods of skin modelling have been investigated (Pang and DaPeng 2009). The results of these skin models may be useful in applications such as medical device calibration in the field of transdermal extraction, or drug dose control in the field of topical drug delivery.

Transdermal monitoring is the measurement of body parameters across the skin. One of the main goals of transdermal monitoring is to provide a non-invasive/minimally invasive and continuous method for measuring blood parameters without the need of collecting a blood sample and the associated discomfort of collection. For example, certain illnesses such as diabetes, anaemia, alcoholism, thyroidism, or conditions such as imbalance in hormone levels and pregnancy may require a constant monitoring of glucose, haemoglobin, ethyl alcohol or hormone levels respectively within the blood (Phillips, Greenberg et al. 1995; Gabriely, Wozniak et al. 1999; Cook 2002; Timm, Lewis et al. 2009). On the other hand, the field of topical drug delivery focuses on introducing substances through the skin. There are two main reasons for this: firstly, because some drugs need to be applied locally to the affected area, and secondly, because stomach acids can degrade the drug and the hepatic

clearance of the liver gets rid of them before they are capable of producing the desired effect (Coston and Li 2001). The quantity of products applied locally to the skin can often be controlled more easily than equivalent oral medication, rendering the dose safer. However, dose control through the skin is not straightforward as the path of the drug to target is complicated by the lipids of the stratum corneum and the cellular membranes (Morganti, Ruocco et al. 2001).

The common factor in both the field of transdermal extraction and transdermal drug delivery is the desire to enhance and model the transport of molecules across the skin. Therefore, the focus of this thesis aims to examine the transport of ions and small molecules across the skin and will seek to model this transport behaviour in this context. This will begin with an overview of transdermal monitoring and transdermal drug delivery techniques discussed in literature. Following on from this, an overview of the relevant background theory will be given to inform the experimental design and modelling techniques.

In order to practically investigate the transport of molecules across the skin an ion and a small electrically neutral molecule will be chosen for study. Ions are small highly mobile charged particles strongly influenced by an electric field. Small neutral molecules are less mobile and less directly influenced by an electric field. Experimentally, observing the behaviour of these two different groups of particles may help inform how different particles are transported across the skin under various conditions. An *in vitro* study arrangement will be constructed to examine this behaviour under tightly controlled conditions. The results from this *in vitro* study will then be examined and modelled. Data from recently completed *in vivo* studies carried out in this lab, and under University ethics, will also be examined and modelled, allowing an *in vitro*/*in vivo* comparison.

The results of these experiments, models and data analysis will then be discussed in the context of their application in transdermal monitoring and transdermal drug delivery.

1.1. Objectives

Recently in vivo studies were carried out under University ethics and in accordance with approved procedures. These studies gathered data on potassium extraction and glucose extraction across the skin of healthy volunteer participants at various times of extraction. Skin impedance data was also gathered during these studies.

The specific objectives of this thesis are to:

- Construct and carry out an *in vitro* study for comparison with the existing *in vivo* studies.
- Determine, if any, and model the extraction behaviour of potassium and glucose *in vitro* and *in vivo.*
- Compare the extraction behaviour *in vitro* and *in vivo* for potassium and glucose and comment on the suitability of the *in vitro* synthetic membrane as an artificial skin membrane.
- Analyse the impedance of the *in vitro* synthetic membrane and analyse the impedance of the skin *in vivo* in response to reverse iontophoresis, comparing and contrasting the results.
- Use the impedance data to model the characteristics of the *in vitro* synthetic membrane and human skin *in vivo.*
- Use modelled parameters, or other parameters, to describe the extraction rate of potassium and glucose *in vivo* and *in vitro.*

Chapter 2: Literature Review and Theory

Mineral ions and small molecules such as glucose, fatty acids, haemoglobin, amino acids and urea (Das 1978), constitute an essential part of the physiological activities within the body and the tight control of their concentration within the body are essential in maintaining normal physiological health. It is often of interest to measure the blood concentration of important compounds or to deliver drugs to the body in order to help monitor or restore normal function.

Ions and small molecules enter into the body through the food we consume as part of our diet. Ions such as sodium, potassium, chlorine, calcium, phosphorus and magnesium are examples of bulk minerals and play important functions in the body. They control the osmotic concentration of the cytoplasm, maintain the transmembrane potential, act in the muscle contraction and interact in the blood clotting cycle. The other group of minerals is called trace minerals due to the low content in the body. The trace minerals mainly work as cofactors during chemical reactions, such as the conversion of glucose to pyruvic acid or the synthesis of haemoglobin. Nonetheless they are still important (Martini, Nath et al. 2009).

The total body content of key bulk and trace minerals is detailed in the Table 1 and Table 2 respectively.

Bulk Minerals	**Total Body Content**	**Recommended Daily Allowance (RDA)**
Sodium	110 g, primarily in body fluids	1.5 g
Potassium	140 g, primarily in cytoplasm	4.7 g
Chloride	89 g, primarily in body fluids	2.3 g
Calcium	1.36 kg, primarily in skeleton	1-1.2 g
Phosphorus	744 g, primarily in skeleton	0.7 g
Magnesium	29 g, (skeleton, 17 g; cytoplasm and body fluids, 12 g)	310-400 mg

Table 1: Total body content of bulk minerals (Martini, Nath et al. 2009)

Trace Minerals	Total Body Content	Recommended Daily Allowance (RDA)
Iron	3.9 g (1.6 g stored as ferritin or hemosiderin)	8-18 mg
Zinc	2 g	8-11 mg
Copper	127 mg	900 μg
Manganese	11 mg	1.8-2.3 mg
Cobalt	1.1 g	0.0001 mg
Selenium	Variable	55 μg
Chromium	0.0006 mg	20-35 μg

Table 2: Total body content of trace minerals (Martini, Nath et al. 2009)

In addition to ions and minerals there are many molecules such as glucose lactate, vitamins and hormones that play an equally important role in normal body function. For the purpose of this project only one ion (potassium) and one small molecule (glucose) have been chosen for investigation. Potassium and glucose have been chosen as they are representative of two different types of molecule that can move across the skin membrane. Potassium is very small, mobile and charged, whereas, glucose is much larger than potassium, less mobile and uncharged. However, both potassium and glucose are also important in their own right.

Potassium is one of the most important and abundant ions in the body. It accounts for the 0.4% of the total body weight and is a basic element required for proper membrane function, nerve impulses and muscle contractions. Its transport mechanism is through channel-mediated diffusion and at resting potential 95% of potassium concentration remains inside the cell due to the sodium-potassium exchange pumps. Thus, it plays an important role in the resting potential and transmission of impulses along the body. As with any other mineral, there is a daily loss of potassium of about 2 grams depending on the diet, urine pH, and hormone activity. For an average adult the recommended daily intake is 4.7 g in order to maintain normal plasma concentration levels in the range of 3.5 and 5.5 mEq/l (Martini, Nath et al. 2009). Blood potassium levels are tightly controlled in the body as potassium levels out with the normal range can lead to cardiac events, such as arrhythmias, or other cardiovascular complications.

Glucose is one of the most important metabolic molecules in the body. It is the basic and most used form of energy for the cells accounting for a blood concentration

between 70 and 110 mg/dl (3.9 and 6.1 mM) in healthy people under fasting conditions. Glucose can either be ingested in the diet, synthesized in the liver from carbohydrates or from non-carbohydrates precursors such as lactic acid, glycerol or amino acids. Once in glucose form, it enters the cells through the mechanism of facilitated diffusion and provides the energy to maintain cell life (Martini, Nath et al. 2009).

Diabetes is a disease where the body can no longer control blood glucose concentrations between tight limits. This can lead to blood glucose levels dropping below safe limits (hypoglycaemia) or rising dangerously high (hyperglycaemia). Patients with diabetes are recommended to control their blood glucose levels within as normal a range as possible. Monitoring of blood glucose plays an important role in this (Martini, Nath et al. 2009). At present the main method of monitoring blood glucose is with invasive finger-prick measurements that involve sampling a drop of blood and measuring the content of that sample on a reagent strip.

As regular blood sampling is required, a non-invasive (less painful) and continuous method of blood glucose monitoring is desired. There is much research underway in the field of transdermal monitoring to develop a non-invasive and continuous blood glucose monitor. A brief overview of the main technologies used in transdermal monitoring will be discussed with a focus on measuring blood glucose.

2.1. Transdermal Monitoring

Many technologies have been examined for their potential in patient monitoring. These methods range from fully invasive methods, such as implantable sensors, through minimally invasive methods, such as micro-needle arrays and miniaturised lancets, to non-invasive methods of monitoring, such as infrared spectroscopy, enhanced diffusion, florescence, electroporation and reverse iontophoresis (Kost, Mitragotri et al. 2000; McShane 2002; Ballerstadt, Gowda et al. 2004). Some of these methods will be explored in more detail shortly with a particular focus on reverse iontophoresis.

Due to the high prevalence of diabetes (IDF 2011) the greatest achievements in transdermal monitoring have come from monitoring glucose. One of the most recent advances in transdermal glucose monitoring was the portable GlucoWatch made by Cygnus Inc., which appeared on the market in 2001 (FDA 2001). It was a glucose monitoring device based on reversed iontophoresis and was used in conjunction with the finger-stick blood glucose measurement devices to provide regular blood glucose readings. However, it was withdrawn from the market in 2006 as it was considered unreliable when excessive sweat was produced. Other complaints with the device included unreliable readings (particularly at low blood glucose), missed readings and long calibration times. Newer devices are still fighting to take its place. There are too many to review in detail, but examples include the OrSense's NBM-200G (Orsense 2011) based on occlusion spectroscopy. The manufacturer claims this device to be able to measure blood glucose levels with comparable accuracy to invasive solutions. Experiments carried out by Amir et al. on the model NBM showed that 95.5% of the measurements lay within the clinically acceptable regions (Amir, Weinstein et al. 2007). In addition, the latest model includes a number of other parameters such as blood haemoglobin, oxygenation and pulse rate, although this device does not appear to be available on the market. Other examples still to be approved by the FDA or in design stage, include the Glucoband Diabetic Watch Monitor made by Calisto Medical Inc. (CalistoMedical 2011) which is based on bio-electromagnetic resonance; the Glucon Glucose Watch made by Glucon and based on photoacoustic waves to calculate glucose levels; the family of devices based on the insertion of sensors subcutaneously such as Dexcom SEVEN manufactured by DexCom, Inc., Minimed Guardian REAL-Time System by Medtronic or Abbott Freestyle Navigator by Abbott Laboratories (Cox). The high number of devices seeking to measure blood glucose levels non-invasively or continuously demonstrates the both the high level of interest in the field of non-invasive patient monitoring as well as the variety of technologies under investigation.

The following table, Table 3, summarises the main research areas under investigation in the field of transdermal monitoring:

Method	Description
Reverse iontophoresis	It is the chosen method of investigation in this project so it will be discussed in more detail later. However, briefly, reverse iontophoresis is a technique based on the application of an electric current to the skin. That current enhances the movement of charged molecules and neutral but polar molecules through the skin such as sodium, potassium, glucose, urea, and phenylalanine. Results performed by Degim et al. (Degim, Ilbasmis et al. 2003) in the extraction of urea showed a correlation with blood levels of 88%. Reverse iontophoresis has the same principle approach as iontophoresis, but with the opposite desired effect. Iontophoresis is a method used to deliver drugs transdermally, whereas reverse iontophoresis is used to extract molecules transdermally. (Leboulanger, Guy et al. 2004).
Electroporation	It is the mechanism used to enhance membrane permeability with the application of a high electric field. Electroporation applies a high voltage of very short duration to the membrane or skin. Chosen pulse profiles are generally either a rectangular pulse with a duration of 10 ns (Chang 1989) or a decaying exponential in the range of milliseconds and can reach up to several hundreds of volts creating a transient pore in the membrane (Coston and Li 2001). Prausnitz et al. (Prausnitz, Edelman et al. 1995) showed the efficiency in the delivery of heparin which was an order of magnitude greater than iontophoresis.
Phonophoresis	Also known as Sonophoresis uses ultrasound to modify the permeability of the skin for enhanced delivery of drugs such as insulin, mannitol, glucose, heparin or molecular extraction such as glucose (Coston and Li 2001; Lavon and Kost 2004; Escobar-Chavez, Bonilla-Martinez et al. 2009). Some researchers believe it produces thermal, mechanical or chemical alteration in the tissue and so it induces structural changes in the intercellular lipid domains, which reduces barrier properties. (Morganti, Ruocco et al. 2001; Escobar-Chavez, Bonilla-Martinez et al. 2009). Other researchers suggest that cavitation is the main mechanism. Cavitation is produced when ultrasound passes through a liquid and bubbles implode producing energy (Coston and Li 2001; Escobar-Chavez, Bonilla-Martinez et al. 2009), that energy creates a shock wave which produces structural changes in the surrounding tissues what in turn helps with drug delivery (Lavon and Kost 2004). Mitragotri et al. in their experiments showed an enhancement in delivery of several permeants of up to 3000 times when compared with the control (Mitragotri, Blankschtein et al. 1996).
Implantable sensors	They are immunoelectrochemical sensors that are enclosed within a dialysis membrane and combine immunochemical methods with electrochemical systems. An electrode containing a immunoreagent is labelled with an enzyme which activity can be detected electrochemically (Cook 1997).
Near-infrared spectroscopy	This method uses fibre optic technology to illuminate the area and detect the reflected spectra. That represents the molecular vibration of all molecules within the tissue, but using advanced processing the energy absorbed/reflected from the molecule of interest can be isolated. Gabriely in his experiments measured glucose using standard glucose oxidase methods and near infrared spectroscopy. The results showed that 97.7% of the predictions were within the A-zone in the error grid analysis (Gabriely, Wozniak et al. 1999).

Near-infrared (NIR) fluorescence affinity sensors	There are many sensors under investigation with the aim of being used to monitor glucose. A sensor developed and characterised by Ballerstadt et al. was sealed in a hollow dialysis fibre and the mechanism is based on fluorescence resonance energy transfer between a NIR chromophore and an NIR fluorophore (Ballerstadt, Gowda et al. 2004). Besides the sensor showed a good dynamic range (15% change over 2.5-30 mM without hysteresis), fast response time (2-4 min) and long term stability (6 months).
Electro - sonophoresis	It is the combination of an electrical field and ultrasound techniques to enhance the movement of analytes to the skin surface, especially those that are hydrophobic or complex in carrier charge. Cook et al. (Cook 2002) in their experiments measured testosterone, insulin 17-b estradiol, and cortisol amongst others and the results compared with those in blood had a correlation greater than 82%.
Microneedles arrays	Microneedle arrays have been used to extract glucose from the interstitial fluid successfully, unfortunately the method seems to be painful as reported by Wang et al. in their experiments (Wang, Cornwell et al. 2005). They can also be used for drug delivery as it will be explained in the next section.

Table 3: Transdermal monitoring research areas

Transdermal monitoring is not limited to monitoring glucose or applications to control levels of glucose and lactate (Ching and Connolly 2008), other compounds such as prostaglandin E2 (Mize, Buttery et al. 1997), urea (Degim, Ilbasmis et al. 2003), phenytoin (Leboulanger, Guy et al. 2004) and potassium (Wascotte, Delgado-Charro et al. 2007) have been studied too.

Another field where knowledge of the transport of molecules across the skin is very important is the field of transdermal drug delivery. This will be discussed briefly in the next section.

2.2. Drug Delivery

Compounds that cannot overcome the acids of the stomach or the hepatic clearance of the liver were traditionally given as intravenous, subcutaneous or intramuscular injections. Subcutaneous and intramuscular means of delivery injected a fixed amount onto the site, but the drug was distributed to other unnecessary areas quickly and higher amounts of drug were necessary. The effect on other parts of the body can be detrimental (Coston and Li 2001).

Drug delivery through the skin is often a preferred route of delivery over oral drug delivery. For example, topical delivery of analgesics is often preferred over oral delivery for mild pain management. However, it is often difficult to quantify the dose of drug passed through the skin and how quickly a given dose is delivered. Many methods have been researched with the aim of enhancing and controlling drug delivery through the skin.

There are a vast number of mechanisms and possible combinations of mechanisms available for application in transdermal delivery enhancement. There are interests in assessing absorption regarding local effects such as corticosteroids for dermatitis; create a systemic effect as in the case of nicotine patches, hormonal drug patches; create a surface effect desired in sunscreens, cosmetics and anti-infectives; targeting deeper tissues for non-steroidal anti-inflammatory agents; prevent unwanted absorption such as solvents, pesticides or allergens (Escobar-Chavez, Bonilla-Martinez et al. 2009). Iontophoresis, for example, has been used in the delivery of lidocaine for analgesia, heparin for anticoagulation, metoprolol for treatment of hypertension and angina pectoris, fentanyl for chronic pain management, insulin, procainamide for antiarrhythmic therapy and heparin and hirudin for combating restenosis (Coston and Li 2001). Microneedles also have been demonstrated *in vivo* for delivery of oligonucleotides, reduction of blood glucose level by insulin, and induction of immune responses from protein and DNA vaccines (Prausnitz 2004).

In a similar manner to transdermal monitoring, methods of transdermal drug delivery can be classified as invasive, minimally invasive or non-invasive. The difference between non-invasive and minimally invasive is not clear from the literature. The definition assumed here is that non-invasive refers to methods where the skin is not breached and minimally invasive methods where the skin is breached, but nerves and blood vessels are not contacted, as in the case of microneedles (Pang and DaPeng 2009). With this definition, the following drug delivery technologies can be divided as follows in Table 4.

Non-invasive methods	Minimally invasive methods
Diffusion Absorption Thermal energy Radio frequency energy Ultrasound Electrostatic force (electrophoresis) Electric field (iontophoresis) Magnetic field Transdermal skin patch	Microneedles (they puncture the skin but less than 1 mm without piercing blood vessels or damaging nerves).

Table 4: Classification of delivery methods according to their interaction with the body

Many of the non-invasive methods have already been discussed in the context of transdermal monitoring so will not be discussed further. However, the use of micro-needle arrays will be briefly described here.

Micro needle arrays has been shown to be a successful method of compound delivery across the skin (Prausnitz 2004). The needle arrays have been manufactured in various sizes, shapes and materials including silicon and metal. They have been used to deliver drugs, proteins, genetic material, and vaccines successfully. Two main variations of microneedles exist. Firstly, solid microneedles puncture micro holes in the skin to facilitate the transport of molecules. These solid versions of microneedles have been used in three configurations. The "poke with patch" approach first punctures the skin with the microneedles and then applies the patch onto the skin. The "coat and poke" approach coats the needles with drug and insert them into the skin. And the "dip and scrape" approach that dips the needles into a drug solution and then leave the drug on the microabrasions created with the needles. Secondly, there are also hollow microneedles which contain a hollow bore and transport the substances through their interior and deliver it by diffusion or by pressure driven force.

Some of the methods above can be further enhanced. The "poke with patch" version of the solid microneedles uses diffusion for the transport of molecules but it can be further enhanced using additional techniques such as iontophoresis, where an electric field is applied (Prausnitz 2004). Microneedles have also been used with sonophoresis (Chen, Wei et al. 2010).

Out of all the methods discussed so far, iontophoresis has shown particular promise. Reverse iontophoresis was the core technology behind the GlucoWatch device, which successfully acquired FDA approval, and is applicable to both transdermal monitoring and drug delivery. Reverse iontophoresis will be discussed in more detail shortly, but before the effects of iontophoresis on the skin can be discussed and before discussing how ions and molecules move across the skin ,we must first consider the structure of skin.

2.3. Skin

2.3.1. Skin structure

The largest organ in the body, the integumentary system, is a very complex structure made up of synchronized layers of skin and accessory structures including hair follicles, nails, sweat glands and sebaceous glands. Figure 1 illustrates various components that make up the integumentary system.

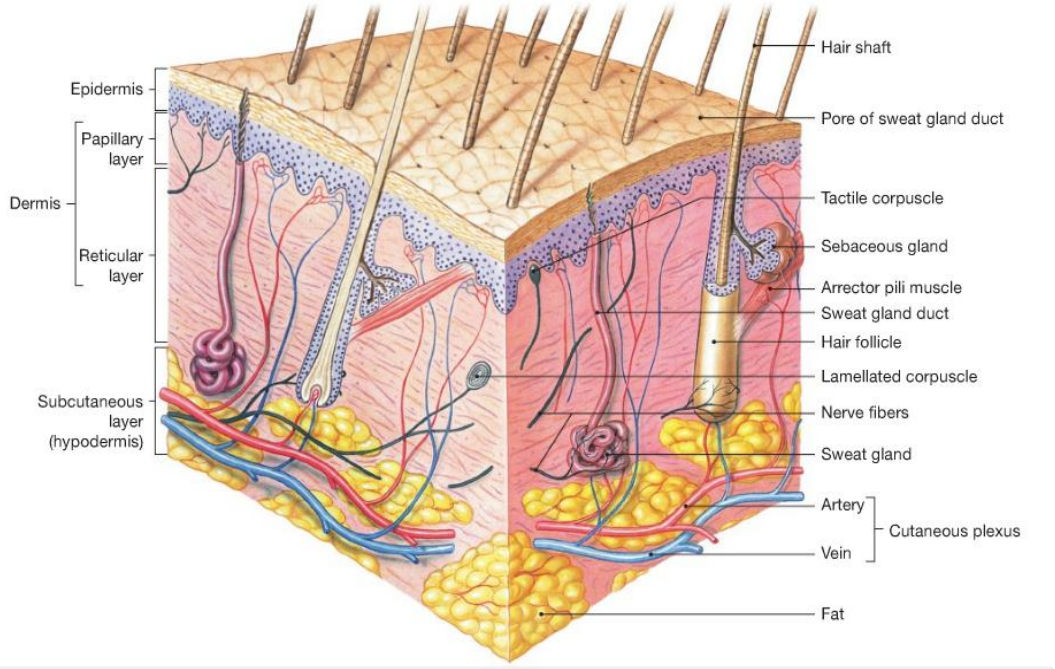

Figure 1: The components of the integumentary system (Martini, Nath et al. 2009)

The skin is divided into two layers, the epidermis and the dermis.

The outermost layer, the epidermis, has many duties, but mainly it is in charge of protecting the body against abrasion, it prevents the body from fluid loss and offers protection against the intrusion of microorganisms.

The epidermis is also avascular, meaning, that there is no direct blood supply, therefore the nutrients need to diffuse from cell to cell. Nerves do not reach this part of the skin either; hence there is no consciousness about any damages.

The most abundant type of cell in the epidermis is the keratinocyte and depending on the state of maturity they form different layers. The name of these cells from the outermost to the innermost are the: stratum corneum, stratum lucidum, stratum granulosum, stratum spinosum and stratum germinativum. The epidermis containing keratinized cells and dead cells offers the first protection, but from the perspective of moving molecules across the skin, this is the first barrier to overcome. One observation about this layer is that it is water resistant but not water proof (Martini, Nath et al. 2009), that means that polar molecules will be able to cross the skin, although with some difficulties.

- The origin of the epidermis starts in the stratum germinativum. At this level cells are large and columnar attaching to adjacent cells by desmosomes and to the basal lamina by hemidesmosomes, laminin and integrins. The network is mainly formed of keratins K5 and K14. They are responsible for the prevention of water loss and the prevention of absorption of foreign substances.

- At the next level, the stratum spinosum, cells differentiate into corneocytes which have less water content and are flatter and bigger. Production of keratin K5 and K14 is interrupted to permit the production of Keratin K1 and K10 which are aggregated to form filaments.

- In the stratum granulosum stage the filaments are packed together with filaggrin and two granule-like structures are formed: the lamellar bodies and a stable protein envelope.

- In a later step, the stratum lucidum, the keratinocytes differentiated into corneocytes are filled with keratin bundles in a lipid-enriched intercellular matrix. Ceramides, cholesterol and free fatty acids help maintain cohesion between corneocytes.

- In the final stage, in the stratum corneum, the cells are flat and the lipid lamellae are released into the intracellular space to help with the cohesion as well as blocking the diffusion of aqueous material (Morganti, Ruocco et al. 2001).

The second main layer of the skin is the dermis. It supports the epidermis and is also divided into 2 layers. The papillary layer contains capillaries, lymphatic vessels and sensory neurons and the reticular layer is made of connective tissue and all the accessory organs. (Martini, Nath et al. 2009)(p.158-168).

This layering of different cells illustrates the complexity and very heterogeneous path the molecules must take to cross the skin barrier. The stratification of the skin together with the channels created due to the accessory structures do however provide potential pathways of molecules through the skin for molecular transport. These potential routes of transport will now be considered.

2.3.2. Routes of transport across the skin barrier

Ions and small molecules find several pathways to cross the skin. Those pathways can be classified into two groups. The first group benefits of the existing passages on the skin, the appendageal ducts and pores, such as hair follicles, sweat ducts and sebaceous glands. The second group includes transcellular pathways across the cells and paracellular pathways around them (Coston and Li 2001).

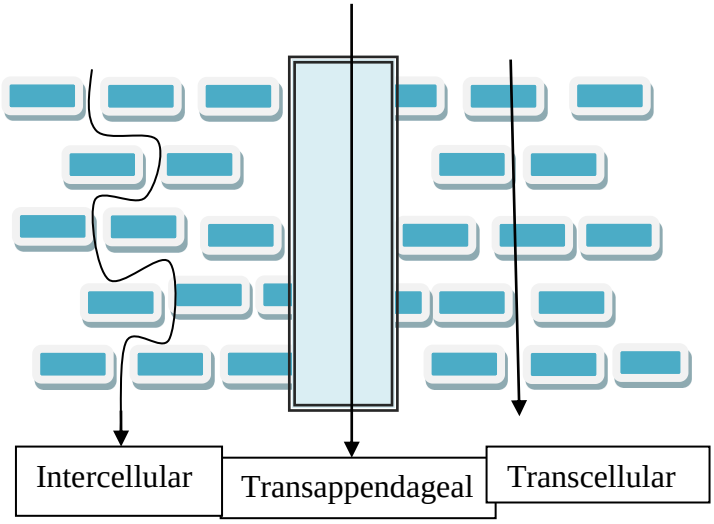

Figure 2: Routes of transport through skin

The transappendageal paths are tube-like pores that reach directly into deep layers of the skin from the surface (Coston and Li 2001). The ducts are covered with a double layer of epithelial cells, which is much less resistant to transport of drugs than the stratum corneum (Hui 1998).

Although transappendageal paths reach deeper into the skin the major route of penetration across the stratum corneum has been reported to be through the intercellular spaces (Coston and Li 2001), which are filled with structured lipids (Morganti, Ruocco et al. 2001; Hadgraft 2004). Therefore a diffusing molecule has to overcome lipophilic and hydrophilic domains before reaching the epidermis. The simple mechanisms of diffusion can be described by Fick's laws as discussed later in section 2.6.2.1.

2.3.3. Skin variation

As has been discussed, skin is not a homogenous material, but rather very heterogeneous. Such heterogeneity is due to many factors such as the site of measurement, the state of disease, age, gender, ethnic origin, species differences (human/animal), metabolic status of the skin, environmental conditions, physiological conditions, diet, the reservoir capacity of the skin, irritation and

toxicity caused by other materials (Frances, Branchet et al. 1990; Diridollou, Black et al. 2000; Harding 2004; Giacomoni, Mammone et al. 2010; Chu and Kollias 2011).

The site of measurement/delivery is important as the thickness of the skin changes along the body. Experiments carried out by Diridollou et al. showed that the skin was thicker in the forehead than in the anterior side of the forearm (Diridollou, Black et al. 2000). Other experiments carried out by Chu et al. showed that scaling was greater in dorsal forearm than in the upper inner arm (Chu and Kollias 2011).

Ageing also produces changes in the metabolism and composition of the cells, especially in the skin. Elderly people show an increase in fibres length and a decrease of skin thickness (Frances, Branchet et al. 1990). Other changes affect the corneocytes, they becomes bigger in size (Harding 2004) and are easier to detach (Chu and Kollias 2011).

Men and women show differences not only in the thickness of the skin, but the number of hair follicles present at site or the sweat production. Men and women also differ in hormone metabolism, sebum production, surface pH, fat accumulation and serum leptins (Giacomoni, Mammone et al. 2010) which lead to the following numbers in Table 5:

Characteristics	**Males**	**Females**
Sweat rate during exercise (ml/h)	800	450
Sebum (µg/cm2)	3	0.7
pH (surface)	5.8	5.5
pH (intra-epidermal)	4.6	5.6
Leptin (serum level, ng/ml)	16	3
Skin thickness (ratio men/women)	1.2	
SCC (incidence ratio men/women)	2	
Systemic lupus (incidence ratio men/women)	0.11	
Melanoma (mortality ratio men/women)	2	

Table 5: Skin difference between men and women (Giacomoni, Mammone et al. 2010)

Ethnic differences also exist. Chu et al. reported using dermatoscopy that corneocyte detachment was easier in Caucasians than in Afro-American population in New Jersey. Elderly Caucasian people showed a rate of corneocyte detachment which was twice the rate as for Afro-American people. (Chu and Kollias 2011).

Other variations of the skin occur during changes in environmental conditions, such as the weather, which influences the intercellular lipids rendering the skin dryer in winter months; or the psychological stress which delays the barrier recovery by elevating the circulating glucocorticoids (Harding 2004).

Animal skin has been studied to establish similarities with human skin. Pig skin is often regarded as having the most similar properties to human skin. Although pig skin is used for *in vitro* experiments to simulate human skin there still exits some differences in permeability as shown by Barbero et al. (Barbero and Frasch 2009). Common pig or hairless guinea pig have a similar skin to human skin due to the distribution of hair on the surface, the thickness of the epidermis with distribution of strata and the large content of elastic tissue, but the permeability is still greater in that observed in human skin.

Finally the state of disease needs to be considered. Diseases such as skin cancer can increase the number of layers of skin and type of cells whereas other diseases such as eczema can decrease the hydration (Glickman, Filo et al. 2003; Nicander and Ollmar 2004).

Due to this high degree of variation in skin permeability, a number of methods have been developed to measure the permeability of skin samples by assessing the integrity of the skin barrier function. The most common techniques found in literature will now be discussed.

2.3.4. Methods of assessing skin permeability

Skin permeability is an important parameter in areas of drug delivery of transdermal monitoring. It is this parameter which determinates the rate at which the ions and molecules will be able to cross the skin.

There are a number of techniques used for measuring skin barrier function, and in turn permeability, in the context of assessing skin integrity. These techniques include Trans Epidermal Water Loss (TEWL), Attenuated Total Reflectance-Fourier Transform Infrared (ATR-FTIR) spectroscopy, Laser Doppler Flowmetry (or

velocimetry) (LDF) and impedance spectroscopy. Some of them will be presented in this section.

Transepidermal Water Loss (TEWL) is one of the most important and used methods of assessing the state of the skin. It is not only used in medical applications but also in areas of cosmetology. The method is based on the measurement on the water evaporated from the skin and so the method measures the rate at which the water evaporates from the body. In order to measure the quantity of water released an evaporimeter is used which besides is non-invasive. Taking several measurements statistical calculations are performed and any disorder with the skin can be found (Gioia and Celleno 2002).

Visual methods also exist such as attenuated total reflectance-Fourier transform infra-red (ATR-FTIR) spectroscopy. This technique shows changes on the stratum corneum, the space between cells and thus it is useful to measure permeation and state of disease of skin. Other methods used to measure the penetration of the permeant, the space between cells or the state of them are laser confocal microscopy, nuclear magnetic resonance (NMR), X-ray scattering, neutron scattering, neutron reflectometry, electron spin resonance, differential scanning calorimetry. (Hadgraft 2004).

The electrical resistance (ER) measurement performed by Davies et al. (Davies, Ward et al. 2004) showed that it was a good method to evaluate integrity of skin. Compared to traditional tritiated water flux method it has the advantage of being quicker and safer as it does not use any radioactive element. The electrical resistance of the skin is measured passing a fixed current across the skin.

Electrical impedance measurements have been used in more advanced ways to assess skin health. Benignant and malignant skin lesions can be differentiated with electrical impedance scanning. The experiments carried out by Glickman, Filo et al. at 2 KHz showed that the size of the skin tumour produces changes in the conductivity and capacitance increasing both values. Necrosis, in the centre of the lesion, is associated with a decrease in the electrical conductivity (Glickman, Filo et al. 2003). It is important to note here that impedance was used, not just skin

resistance, therefore information was gathered from both the conductive and capacitive parameters recorded.

The lipid content of the stratum has also been measured using electrical impedance spectroscopy. This method reflects structural and chemical alterations of living tissues. The test performed on patients with atopic dermatitis showed a larger reactivity than on healthy skin patients (Nicander and Ollmar 2004), which was attributed to lower amounts of intercellular lipids. Again electrical impedance was used here not just resistance and information was gathered from the reactance measurement.

Skin impedance is an attractive method for assessing skin integrity and skin permeability, as it is safe, fast and inexpensive when compared to the alternatives listed above. It can also be seen that recording both the resistive and reactive parts of impedance can help provide more information about the skin rather than recording electrical resistance alone. To achieve this, electrical equivalent circuit models of the skin can be constructed. These will be discussed in the next section.

2.4. Electrical Equivalent Circuit Modelling of Skin

Electrical properties of skin can be examined and related to various properties or conditions of skin, such as skin hydration (Martinsen and Grimnes 2001), permeability (Potts and Guy 1995) or skin health (Harding 2004). To achieve this, skin has been modelled using electrical equivalent circuits models (Lykken 1970; Elden 1971; Pang and DaPeng 2009). The models considered in this thesis will be limited to models containing only resistors and capacitors as the skin is not considered to possess inductive properties (Coston and Li 2001; Pang and DaPeng 2009). However, before considering specific electrical circuit models of the skin, some preliminary circuit theory will first be discussed (Coston and Li 2001).

Resistance (R) is the ability of the material to oppose to a direct current (DC). According to Ohm's law the voltage across a resistance is proportional to the current circulating through the material:

$$V = I \cdot R$$

Equation 1: Ohm's Law

When the resistance depends on the frequency of the current or voltage it is referred to as impedance and represents the complex resistance.

$$V = I \cdot Z$$

Equation 2: Ohm's Law for impedances

Therefore, Impedance (Z) is the ability of the material to oppose an alternating current (AC). The impedance is defined as a complex quantity and can be expressed in several forms. The most common forms are the polar form and the Cartesian form.

$$Z = |Z|e^{j\theta}$$

Equation 3: Impedance in its polar form

Where |Z| represents the magnitude and Θ is the phase.

$$Z = Z' + jZ''$$

Equation 4: Impedance in its Cartesian form

Where Z' is the real part or resistance and Z'' is the imaginary part.

Capacitance is the ability of the material to create an opposing voltage when the current or voltage is of alternating nature. The effect created results in the storage of charge. There are two types of capacitance. The most common form of capacitance is electrical capacitance, which is created when a dielectric material separates two conducting materials. The second type of capacitance is referred to as polarization capacitance, and results from the movement of ions in a solution.

In the case of a simple RC series circuit:

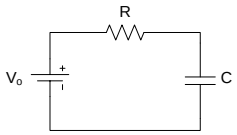

Figure 3: R-C Series Circuit

The voltage across the capacitor with respect to time is given by:

$$V_c(t) = V_o(1 - e^{-t/\tau_o})$$

Equation 5: Voltage across a capacitor in a series RC circuit

Where V_o is the voltage of the power supply, t is the time and τ_o is the time constant of the system given by:

$$\tau_o = RC$$

Equation 6: Time constant equation

This means that if the current is DC, the capacitor will fully charge and will not discharged until the source of voltage has been disconnected.

The stratum corneum possesses both capacitive and resistive properties. Whereas, the tissue found deeper in are often regarded as behaving in a purely resistive manner (Pang and DaPeng 2009).

According to several investigators (Lykken 1970; Elden 1971; Yamamoto and Yamamoto 1977; Pang and DaPeng 2009) skin impedance can be modelled using resistor-capacitor (RC) circuits and no inductive components. Upon the agreement that only resistance and capacitance forms can be used to model the skin, several models can be designed.

Three example electrical equivalent skin models, based solely on resistors and capacitors, will now be considered.

2.4.1. Model A

The simplest of the models studied by (Elden 1971) considers the stratum corneum as a parallel combination of a resistor and capacitor in series with another resistor. This model reflects the frequency dependence of skin. In particular, the magnitude of the impedance decreases as frequency increases, which is representative of skin. However, as this is a simple model, some limitations have been identified. In particular, this model does not represent the layered structure of skin (as described in section 2.3 Skin) (Coston and Li 2001). An illustration of the electrical equivalent circuit model is given in Figure 4:

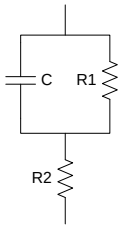

Figure 4: Model A (Pang and DaPeng 2009)

Where C and R_1 represent the capacitance and resistance of the outermost layer of the stratum corneum and R_2 represents the resistance found in deeper layers of the stratum corneum.

Typical values for R_1 range from 100 Ω to 5 MΩ cm^2 and R_2 from 0.1 Ω to 1 kΩ cm^2 (Pang and DaPeng 2009).

2.4.2. Model B

To address the limitations of Model A a more complex model was proposed by Tregear (Tregear 1966) to represent the layered structure of skin. This model consists of multiple parallel RC circuits in series. Each of the parallel blocks represents the different skin layers. The lipid matrix subsystem includes 70-100 bilayers in sequence (Elias, McNutt et al. 1977; Elias 1983; Goldsmith 1983; Madison, Swartzendruber et al. 1987). This model also shows the distribution of the impedance within the skin. It has been observed that stratum corneum accounts for the majority of impedance measured (Pang and DaPeng 2009).

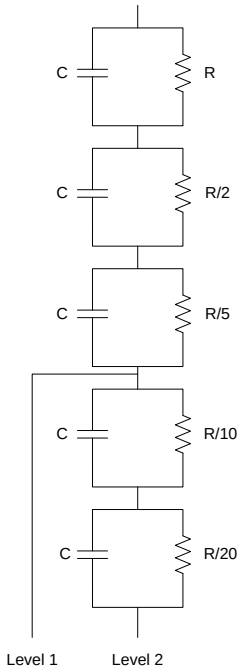

Figure 5: Model B (Pang and DaPeng 2009)

2.4.3. Model C

A third, and again more complex, model has been proposed to further represent the layered structure of skin Lykken in (Lykken 1970). This model consists of parallel lines, each containing parallel blocks in series with a resistor. As in the previous method, the parallel blocks represent the layers of the skin. And the parallel lines represent the different paths through the skin. In order to find an accurate impedance model of the skin Lykken performed a square wave analysis. In this analysis he chose pulses of sufficient duration so as to keep capacitors fully charged. When capacitors are fully charged all current is forced to flow through the parallel resistance and travel to deeper layers of the skin. In this way he showed the resistive properties in deeper layers.

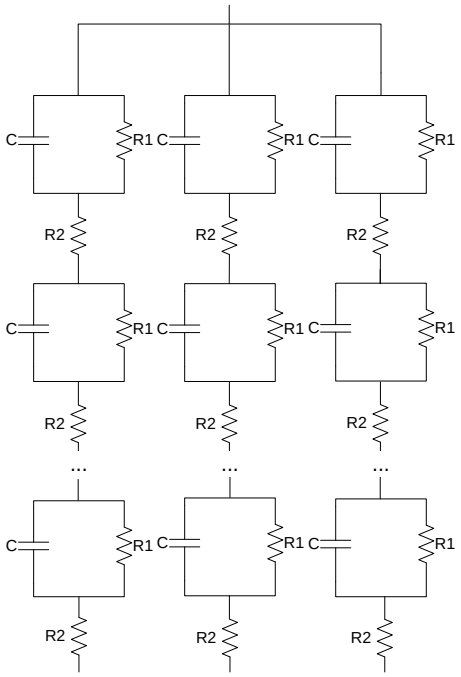

Figure 6: Model C (Pang and DaPeng 2009)

2.5. Skin Models Used in Analysis

To fulfil the aims of this project model A will be used. It is the simplest model but very complete as well. The model is made up of a resistor in series with a resistor and capacitor in parallel.

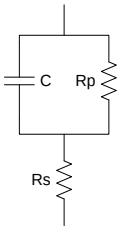

Figure 7: Model A (Pang and DaPeng 2009)

Where R_s represents the deeper layers or the solution in the *in vitro* case and C/R_p represents the outer layers or the membrane. Together with the theory for biological tissues studied by the Cole brothers the values of R_s, R_p and C will be calculated.

Figure 8 shows the typical complex plot obtained when impedance of any biological tissue is analysed.

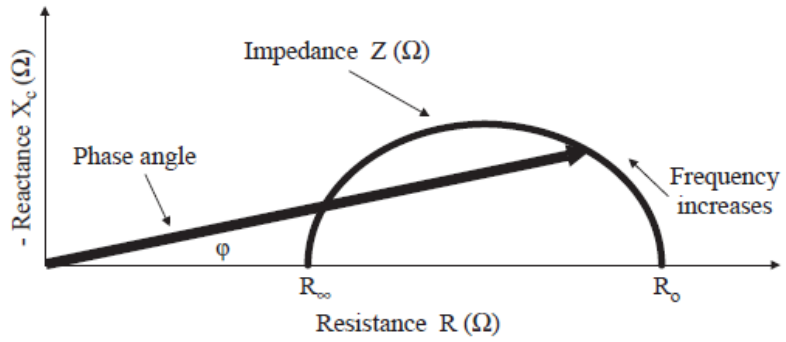

Figure 8: Typical Cole-Cole plot of tissue (Kyle, Bosaeus et al. 2004)

According to the Cole empirical equation the impedance is given by Equation 7:

$$Z = R_\infty + \frac{R_0 - R_\infty}{1 + (j\omega\tau)^\alpha}$$

Equation 7: Cole empirical equation (Martinsen, Grimnes et al. 2002)

Where R_∞ is the resistance at very high frequencies, R_0 is the resistance at very low frequencies, ω is the angular frequency, τ is a time constant and $\varphi=\alpha(\pi/2)$ is the constant phase angle (Martinsen, Grimnes et al. 2002).

The general equation for circuit in Figure 7 can be written as in Equation 8.

$$Z = Z_{series} + Z_{parallel}$$

Equation 8: General impedance form of Model A

Comparing Equation 7 with Equation 8 and using names for the components as in Figure 7 the following results apply:

$$Z_{series} = R_\infty = R_s$$

Equation 9: Z series

$$Z_{parallel} = \frac{R_0 - R_\infty}{1 + (j\omega\tau)^\alpha} = \frac{R_p}{1 + j\omega R_p C}$$

Equation 10: Z parallel

The parallel part has real and imaginary parts and can be shown in the Cartesian form:

$$Z_{parallel} = Z' + Z'' = \frac{R_p}{1 + \omega^2 R_p^2 C^2} - j\frac{\omega R_p^2 C}{1 + \omega^2 R_p^2 C^2}$$

Equation 11: Z parallel in Cartesian form

Where Z'' is the part of interest to calculate the value of C.

$$Z'' = j\frac{\omega R_p^2 C}{1 + \omega^2 R_p^2 C^2}$$

Equation 12: Imaginary part of the parallel part of the circuit in Model A

As Z'', R_p and ω are given value, the equation can be solved for C.

2.6. Iontophoresis and Reverse Iontophoresis

Previous sections of this chapter (Section 2.1 and 2.2) have already discussed a number of methods in development for enhanced drug delivery and molecular extraction. The structure of skin and the electrical properties of skin have also been discussed (Section 2.3 and 2.4). Here iontophoresis will be discussed in detail in the context of enhanced drug delivery and molecular extraction.

Iontophoresis is a potential non-invasive and painless method of delivering drugs transdermally and allows certain drugs including peptides, proteins and hormones to be delivered safely in controlled doses without serious pain to the patient (Pang and DaPeng 2009). This allows the drug to be delivered in lower quantities. The lower the quantity the less risk there is to other parts of the body (Coston and Li 2001).

As has been previously mentioned, Iontophoresis is based on the application of an electric field over a permeable or semipermeable membrane. Iontophoresis is usually

applied by establishing a voltage across an electrode pair in order to drive a constant DC current between the two electrodes. The voltage that is created and the current that is generated leads to the movement of particles.

Reverse iontophoresis (RI) is the same application of an electric field, but with the aim of extracting molecules out of the body through the skin instead of delivering them. There are three forces that act during the application of reverse iontophoresis; passive diffusion, electromigration and electroosmotic flow.

The first force that will be described is passive diffusion. This force is independent of RI, but still needs to be considered. Passive diffusion is due to the concentration of molecules within a solution. When different concentrations of molecules exist in the same solution a gradient of concentrations appears and the force moves down the gradient concentration (Coston and Li 2001).

The second force that will be discussed is electromigration. Electromigration is caused by the electric field applied during RI. Within the skin, the permeation of both charged molecules and uncharged, but very polar species, will be enhanced significantly under the influence of an electrical field (Curdy, Kalia et al. 2001). This electrical current movement acts on charged substances and is independent from the passive diffusion.

A third force that will be discussed is electroosmotic flow (Sieg, Guy et al. 2004). This is the main transport mechanism of uncharged molecules and high molecular weight cations. The skin is a permselective membrane that, at physiological pH (~5.0-6.0), supports a net negative charge. As a result a positively charged ion will penetrate more easily across the skin than a comparably sized negative ion. Therefore, more momentum is transferred to the solvent by cations than by anions. This momentum generated by the cation movement causes a net convective flow of volume (electroosmotic flow) from anode to cathode and, as a result, there will be enhanced transport of dissolved polar (but uncharged) solutes in the same direction (Coston and Li 2001).

In an ionic solution ions will move due to an applied driving force. An electron flux is transformed into an ionic current at the electrode/liquid and electrode/skin

interfaces. That ionic current proceeds through the skin (Sieg, Guy et al. 2004) and is the one responsible for the movement of the drug into the skin (Coston and Li 2001).

In the following diagram (Figure 9) all three forces are shown. In the cathode, cations and neutral molecules are pulled due to the passive diffusion, the electromigration and the electroosmotic flow. On the other side, in the anode, anions are attracted due to the passive and electromigration while the electroosmotic flow repels them.

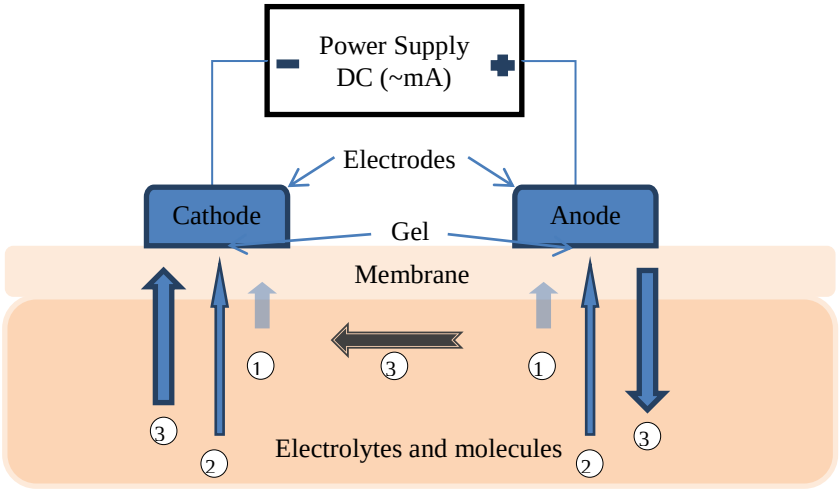

Figure 9: Diagram of the movement of elements due to the different existing forces

Where 1 is the force due to passive diffusion, 2 is the force due to electromigration and 3 is the force due to electroosmotic flow.

2.6.1. Effects of iontophoresis and alternative profiles

Generally, iontophoresis is regarded as a safe method of delivering drug transdermally, but certain limitations and disadvantages have been reported and should be taken into consideration. The applied constant current during a period of time can produce erythema, burns, and blisters and can lead to an insufficient delivery (Coston and Li 2001).

Studies carried out by Catherine Curdy et al. (Curdy, Kalia et al. 2001) to assess the effects of iontophoresis on the skin integrity drew the following conclusion:

1. The sensations produced using current densities below 0.5 mA/cm^2 are within acceptable limits.

2. The passage of current does not change skin's basic barrier functions significantly as it was tested using transepidermal water loss (TEWL) technique and reflectance infra-red (IR) spectroscopy. IR spectroscopy revealed that the current does not produce a significant perturbation in the conformational order of the stratum corneum or on the protein conformation.

3. The changes in skin properties were observed to be reversible. This was shown by measuring the electrical properties of the skin before and after the application of iontophoresis.

4. The transient erythema provoked by iontophoresis has a quick recovery. Its intensity and duration is related to the intensity and duration of the current as it was measured with laser Doppler flowmetry (LDF).

Traditionally a direct current (DC) has been used to perform iontophoretic transport, but different signals have also been used to create the driving force (Coston and Li 2001). The direct current profile is the simplest profile to apply, but it has several drawbacks including erythema or mild burns as explained above. A constant current applied over a long period can charge completely a capacitor. And due to the capacitance nature of the skin the effect can result in erythemas, burns and shocks (Coston and Li 2001). To minimise these unwanted side effects a number of measures can be taken. Negative side effects can be minimised by reducing the current density and duration of the applied direct current. However, this will likely reduce the quantity of analyte extracted or drug delivered. Alternative profiles have suggested maximising the desired enhanced transport effects of iontophoresis while minimising the unwanted negative effects observed on the skin.

One alternative profile tested seeks to deliver the direct current in pulses (Coston and Li 2001). That is called a pulsed DC. Selecting an appropriate duty cycle allows the skin to de-polarise in a similar way that a charged capacitor would discharge when the voltage source is removed. According to some researchers the time constant of the skin has been estimated at 2.4 ms (Coston and Li 2001). Using a signal with

frequency above 1 KHz has been suggested as a sufficient duty cycle to minimise the negative effects of the current on skin (Coston and Li 2001).

The third profile option that will be discussed is an alternating waveform. AC current has been reported to operate for up to 4 hours with no damage to the patient and increases delivery with duration of application (Howard, Drake et al. 1995). AC iontophoresis does not change the electrochemical properties of the solution surrounding the electrodes either, but in order to enhance the flux the frequency must be low (Yan, Xu et al. 2008).

The final profile that will be discussed is a switched DC profile where the polarity of the DC application is reversed periodically. This retains the advantages of DC iontophoresis, but allows the skin to depolarise. This will be the profile chosen for this project.

2.6.2. Algebraic representation of forces

The movement of molecules can also be explained algebraically. As explained by Coston and Li (Coston and Li 2001), iontophoresis transport has several components.

2.6.2.1. Passive diffusion

First mechanism, the passive diffusion, is due to the difference in the concentration in both sides of the membrane. That difference creates a gradient which makes molecules cross the membrane to equilibrate concentration of both sides. The equation that states the first mechanism is described by Fick's 1st law of diffusion:

$$J_i = -D_i \frac{dc_i}{dx}$$

Equation 13: Passive diffusion (Coston and Li 2001)

Where D_i is the diffusion coefficient, c_i is the concentration of species i and x is the distance or the diffusional path length.

Hadgraft (Hadgraft 2004) also shows a more developed equation of Fick's first law of diffusion in the context of drug delivery, which describes the diffusion of the permeant with the aid of another constant, the partition coefficient:

$$J = \frac{K \cdot D}{h}(c_{app} - c_{rec})$$

Equation 14: Passive diffusion with partition coefficient (Hadgraft 2004)

Where k is the partition coefficient of the permeant between the skin and the applied drug, D is the diffusion coefficient, h is the diffusional path length, c_{app} is the applied concentration of the permeant in the vehicle and c_{rec} is the concentration of the permeant in the receptor.

Revising the second equation it can be seen that the most important physicochemical properties are partition coefficient (K), diffusion coefficient (D) and solubility of the permeant (which is the optimum value c_{app} could reach). Hadgraft highlights some conclusion from the derived relationship and from their results. Firstly, they conclude that a high partition coefficient (K) should produce a high flow (J), however high partition coefficients are related to molecules with poor solubility (and therefore a low c_{app}), thus producing a low flow. Secondly, a high diffusion coefficient (D) is also desirable to produce a higher flow (J), but high diffusion coefficients (D) are related to small molecules and therefore less amount of drug is transported in each of them. Finally, solubility is one of the key factors. The higher the solubility the higher the permeability, but also good solubility (which means a high c_{app}) is related to low partition coefficients (K) which results in a low flow (J) (Hadgraft 2004).

The rate at which the compounds permeate the skin can be shown with the equation presented by Hadgraft (Hadgraft 2004). Morganti et al. in line with the results presented by Hadgraft also suggest that the rate of permeation is due to the concentration of permeant applied, the partition coefficient of the permeant between the stratum corneum and the vehicle and the diffusivity of the compound within the stratum corneum (Morganti, Ruocco et al. 2001).

2.6.2.2. Electromigration

The second mechanism is due to the application of an electric field. The driving force will take the molecules from one side to the other due to the force a charge experiences in the applied electric field. This is often called active diffusion, electrotransport or electromigration (Sieg, Guy et al. 2004) and together with the first mechanism (passive diffusion) constitutes the Nernst-Planck equation. In this case the particles are considered to be charged and they cross the skin under the influence of the electric field and not due to the concentration gradient alone (Coston and Li 2001). The equation representing this second mechanism is as follows:

$$J_i = -\frac{D_i z_i F c_i}{RT}\frac{d\Phi}{dx}$$

Equation 15: Electrotransport or Electromigration (Coston and Li 2001)

Where D_i is the diffusion coefficient, z_i is the charge on species i, F is the Faraday constant (96,500 C/mol), R is the gas constant (8.31 J/(mol K)), T is the absolute temperature in Kelvin, c_i is the concentration of species I, x is the distance and ϕ is the electric potential.

2.6.2.3. Electroosmotic flow

The third mechanism is often called the electroosmotic flow or convective flux. Drug ions surrounded by water molecules follow the flow of water when a transport of these occurs. The respective equation is:

$$J_i = c_i v$$

Equation 16: Electroosmotic flow (Coston and Li 2001)

Where c_i is the concentration of species i and v is the solvent velocity.

Putting all terms together the equation containing all parameters can be written as:

$$J_i = -D_i \frac{dc_i}{dx} - \frac{D_i z_i F c_i}{RT} \frac{d\Phi}{dx} + c_i v$$

Equation 17: Total flux of solute during iontophoresis

2.6.3. Electroporation

As reverse iontophoresis is the application of an electric field, electroporation and the effects of electroporation on the skin must be considered. The Nernst-Planck electrodiffusion equation (Equation 13 + Equation 15) describes the current density at low voltages near 1 V. In this situation if there are no concentration gradients the current-voltage dependence becomes linear. But at higher voltages that dependence is no longer linear and the changes that appear on the skin cannot be described with electrodiffusion but rather with electroporation (Chizmadzhev, Indenbom et al. 1998).

Skin resistance can be changed using electroporation, i.e. application of short electrical pulses to create a reversible permeabilization of the cell membrane (Chang 1989). Taking into account the existing electrical pathways in the skin (appendageal and intercellular) two electrical intervals can be found (Chizmadzhev, Indenbom et al. 1998). At low voltage levels (under 30 V) electroporation of the appendageal ducts is the main cause of the skin resistance variation. When the voltage is increased, it is the electroporation of the lipid-corneocyte matrix which has a higher and longer effect on the skin resistance. Hence new aqueous pathways are created (Pliquett, Langer et al. 1995).

Considering the different pathways existing in the skin the applied voltage will have a different effect on the appendageal pores or the intercellular paths. When a pulse voltage of 1 V is applied it creates a potential drop of approximately 250-500 mV/bilayer in the macropore duct because the epithelial cells in the macropore cause the duct to have a high current density. This is enough for electroporation of the macropore but not for the stratum corneum (Coston and Li 2001). The latter is made up of 70 to 100 layers. Therefore a voltage of 1 V will become a potential difference

of 10 mV per layer, each layer is considered as a series of resistors, which is not enough for electroporation. To get a similar effect as in the macropore, i.e. to have a 250-500 mV potential per layer the potential applied should be more than 30 V (Chizmadzhev, Indenbom et al. 1998; Hui 1998). As high voltages are required for depolarisation of stratum corneum, the duration of the chosen pulses are also very important. As voltages used for depolarisation can reach up to 100 V, pulses of short duration in the range of 1 ms are generally used (Pliquett, Langer et al. 1995).

2.7. Factors affecting transport of molecules through skin

As can be seen from the mechanisms of transport, there are several factors affecting skin permeation and hence the amount of drug that can be delivered, or molecule extracted, through the skin. These factors can be divided into exogenous and biological factors (Sieg, Guy et al. 2004) and will be discussed in turn here.

Biological factors are more related to the skin and internal composition of the skin. They include the properties of the cells membrane, the net charge of the skin, the local blood flow or the local composition of the skin including hair follicles, sebaceous glands, etc. Therefore the amount, density and ratio of each element contributing to the skin structure have an impact on its behaviour as a barrier. Ceramides, cholesterol and saturated free fatty acids act as a barrier and may alter the skin permeability, rendering it less permeable to aqueous material. On the other hand phospholipids and unsaturated fatty acids make the membrane more permeable (Morganti, Ruocco et al. 2001). Water and salt from sudoriparous and sebaceous glands also interfere in the electrical properties of the skin. Because a component of the transport mechanism is diffusional, the degree of hydration is important in the permeability. And hydration is a function of water concentration. Permeability is also influenced by the hydrophobicity and size of penetrants and presence or absence of electric charge (Morganti, Ruocco et al. 2001).

Exogenous parameters are those related to external items such as the metals, gels and currents applied. They include the current profile, the current amplitude, the duration of the current applied, the intensity of the electric field, the electrolyte composition,

the pH of the solution or gel, the drug concentration, the dose, the carrier, the properties of the drug, the physicochemical properties of the active element (Hadgraft 2004) and the duration of exposure (Coston and Li 2001; Curdy, Kalia et al. 2001; Sieg, Guy et al. 2004). It must be kept in mind that the carrier (e.g. doped gel) has to release the active principle (e.g. desired drug) and remain on the site for the time needed to fulfil its function (Morganti, Ruocco et al. 2001).

During iontophoresis there are a number of factors that can be modified to alter the transport of permeants through the skin. These factors include: concentration of permeant applied, the partition coefficient of the permeant between the stratum corneum and the vehicle and the diffusivity of the compound within the stratum corneum. The concentration of the permeant can be increased up to limits of superconcentration. This is the point where any further increase in permeant concentration will no longer result in increased skin absorption. The partition coefficient can be modified by introducing penetration enhancers in order to alter the properties of the skin barrier to allow easier molecular transport. This would increase molecular transport during passive diffusion as well as during iontophoresis. The solubility of the permeant can also be changed using solvents (Hadgraft 2004).

Costello and Jeske (Costello and Jeske 1995) in their review explain some of the influences of certain factors affecting transdermal drug delivery in the context of iontophoresis. For example, pH affects the skin charge and therefore the electroosmotic flow. It also affects the degree of ionization of organic compounds. The size of the ions is important too, those smaller are more readily to pass compared with those of bigger size and biovalent ions are more readily to bind to receptors on the walls of the pores impeding their own transit through the skin. The concentration of ions in the solution must also be considered. A sufficient concentration of ions is required for carrying charge across the skin, but if the ionic concentration is too high they will compete amongst themselves and significantly reduce the amount of drug delivered.

2.8. Membranes

The structure of skin has been discussed previously in this chapter. A useful description to consider is the definition of the skin as a "brick and mortar" structure (Michaels, Chandrasekaran et al. 1975). The brick part is due to the keratinocytes and the mortar due to the lipid bilayer (Coston and Li 2001). That definition makes a clear contrast in that the skin has some routes of transport that can be compared to artificial materials with pores of similar size and distribution.

Many studies have been carried out to obtain membranes with similar features to human skin. Many of them have been studied in the literature but they all present some limitations. Liquid membranes have a simple structure even when lipids have been incorporated, however, they do not display the heterogeneous nature of the intercellular channels. Polymeric systems including the most basics ones like silicone membranes were able to reach similar transfer rates as skin, but only when the chemical potential was dominant enough. Carbosil membranes have been used too. Tissue from animals, especially pig ear has a more similar behaviour to human skin. Also, cultured skin has been tried in an effort to find a good representation of the human skin *in vitro*. However, the best results are often reported from studies *in vivo* human and then from *in vitro* human (Hadgraft 2004).

Nevertheless the following considerations when using membranes must be considered:

- Advantages of use of artificial membranes:
    - Provide a good means of repeatable experiments.
    - Are more reproducible than human skin.
    - The use of the membrane does not need to be ethically approved.
    - Artificial membranes can approximate the physicochemical properties of the skin due to the mechanical structure with size of pores, distribution and thickness of the membrane.

- Disadvantages of use of artificial membranes:
    - *In vitro* experiments should be considered a previous form of experiment to *in vivo* experiments and the results cannot be the basis of the *in vivo* part.
    - Artificial membranes cannot represent the actual anatomical, biological or physiological properties of the skin.

Chapter 3: Methodology

This chapter describes the materials and procedures used in this project.

3.1. *In vitro* vs. *In vivo*

Choosing the right materials to carry on an experiment is not always a straightforward issue. In particular, when multiple experiments need to be accomplished there are often limitations in the availability of materials. As has been discussed, human skin *in vivo* shows a high degree of variation due to factors including, age, gender, ethnic origin and environmental factors. One of the aims of this project is to construct an appropriate *in vitro* arrangement to mimic an existing *in vivo* data set. A key component to the in vitro arrangement is the choice of membrane used as a substitute for human skin.

For the purpose of this project *in vivo* skin from human is not feasible and a simple dialysis membrane has been chosen. It is a cost-effective solution which allows repeatability as well as a good approximation to the intercellular channels. The following diagram shows the parts and order of the *in vitro* cell chamber:

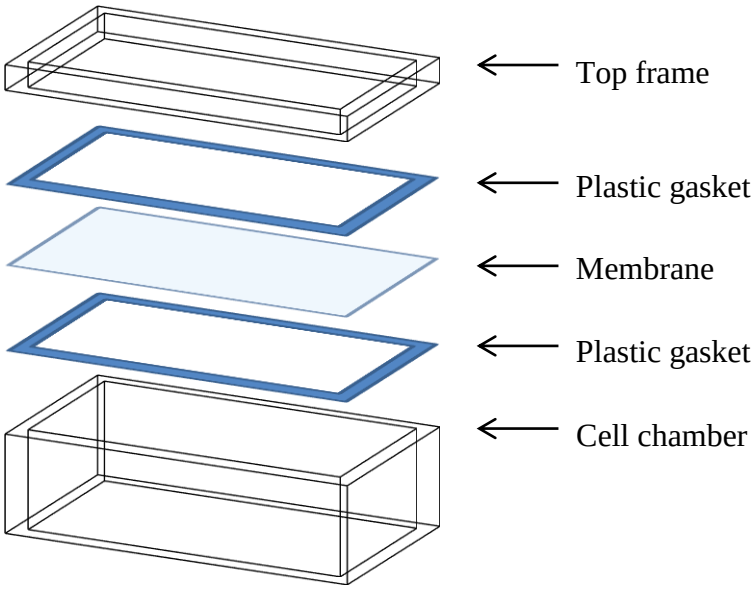

Figure 10: Diagram of the In vitro cell preparation

3.2. *In vitro* study

In order to carry out the *in vitro* experiments a complete list of materials is needed before the experiments are started and they need to be prepared. The complete set of materials with manufacturer and model can be checked in Appendix A.

A total amount of 26 *in vitro* experiments were completed. Each *in vitro* experiment was a replicate, i.e., for each experiment the in vitro cell was fixed with a cell buffer concentration of 5 mM glucose and 4 mM potassium to mimic the concentrations expected in healthy individuals under fasting conditions. Due to the process chosen using replicates an uncertainty is introduced. Steps were taken to minimise uncertainties using the same membrane and same gel. Time of extraction by reverse iontophoresis was then varied. The following table (Table 6) shows the number of experiments performed for each extraction time chosen.

Extraction Time (m)	**Number of experiments**
2 (fixed RI polarity)	4
5 (fixed RI polarity)	4
10 (fixed RI polarity)	4
15 (fixed RI polarity)	4
30 (switching the RI polarity every 15 minutes)	3
30 (fixed RI polarity)	3
60 (switching the RI polarity every 15 minutes)	4
Total	26 experiments

Table 6: Number of in vitro experiments for each RI extraction time

Each experiment included a process of:

- Application of reverse iontophoresis
- Impedance measurement before and after the RI application
- Collection of the gel from the electrodes
- Potassium measurement from the gel
- Glucose measurement from the gel

Three electrodes were used. Electrode 1 and electrode 2 were used as a pair for reverse iontophoresis. When the polarity was not switched, electrode 1 was the anode and electrode 2 was the cathode. When the polarity was switched, electrode 1 would

start as the anode (and electrode 2 as the cathode) and then switch to give the opposite case i.e. electrode 1 would switch to become the cathode and electrode 2 would switch to become the anode. In all cases electrode 3 was the diffusion chamber and did not have any electric field applied to it.

3.2.1. Preparation of materials for experiments

Each of the steps in the project includes the preparation of the materials according to given procedures. A brief description of each of them is presented next and the list of materials used in each of them as well as the description of the methods can be found in Appendix B.

In vitro cell

The *in vitro* cell is the chamber which contains the solution that simulates the interstitial fluid. It holds the membrane between two plastic gaskets and keeps it in contact with the solution in the internal side as it was shown if Figure 10. The electrodes filled with gel are stuck on the external side. This *in vitro* cell was designed within the department.

Membrane

The membrane used to simulate the epidermis is a dialysis type one. Dialysis membranes are permselective; they are designed to simulate the filtering effect of the kidneys and allow ions and small molecules to go through their pores. It is sold in a tube–like shape and has to be kept refrigerated in preservative solution, sodium azide, which is rinsed off before use. For the purpose of this experiment one of the edges of the tube is cut and the membrane unfolded to give a rectangular plane. This is then placed on the *in vitro* cell to keep it in contact with the solution only on one of the sides allowing the other side to be accessible for placement of the electrodes.

HEPES buffer

The HEPES buffer simulates the interstitial fluid. It must therefore have a similar pH and concentration of solutes (Sodium, Chloride, Potassium, Glucose…). For the

experiments under study the amount of sodium, chloride, glucose and potassium will be fixed. For the calculation of the quantity of the solutes please refer to Appendix D.

Electrodes

Electrodes are used to interconnect a device with a surface and drive a current through it, which in this case it is the membrane. They attract ions and charged molecules to them. Anions are attracted to the anode and cations to the cathode. The electrodes are custom made and can have any desirable shape. For the experiments under test only one contact (track) is necessary. The chosen design is shown in Figure 11:

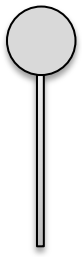

Figure 11: Shape of electrode

Phosphate Buffer

A buffer solution capable of keeping pH at a constant value is necessary to prepare gels or dilute them so, for example, the ion selective electrode can measure the quantity of ions in the given solution. An aqueous solution can be more accurately measured than a more viscous solution. Phosphate buffer solution has been chosen for the experiments in this project.

Hydrogel

The gel is used to keep the electrodes in contact with the membrane in the *in vitro* experiments or the skin in the *in vivo* experiments. Due to the conducting nature of the gel it helps in the movements of electrons as well as in the movement of ions and charged molecules. Extracted ions and molecules through the membrane will be captured into the gel which can be used later to measure the quantity of them.

3.2.2. Preparation of materials for measurements and calibration

Reverse Iontophoresis Device

For the reverse iontophoresis procedure a device was designed by staff in the department. The device can be configured so as to work for a finite period of time or switch direction of current between electrodes every given time.

The device will be set with direct current for experiments lasting 2, 5, 10, 15 and 30 minutes. For another set of experiments the device will be programmed for extractions lasting 30 and 60 minutes with switching polarity every 15 minutes.

1260/1294 Impedance Interface

The impedance interface is used to measure the impedance of the material under test. In *in vivo* experiments it is necessary to comply with safety rules such as electrical isolation and current limitation. In case of *in vitro* experiments such rules would not be necessary, however, in order to obtain a good comparison of results *in vivo* vs. *in vitro* the same devices and configurations will be used. As the Human interface inserts some extra noise in the system and reduces the accuracy range some tests without Human interface will be performed as well. All those tests will show the differences in results.

The differences of accuracy using 1260 interface by itself (left) and using the 1294 human interface (right) are shown in the following figure (Figure 12):

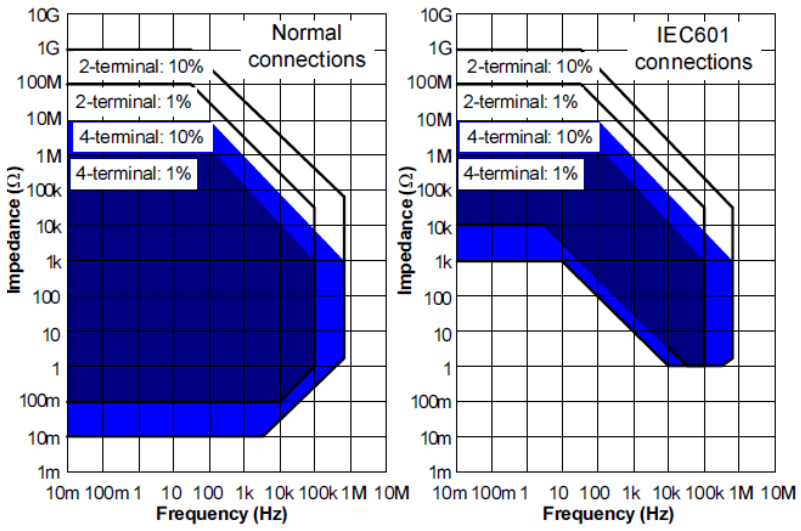

Figure 12: 1294 Typical Measurement Accuracy (Solartron 2011)

Potassium Flow Plus Ion Selective Electrode (ISE)

The potassium flow plus ion selective electrode is a special electrode sensitive to potassium ions. Although it has been made to measure potassium it must be noted than some other ions can interfere in the measurements.

In order to get the most accurate values a calibration must be performed every time it is used. The range of the concentrations chosen depends either on the range of the sensor as well as the range of the expected measurements.

Enzyme Assay Kit

The glucose extracted in the gels can be measured as well using a colorimetric assay. For the correct functioning of the device an enzyme assay kit with 96-well plates has to be used. That is possible because glucose is oxidised by the application of an enzyme reagent, which changes the colour of the sample. The stronger the colour is, the more glucose there is in the sample. After having applied the enzyme to the samples, the device incubates the samples and then scans the samples at a chosen wavelength that corresponds to the peak wavelength of the colour. In this case this is 490 nm. In this case the device used is a Labsystem Multiskan Ascent and is controlled using software from an attached computer. For the correct calculation of glucose concentration a glucose standard has to be used in each plate. Although for the results in this study it was not followed the procedure strictly. A plate with just calibration standard was read, and then the standard was used in the first and third plate. Because all of the samples were measured the same day and using the same calibration standard gel an average of the values was used for the second plate.

Phosphate buffer with 10 mM KCl

Prior to every use the ion selective electrode has to be calibrated within a range. This calibration is useful to get a linear relationship between the concentration measured and the voltage obtained. The range chosen should cover the concentrations measured. If values are outside the range or within a very narrow spectrum of that range, a new calibration should be performed. To learn how to prepare the range of solutions, please refer to Appendix E.

The solutions used should have the same consistency as the samples to be measured. For the experiments of concern 1 part of gel and 9 parts of solutions have to be mixed.

3.2.3. Experimental arrangement and procedure for the *in vitro* experiments

Before beginning the experimental procedure all materials, electrodes, gels and solutions were prepared according the relevant procedures described in Appendix B. First, electrodes were made. Hydrogel was prepared and stored in a syringe between 2 and 8 degrees Celsius. The gel was used within one month of preparation. HEPES solution and phosphate buffer solution were prepared. The HEPES buffer was modified to reflect physiological concentrations of fasting blood potassium and glucose by dissolving 4 mM KCl and 5 mM glucose in the HEPES buffer. The solutions were stored between 2 and 8 degrees Celsius and were used within one week of preparation. The *in vitro* cell was constructed mounting the membrane across the upper face of the donor solution chamber. It is important to making sure the membrane is tense and screws are tight to prevent leaking. One side of the membrane tube was cut, unfolded and rinsed with deionised water before mounting it in the diffusion cell. After filling the donor solution chamber with the prepared HEPES buffer, all 3 electrodes are covered with 300 μg of hydrogel. For increased accuracy, the electrodes were placed on a weigh scale and an Eppendorf multipipette was used to dispense the gel form the syringe. The electrodes were then connected to their cables and a multimeter was used to ensure good electrical connection. Any exposed conductive track of the electrode was covered with electrical insulation tape avoid an undesired short circuit. Finally the liners of the electrodes were removed to expose the adhesive surface and the electrodes were then secured to the membrane. Additional tape was sued to further secure the electrodes and cables in place.

After fixing the electrodes to the membrane, impedance measurements were taken before the application of reverse iontophoresis. The impedance is measured with the 1260 impedance interface, which must be turned on and configured. A frequency scan from 1 Hz to 1 MHz, (voltage: 200 mV) was measure between the following

electrode pair combinations: 1-2, 1-3, 2-3 to make sure impedances between all electrodes was recorded. Following the initial impedance measurements, reverse iontophoresis was performed using the reverse iontophoresis device, which was programmed in advance to give the desired current output, duration and polarity profile for the given experiment. After the reverse iontophoresis step the impedance is measured again as before.

The next step in the experiment was the collection of gel from electrodes. To achieve this, 50 µl of gel was collected and stored in 7 ml bijou tubes using the multipipette. The tubes containing the gel samples were labelled and frozen for later analysis.

The samples were prepared by adding 450 µl of phosphate buffer to each of the 50 µl gel samples. The diluted samples were then mixed using a vortex mixer and kept in fridge overnight in order to allow the sample to become homogeneous. For the measurement of potassium it is first necessary to prepare a standard gel calibration set with known concentrations. The initial buffer standards used for calibration of the potassium ISE are prepared as explained in Appendix E and kept in 25 ml tubes. Each of those buffer standards were then used to prepare the gel for calibration adding 500 µl of hydrogel and 4500 µl of solution into 7 ml tubes. The resulting gel calibration standards were mixed and left in the fridge overnight to allow the sample to become homogeneous.

In the experiments performed a first range was chosen from 0.001 to 10 mM (0.001, 0.005, 0.01, 0.05, 0.1, 0.5, 1, 5, 10 mM). However, after having analysed the first set of samples it was observed that all of them lay within a very short range (between 0.04 and 0.22 mM) therefore a new calibration standard was designed to gain precision.

The second range chosen extended from 0.001 to 0.2 mM (0.001, 0.002, 0.004, 0.006, 0.01, 0.03, 0.05, 0.07, 0.1, 0.2 mM) and the standards below 0.01 were only used to stabilise the sensor and were discarded to calculate the calibration curve.

The final calibration curves ranged from 0.01 to 0.2 mM. With that range all of them achieved a coefficient of correlation above 95%. Details of this are given in Appendix F.

With the standards prepared, the ISE electrode was used to establish a calibration curve. To achieve this, the electrode was immersed into each calibration solution for 5 minutes to allow the voltage to stabilise and then recorded. Immediately after the calibration process has been finished the samples were measured in the same way, keeping the electrode into the solution for 5 minutes and recording the voltage displayed.

The samples were returned to the freezer for future repetitions of the measurements or to be analysed for glucose content.

To analyse the gels for glucose content, another calibration standard set was prepared. The standard chosen for glucose calibration was made up of 8 samples of gel containing a known quantity of glucose (0, 1.125, 2.225, 4.5, 9, 18, 45 and 450 μM glucose). However, after having read all the unknown concentration it was observed that the values lay within a short range, therefore the 2 highest values and the smallest one were discarded because they fell outside the range of interest. The calibration curves used for the calculation of glucose concentration in the samples are shown in Appendix G.

Once the glucose calibration standards are available, 80 μl of each calibration solution was added to 3 wells of a 96-well plate. Each prepared extraction sample was also pippetted into 3 wells of the 96-well plate. Glucose oxidase enzyme (GlucoPAP, RANDOX) was then added to each well of the plate. The plate was incubated at 37 degrees Celsius for 90 minutes and then an absorption reading was taken at 490nM using the Labsystem Multiskan Ascent.

3.3. *In vivo* study

The data set from *in vivo* experiments (gathered from healthy participants under ethics) was provided and no *in vivo* experiments were carried out. However, the list of materials, their preparation and the experimental arrangement and procedure are detailed in Appendix C.

3.4. Analysis of the data

Potassium and glucose results can be calculated using a simple regression analysis from the calibration curves obtained and statistical analysis.

However, impedance results need further analysis and some assumptions in order to get the correct values of the series and parallel part of the circuit.

3.4.1. Calculation of the components of the equivalent circuit

As it was shown in Section 2.4:

$$R_s = R_\infty$$

Equation 18: Value of R_s

$$R_p = R_0 - R_\infty$$

Equation 19: Value of R_p

$$Z'' = j\frac{\omega R_p^2 C}{1 + \omega^2 R_p^2 C^2}$$

Equation 20: Value of Z''

C can be isolated resulting in a second order equation:

$$Z''\omega^2 R_p^2 C^2 + j\omega R_p^2 C + Z'' = 0$$

Equation 21: Second order equation for C value

Assuming that R_p is much greater than Z'' the solution can be simplified to:

$$C = \frac{1}{2\pi f Z''}$$

Equation 22: Formula used for the calculation of C

Please, refer to Appendix M for the proof of the simplification.

C should have the same value for every frequency, however, its value varies among frequencies, thus it has been calculated averaging the results using the valid range of frequencies (100, 1000, 10000, 100000 Hz).

3.4.2. Statistical analysis

In order to determine the significance of any differences in data from potassium a statistical analysis of the values was performed. That analysis is of special relevance within the first 4 sets of data (2, 5, 10 and 15 minutes) for potassium concentration where the averages seem to be similar as it will be shown in next chapter.

A two sample t-Test for the difference between means method has been chosen to accept or reject such differences. Data from the sample must satisfy several conditions:

1. Samples of less than 30 must be taken from normally distributed populations.
2. The samples must be randomly selected.
3. The samples must be independent.
4. Each population must have a normal distribution.

Once the conditions are met, the standardized test statistic is:

$$t = \frac{(\bar{x}_1 - \bar{x}_2) - (\mu_1 - \mu_2)}{\sigma_{\bar{x}_1 - \bar{x}_2}}$$

Equation 23: Standardized test statistic

Where $\sigma_{\bar{x}_1 - \bar{x}_2} = \sqrt{\frac{s_1^2}{n_1} + \frac{s_2^2}{n_2}}$ and the degree of freedom is the smaller of n_1-1 or n_2-1 if variances are not equal as it will be the case.

The steps to follow to complete the test with a level of significance of 95% are:

1. State the claim mathematically identifying the null and the alternative hypotheses (H_0 and H_a).
2. Specify the level of significance (95%).
3. Identify the degrees of freedom (the smaller of n_1-1 or n_2-1).

4. Determine the critical value using a t-Table.
5. Determine the rejection regions.
6. Find the standardized test statistics using Equation 23.
7. Make a decision to reject or fail to reject the null hypothesis (if t is in the rejection region, reject H_0, otherwise, fail to reject H_0).
8. Interpret the decision in the context of the original claim.

The statistical analysis will be carried out with the help of statistical software (Minitab).

Chapter 4: Results

4.1. *In vitro* results and analysis

4.1.1. Potassium results

Potassium values are not a direct result from the potassium ion selective electrode. The results are given in mV and have to be converted into concentration (mM). In order to get that relationship a calibration curve is needed to convert from mV to mM. The calibration curves used for potassium can be seen in Appendix F.

A summary of the quantity of potassium extracted into each of the electrode chambers for various duration of reverse iontophoresis (RI) extraction, *in vitro*, are shown in Figure 13. The data shown represents the means of 4 experiments for 2, 5, 10, 15 and 60 minutes cases (3 in the case of 30 minutes) and the error bars denote the standard error of the mean.

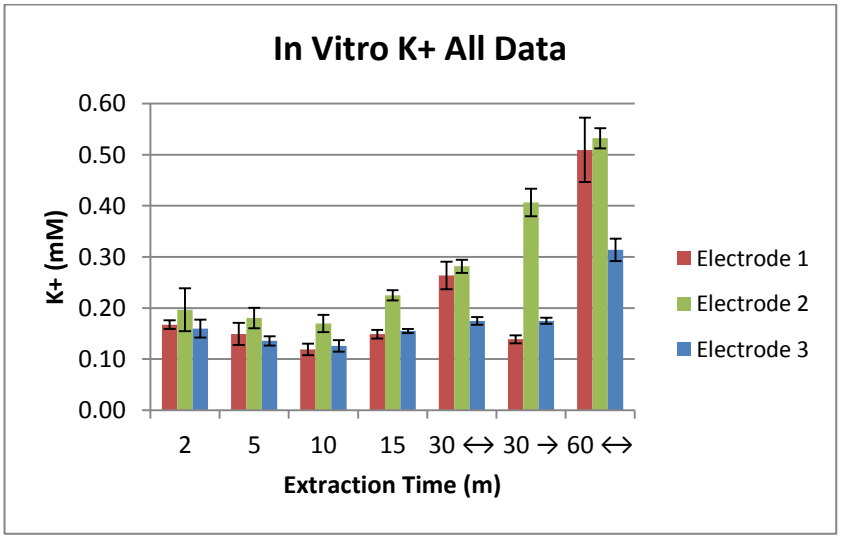

Figure 13: In vitro results of potassium using all data

Where 2, 5, 10, 15 and 30→ stand for experiments of 2, 5, 10, 15 and 30 minutes of Reverse Iontophoresis (RI) extraction in which the polarity was maintained in the same direction and 30 ↔ and 60 ↔ stand for experiments of 30 and 60 minutes RI extraction in which the polarity was reversed every 15 minutes.

At first glance, Figure 13 appears to show a decrease in the amount of potassium extracted with increasing extraction for the first experiments over the 2 minute, 5 minute and 10 minute. This result would be unexpected. However, to investigate this, a statistical analysis was performed to compare all pair of experiments. The chosen analysis was the 2 sample t-test analysis performed with a 95% confidence interval. The values obtained for the p-value are shown in Table 7.

	Pair of experiments	**95% confidence interval P-value**
Electrode 1	2,5	0.496
	2,10	0.018
	2,15	0.185
	5,10	0.281
	5,15	0.986
	10,15	0.087
Electrode 2	2,5	0.747
	2,10	0.594
	2,15	0.558
	5,10	0.696
	5,15	0.116
	10,15	0.047
Electrode 3	2,5	0.288
	2,10	0.164
	2,15	0.806
	5,10	0.522
	5,15	0.121
	10,15	0.092

Table 7: P-value at 95% CI of in vitro potassium analysis

For all cases where the p-value is above 0.05 there is no statistical difference between the means of the experiments compared. Table shows 2 cases in which p-value is below 0.05. This would indicate that the statistical difference is significant, however with a very small sample of n = 4, the statistical power behind this test is not enough to reject any experiment.

Despite the visual trend which seems to show a decreasing concentration extracted with increasing extraction time, the statistical analysis shows that there is not a significant difference between the extraction concentrations between 2 and 15 minutes.

From 15 minutes of extraction time upwards, the potassium extracted increases with increasing extraction time. This result is what would be expected.

The first 3 experiments of 2, 5, 10 and 15 minutes of duration were the first 12 experiments performed. There were practical difficulties encountered when performing the *in vitro* experiments, which resulted in the experiment taking longer than desired and the electrode well remaining on the membrane longer than desired. This was particularly true during the learning phase of the *in vitro* experiments. A fourth repetition of the 2, 5, 10 and 15 minute extraction times were performed when the *in vitro* experiment had been well practiced.

Experiments 1, 2 and 3 of duration 2, 5, 10 and 15 minutes were considered part of the learning process, and although they are considered for the results, it must be noticed that the error introduced for those durations is higher than for the other experiments.

Having a look at experiments 1, 2 and 3 of 2, 5, 10 and 15 minutes (in Figure 14, Figure 16 and Figure 18) and comparing them with experiment 4 of the same durations (in Figure 15, Figure 17 and Figure 19) some observations can be made.

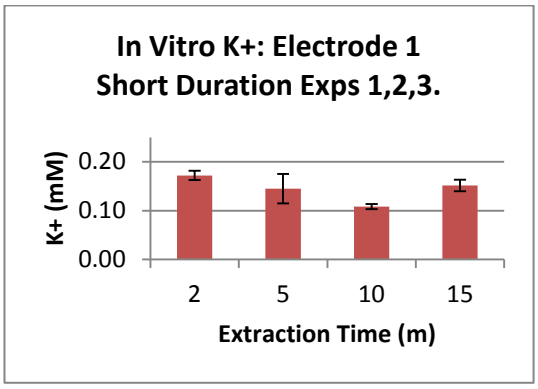

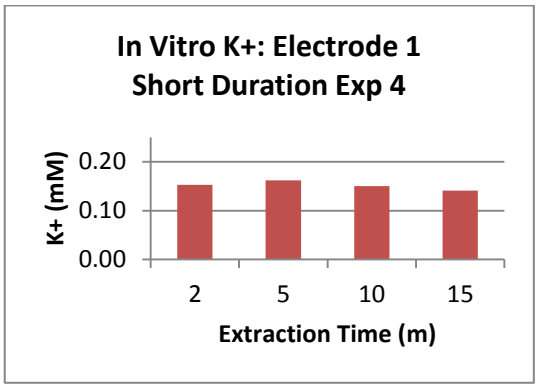

Figure 14: K^+ electrode 1 exp. 1, 2, 3

Figure 15: K^+ electrode 1 exp 4

Electrode 1 for experiments 1, 2 and 3 clearly shows that the experiment of 2 minutes of duration has a higher concentration (0.17 mM) than 5 (0.15 mM) and 10 (0.12 mM) minutes ones. This is unexpected.

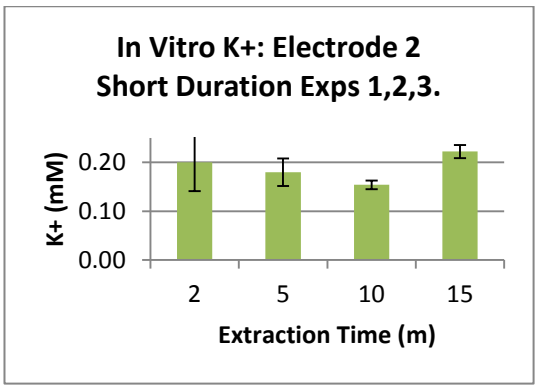

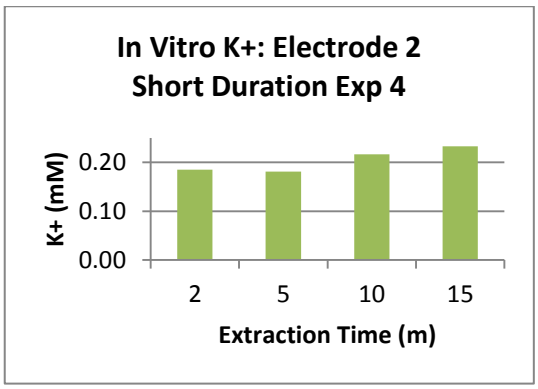

Figure 16: K^+ electrode 2 exps 1, 2, 3

Figure 17: K^+ electrode 2 exp 4

Again, electrode 2 in experiments 1, 2 and 3 shows that 2 minutes experiment (0.20 mM) has a higher concentration than 5 (0.18 mM) or 10 (0.17 mM) minutes experiments. While in experiment 4 the rise of potassium extracted with time is clearly visible.

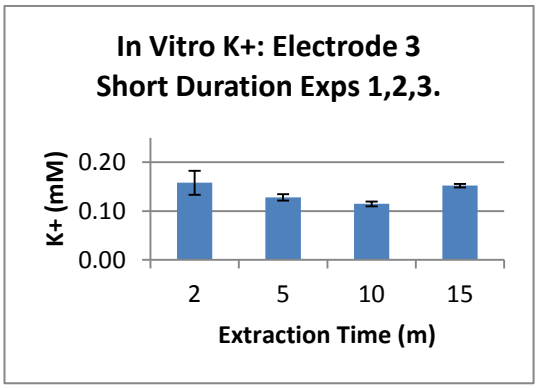

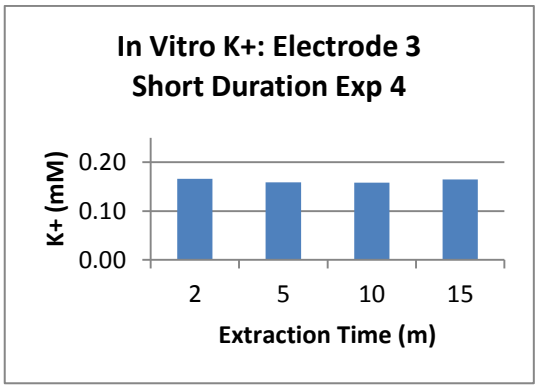

Figure 18: K^+ electrode 3 exps 1, 2, 3

Figure 19: K^+ electrode 3 exp 4

In experiments 1, 2 and 3, as duration of experiment increases the potassium concentration measured in the samples seems to go down except for 15 minutes of duration. If the error bars are considered, it can be deduced that they could produce the same output. For experiment 4 the output in electrode 3 remains constant.

For the results the experiments and times used are shown in Table 8:

Extraction times (minutes)	**Experiment Number**
2→	1, 2, 3, 4
5→	1, 2, 3, 4
10→	1, 2, 3, 4
15→	1, 2, 3, 4
30↔	1, 2, 3
30→	1, 2, 3
60→	1, 2, 3, 4

Table 8: Experiments used of each extraction time for the final results of in vitro potassium concentration

The graphs for each electrode are shown in Figure 20, Figure 21 and Figure 22.

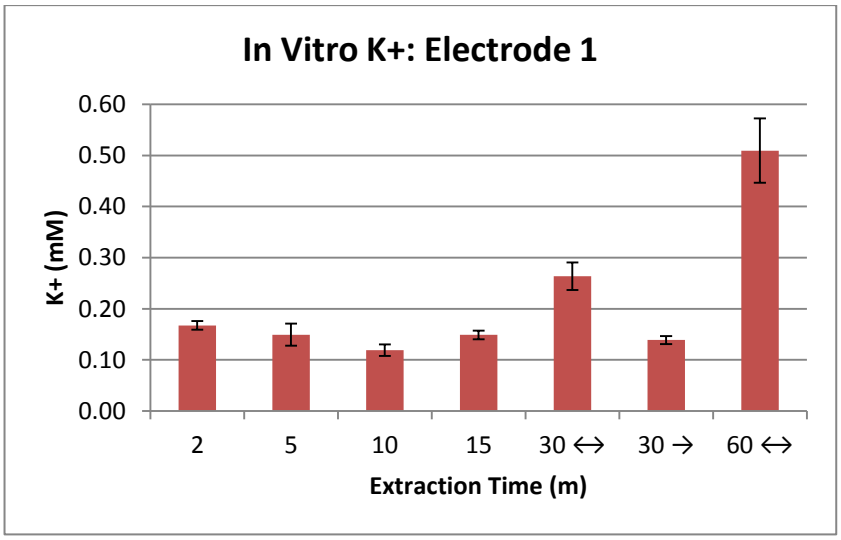

Figure 20: Potassium concentration for electrode 1

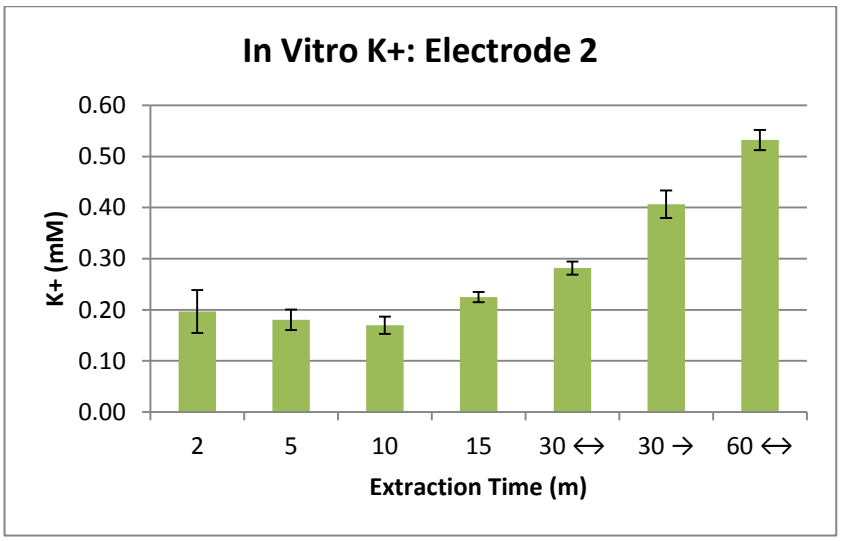

Figure 21: Potassium concentration for electrode 2

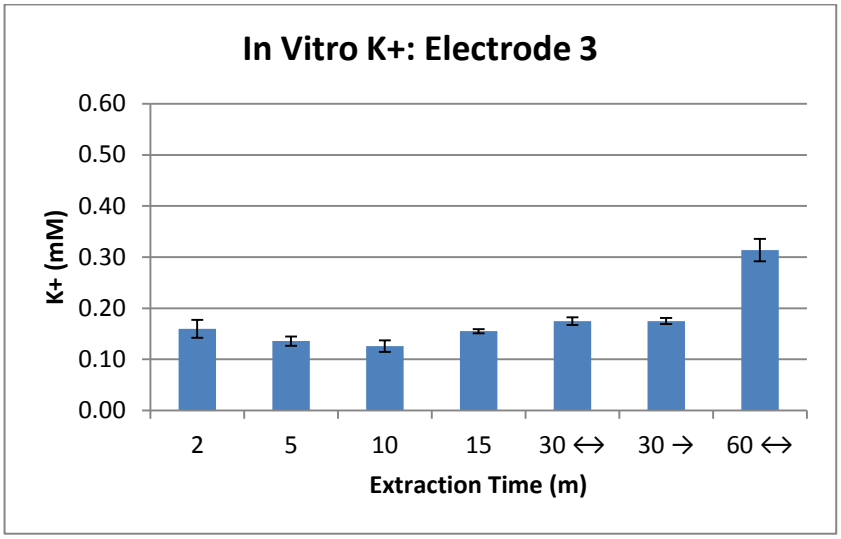

Figure 22: Potassium concentration for electrode 3

Plotting the potassium extraction results for the *in vitro* experiments again in Figure 23 some more observations can be written:

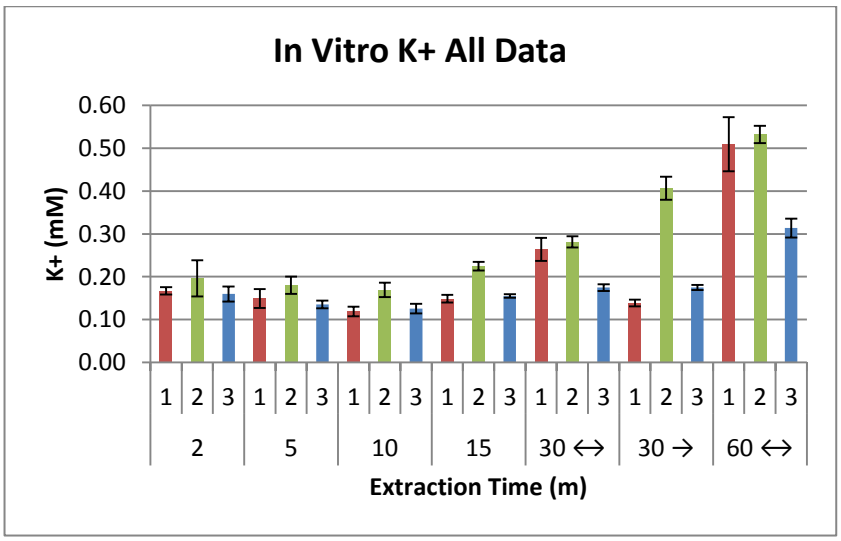

Figure 23: In vitro results of potassium

Comparing all electrodes and experiments it can be noticed that:

Experiments 2, 5 and 10 minutes do not show a significant difference in potassium extracted. The potassium concentration recorded at electrode 2 was 0.18, 0.18 and 0.22 mM for experiments 2, 5 and 10 minutes respectively. From 15 minutes of extraction upwards, there is an evident increase in the potassium concentration extracted with increasing extraction time in electrode 2. The potassium concentration rises from 0.23 to 0.53 mM. A significant increase in potassium extraction into the electrode 1 chamber is only observed when the polarity is switched causing electrode one to become negatively charged. It doubles its value from 30→ to 30↔ and from 30↔ to 60↔. A significant increase in potassium is only observed in electrode 3 after 60 minutes of diffusion, where it increases from an average of 0.16 to 0.31 mM.

In all fixed polarity experiments, electrode 2 attracts a higher concentration of potassium than electrodes 1 and 3 for a fixed time period. During experiments where the polarity is reversed for half of the total time (30 ↔ and 60 ↔) the concentration of potassium found in electrodes 1 and 2 are approximately equal, 0.26 mM and 0.28 mM for the 30 minutes experiment and 0.51 mM and 0.53 mM for 60 minutes experiment.

For electrode 2 a mathematical model was calculated as shown in Figure 24. It must be noticed that the value for 30 minutes performed with the same polarity all the time

has been placed at 45 minutes. It was chosen like that because it was considered that electrode 2 in experiment 30→ had received twice the effects of the electromigration due to RI than experiment 30↔ and also had undergone the same effects due to passive diffusion as experiment 30↔.

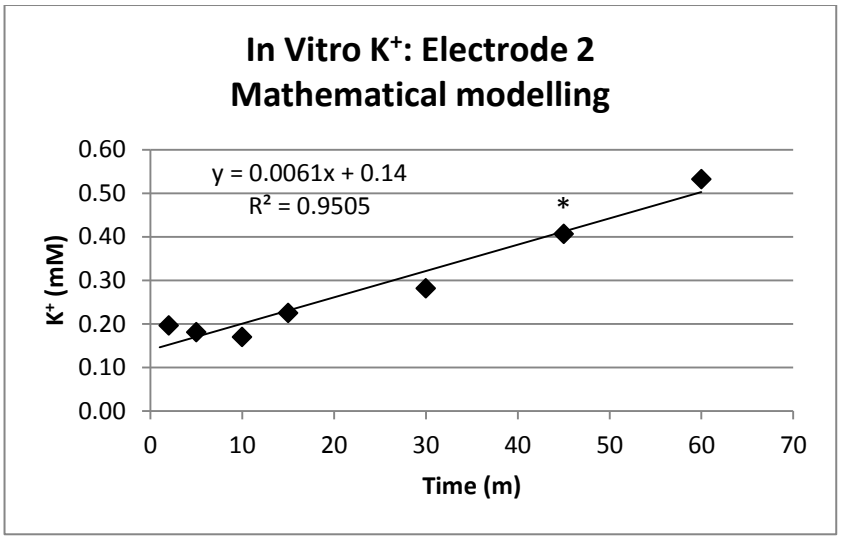

Figure 24: Mathematical modelling of in vitro K^+ electrode 2

* Note that there was no experiment performed at 45 minutes. The data showed belongs to the 30 minutes experiment and has been placed at 45 minutes according to the reasons given above.

The equation shown in Figure 24:

$$y = 0.0061x + 0.14$$

Equation 24: Regression curve for potassium concentration in electrode 2

This is a linear regression line for the potassium concentration and fits with a correlation coefficient of 95%. Where x is the time in minutes and y is the potassium concentration in mM. This demonstrates that the extraction of potassium by reverse iontophoresis is predictable *in vitro.*

The results in Figure 25 appear to trace a slight curve which could be modelled with a polynomial regression curve; however, the coefficient factor (98.74%) does not

represent such improvement as to discard the linear regression line shown in Figure 24 with a regression factor of 95%, but may be worth considering in future analysis.

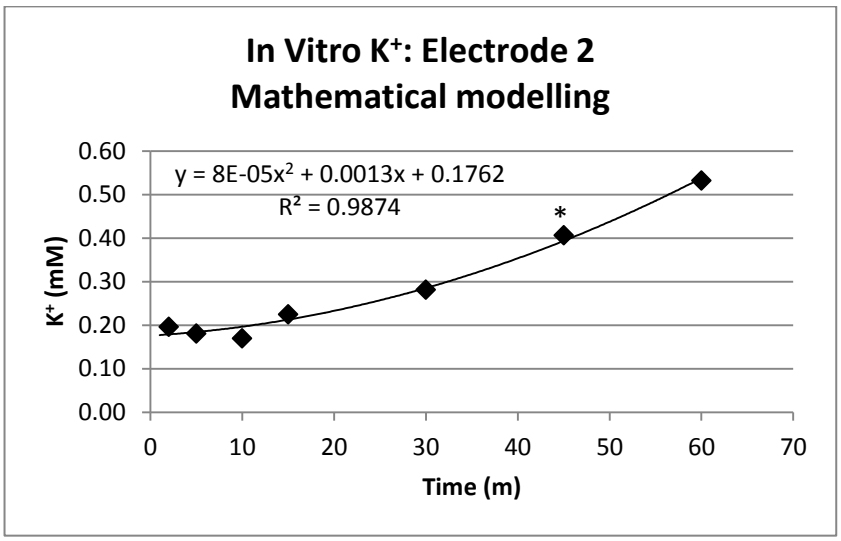

Figure 25: Mathematical modelling of potassium extraction with polynomial regression line

* Note that there was no experiment performed at 45 minutes. The data showed belongs to the 30 minutes experiment and has been placed at 45 minutes according to the reasons given above.

In summary, the quantity of potassium extracted in to the electrode chamber depends on polarity of electrode and duration of reverse iontophoresis (RI) of extraction. The behaviour of this extraction can also be modelled by an exponential function. However, a linear relationship may be an adequate approximation.

4.1.2. Glucose results

The gels samples for the *in vitro* experiments were also analysed to determine the concentration of glucose in each sample. As well as in the potassium case glucose values were not given in μM directly from the enzyme assay kit. Those results were given in absorbance units and then they had to be converted into concentration using several calibration curves.

The calibration curves used for this analysis can be seen in Appendix G. The glucose concentration results are summarised in Figure 26 where the error bars shown denote the standard error of the mean.

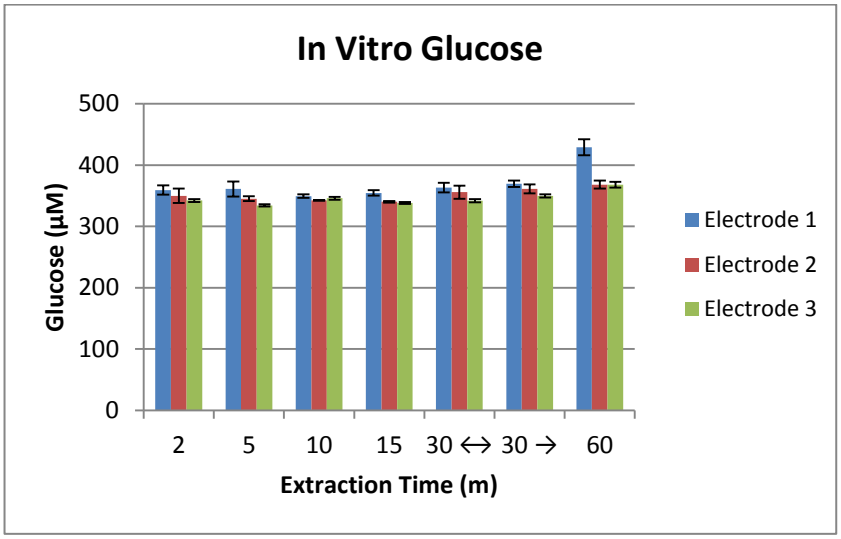

Figure 26: In vitro results of glucose

Looking at each individual experiment they all follow the same pattern. Electrode 1 collected the highest amount of glucose and electrode 3 the lowest, with a maximum difference of 17% in the 5 minutes experiment.

A detailed view of each of the electrodes separately is shown in Figure 27, Figure 28 and Figure 29.

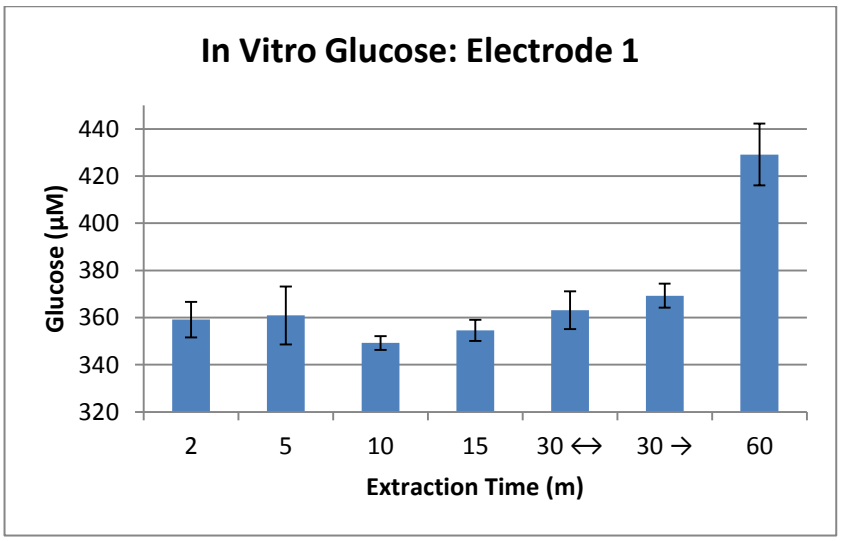

Figure 27: Glucose concentration in electrode 1

For electrode 1, the differences in concentration between experiments are largely inconsistent across the experiments in 2, 5 and 10 minutes. However, from 15 minutes upwards, there is a progressive increase in the amount of glucose extracted into the electrode chamber with increase in extraction time. Where the quantity of glucose extracted rose from 342 µM after 15 minutes to 429 µM after 60 minutes RI.

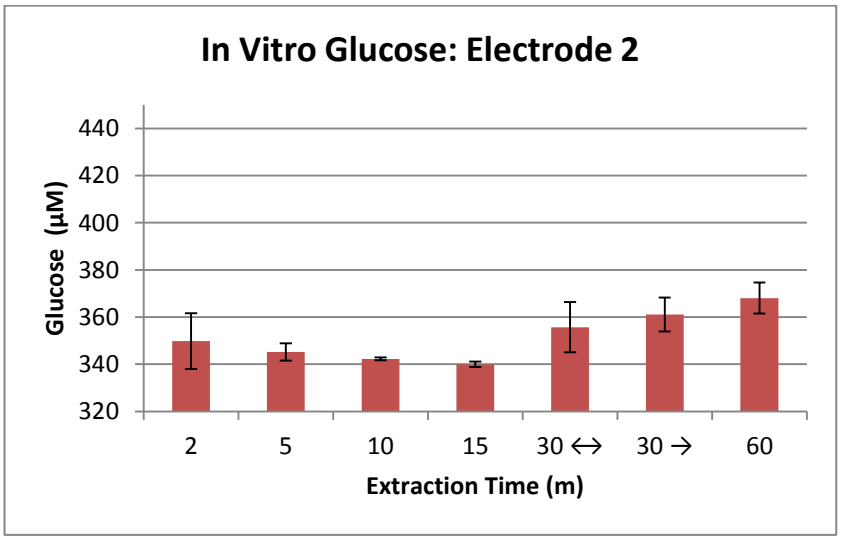

Figure 28: Glucose concentration in electrode 2

Electrode 2 shows a similar behaviour to electrode 1. From 30 minutes upwards there is an increase in glucose concentration extracted rising from 356 to 368 µM, although in this case error bars make the real value to lie within the same range.

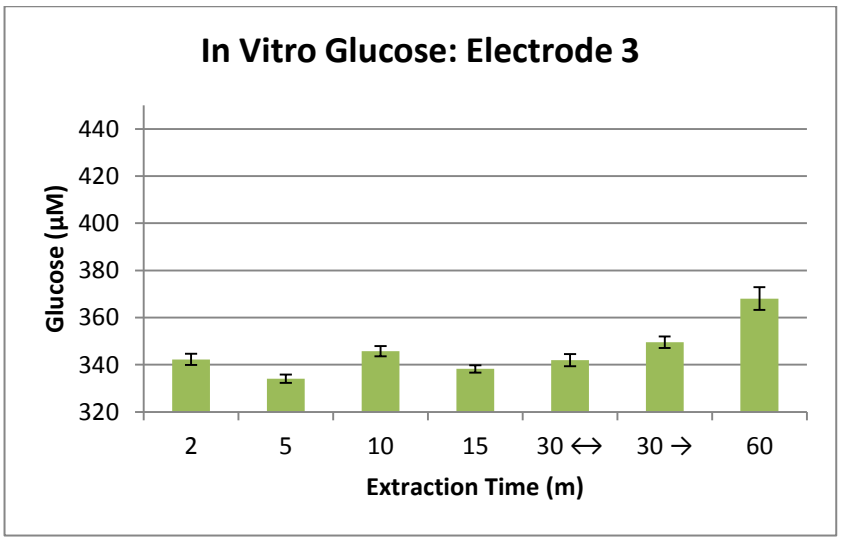

Figure 29: Glucose concentration in electrode 3

Finally, the 3rd electrode shows again the same behaviour as electrode 1 and 2, although in this case error bars do not overlap. In 15 minutes experiment the glucose measured was 339 µM what raised up to 368 µM in experiment 60 minutes.

4.1.3. Impedance results

Impedance data was measured under different circumstances. During the initial *in vitro* experiments the human interface 1294 was used as it was used for the *in vivo* experiment. However, the impedance measurements from the *in vitro* cell were found to fall out with the recommended range of the Solartron 1294 as discussed in section 3.2.1. Therefore, the *in vitro* experiments were then carried out using the Solartron 1260 stand alone. On a limited number of occasions impedance measurements were not recorded. Appendix H shows the impact of using the Solartron 1294 instead of the Solartron 1260. A table with a detailed list of all experiments and their circumstances is shown in Appendix I. For every extraction time, experiments have been performed using the Solartron 1260 stand alone. Therefore, only data where *in vitro* cell was directly connected to the Solartron 1260 analyser will be used for analysis and discussion.

4.1.3.1. Comparison of impedances before and after the application of reverse iontophoresis (Electrode 1 and 2)

It has been observed that the application of reverse iontophoresis (RI) causes a change in measured impedance across the artificial skin membrane. The following graphs (Figure 30) and table (Table 9) show an example of this variation in impedance in response to RI. The example given is the impedance data for 15 minutes of RI between electrodes 1 and 2 and is representative of the trend observed for all durations of RI.

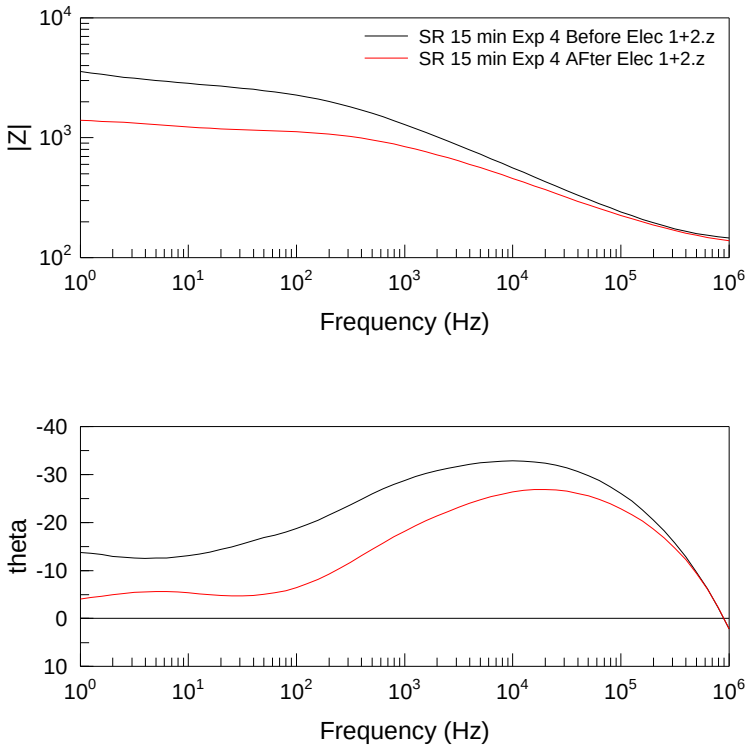

Figure 30: Bode plot and phase plot showing impedance measurements in an in vitro experiment before and after 15 minutes of RI

	Magnitude (Ω)						
Freq (Hz)	**1**	**10**	**100**	**1000**	**10000**	**100000**	**1000000**
E 1,2 Before	3569	2844	2266	1292	562	241	146
E 1,2 After	1401	1231	1121	845	459	226	139
Difference	2168	1613	1145	347	103	15	7

Table 9: Magnitude values for the same pair of electrodes in an in vitro experiment before and after applying 15 minutes of RI

It is clear from these results that the application of reverse iontophoresis (RI) causes a significant decrease in measured impedance. At very low frequencies the impedance values measured after applying RI are 40% of the value measured before the application of RI. However at high frequencies the difference in impedance before and after RI is much less significant with the value after RI remaining at 95% of the value before RI.

The same data is represented in a complex plane plot. Again, the difference in impedance values before and after RI is grater at lower frequencies that at higher frequencies.

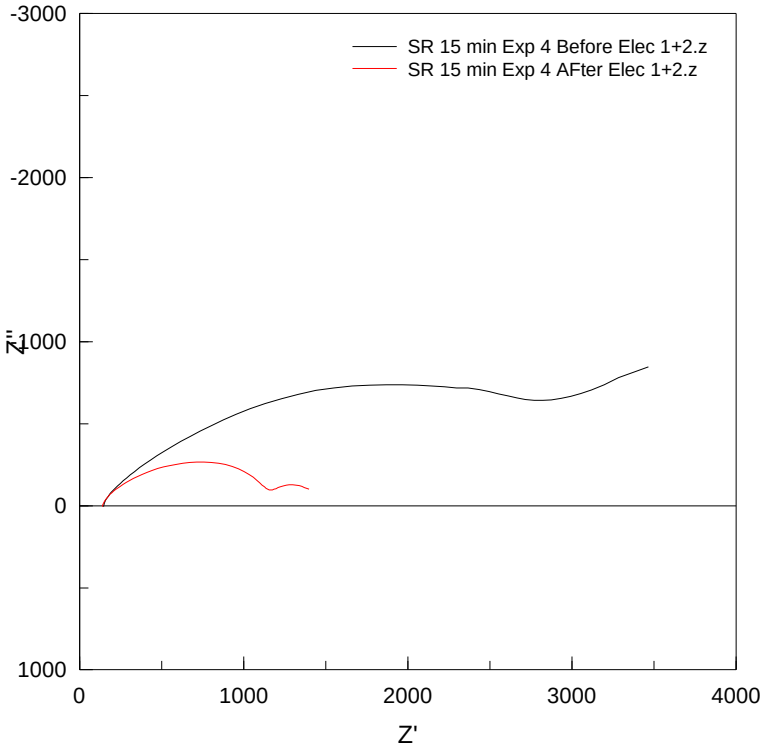

Figure 31: Complex plot showing difference impedance difference before and after applying reverse iontophoresis in in vitro experiment 4 of 15 minutes of duration

An important observation from Figure 31 is the semi-circular curve that is traced. This observation is important in terms of potential impedance analysis and is discussed later.

4.1.3.2. Bar charts for pair of electrodes E1,2

For the 3 pairs of electrodes and the 7 intervals of duration (2, 5, 10, 15, 30↔, 30→ and 60 minutes) all calculations including averages, standard deviations of Z', Z'', magnitude and phase have been made. However, for clarity the pair of electrodes E1,2 will be presented in experiments of all durations and only the most significant graphs will be shown. Secondary graphs will be shown in Appendix J.

4.1.3.2.1. Comparison Z' at all frequencies before and after applying RI

Figure 32 shows the real part of the impedance of the membrane at different frequencies and for the complete set of experiments performed.

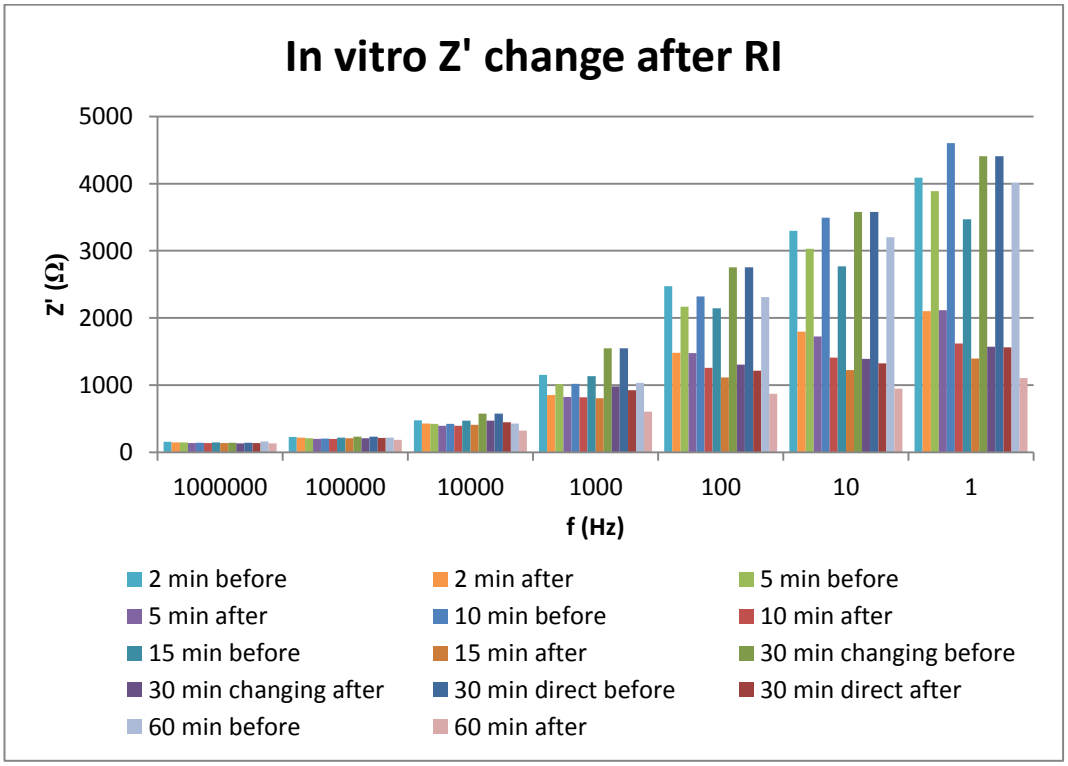

Figure 32: In vitro Z' before and after applying reverse iontophoresis

The impedance values show very interesting findings. First as frequency decreases the real part of the impedance increases for all experiments, from an average value of 148 Ω at 1 MHz to 4.1 KΩ at 1 Hz. Second, comparing results before and after performing the experiments, there is a decrease in their values up to a 60% at 1 Hz. Thus the impedance after the experiment is always lower than before. Finally,

comparing the change in impedance before and after at one frequency it can be noticed that the longer the extraction time the lower the value after the experiment; at 1 Hz for 60 minutes it decreases up to 70%. Therefore there are 2 dependencies: frequency and duration of RI application.

4.1.3.2.2. Comparison of Z'' for all frequencies before and after applying RI

Figure 33 shows the imaginary part of the impedance for the experiments carried out at several frequencies.

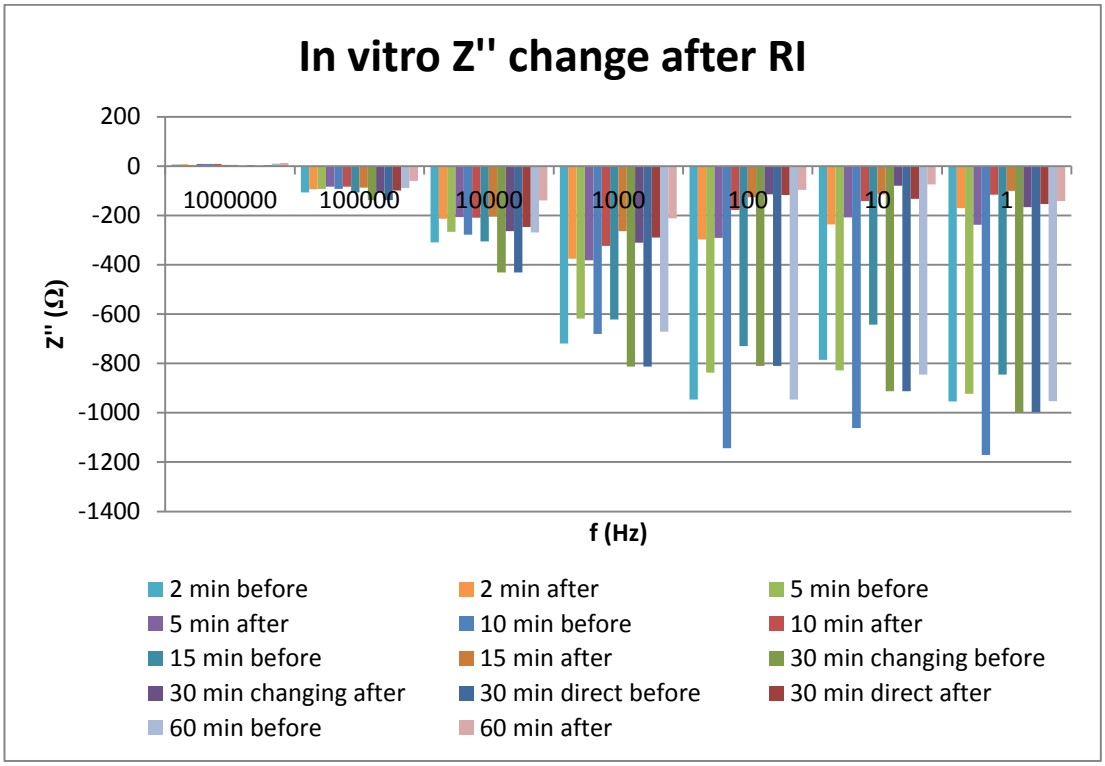

Figure 33: In vitro Z'' before and after applying reverse iontophoresis

The imaginary part of the impedance also throws out very interesting results although the trends observed are not as clear as with the real part. Firstly, before the application of RI, as frequency decreases measured Z'' decreases also in most cases. Although there is an exception at 10 Hz; and after RI it decreases up to 1 KHz and then it increases again. Secondly, there is a notable increase in the measured Z'' value after the application of RI compared to values before, in the case at 1 Hz there is an increase of up to 84%. Thirdly, no straightforward relationship between Z'' and extraction time was found. And finally, at very high frequencies (1 MHz) the value

of the imaginary part changes sign to positive. This suggests the measured reactance has moved from being capacitive to being inductive. The membrane and solution is not expected to exhibit inductive behaviour. This inductive reactance is more likely due to be as a result of measuring at such high frequencies and introducing inductance from the experimental arrangement, such as the attaching cables. It may be necessary to reject the results at 1MHz in later impedance analysis.

4.1.3.2.3. Comparison of modulus of Z for all frequencies before and after applying RI

Figure 34 shows the magnitude of the impedance Z before and after RI for all experiments performed. It is shown merely to observe the tendency when both real and imaginary parts are used for the analysis.

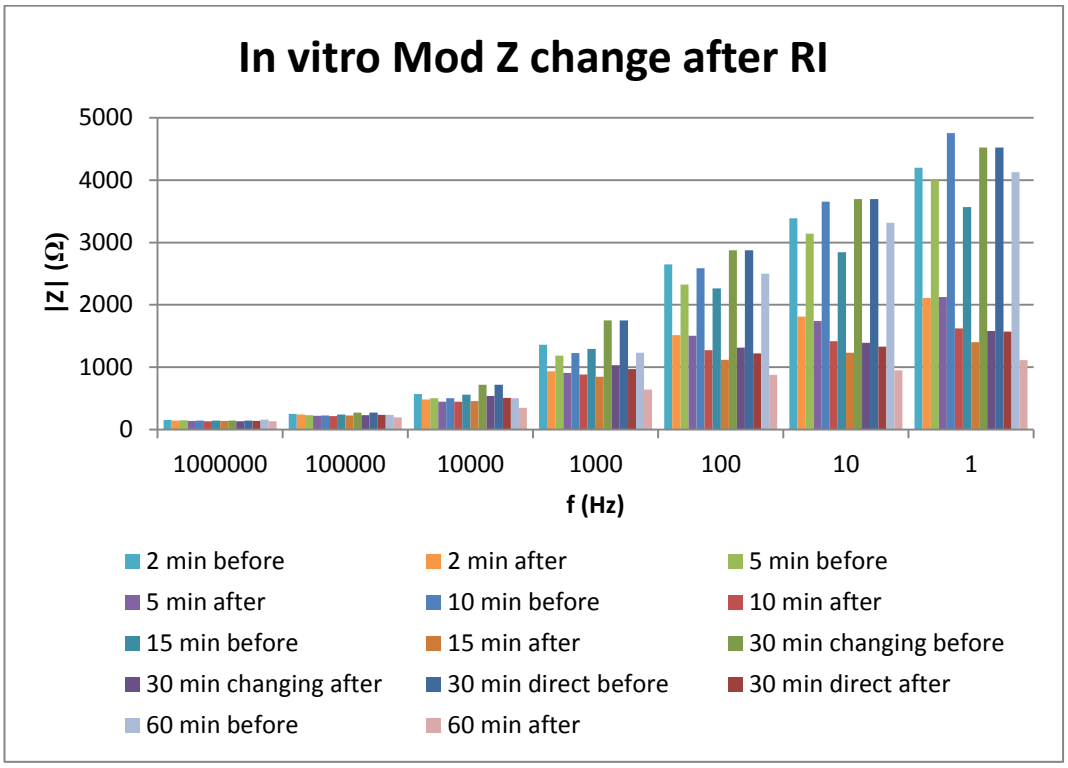

Figure 34: In vitro magnitude of Z before and after applying reverse iontophoresis

The magnitude of the impedance is not straightforward to analyse as it is made up of the real and imaginary parts. In general, the magnitude decreases with frequency, but not linearly. At some frequencies it increases again. For the 10 minutes experiment it

changes from a maximum value of 4.7 KΩ at 1 Hz to a minimum value of 145 Ω at 1 MHz.

4.1.3.3. Electrical modelling *in vitro*

As can be seen in any of the complex plane plots, the shape of the plot is similar to a circular arc locus and the empirical equation for impedance proposed by Cole can be applied as discussed in section 2.5.

Looking at any of the experiments the values of R_∞, R_0 can be found. For example, experiment 4 of 60 minutes of duration has been chosen and is representative of all the *in vitro* experiments. The impedance for the pair E1,2 is represented before and after applying reverse iontophoresis.

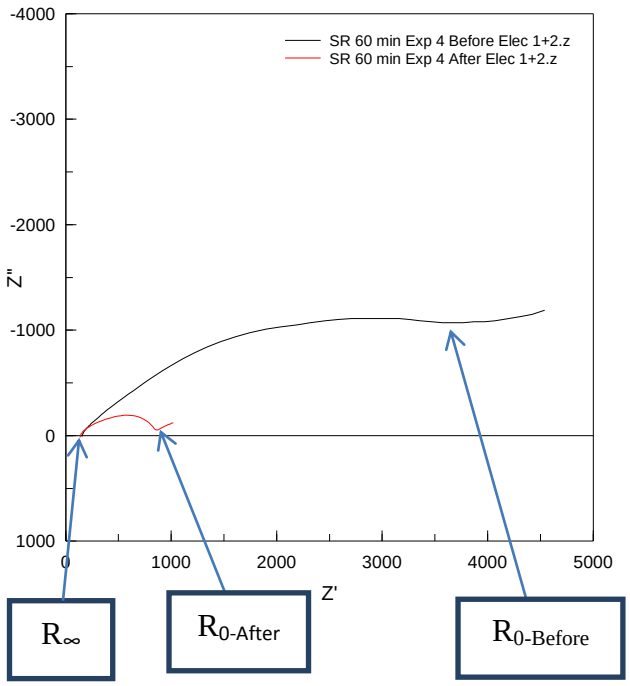

Figure 35: Complex plot showing impedance before and after applying reverse iontophoresis for pair of electrode E1,2 in in vitro experiment 4 of 6o minutes of duration

The large arc corresponds to the values of impedance before applying reverse iontophoresis and the small arc to those after the experiments has been carried out.

Both of the arcs approach the same value as the frequency approaches infinity. It has been represented with R_∞. For the membrane under study infinite means a frequency of 1 MHz.

According to the theory, the other end of the arc represents the impedance when the frequency is near zero or DC. That value has been represented as R_0, and for our results will be the point of inflexion in the curve which is around 10 Hz.

Their values are detailed in Table 10 and Table 11.

Z'(Ω)							
Freq (Hz)	**1**	**10**	**100**	**1000**	**10000**	**100000**	**1000000**
E1,2 Before	4538	3467	2324	1007	423	217	154
E1,2 After	1023	889	825	586	319	184	135

Table 10: Real part of impedance values before and after applying reverse iontophoresis for pair of electrodes E1,2 in in vitro experiment 4 of 60 minutes of duration

Z''(Ω)							
Freq (Hz)	**1**	**10**	**100**	**1000**	**10000**	**100000**	**1000000**
E1,2 Before	-1193	-1080	-1073	-670	-266	-90	9
E1,2 After	-121	-63	-85	-194	-132	-58	16

Table 11: Imaginary part of impedance values before and after applying reverse iontophoresis for pair of electrodes E1,2 in in vitro experiment 4 of 60 minutes of duration

This data will be modelled and analysed in the next section. However, before modelling the data a couple of observation about the shape of the arcs must be made. First, at high frequencies the values for the imaginary part of the impedance change their sign, which means a change from capacitive to inductive behaviour. According to the theory, only capacitive behaviour is expected, therefore the maximum considered frequency will be limited to 100,000 Hz. Second, at low frequencies the imaginary part of the impedance decreases up to an inverting point where it increases again creating a tail in the shape of the arc. Thus, values up to the lowest peak will be considered for further calculations, which means limiting the lowest frequency to 10 Hz.

4.1.4. Electrical skin model

Considering Model A (presented in Section 2.5), the values for the electrical skin model can be calculated. The chosen model has been presented again here in Figure 36:

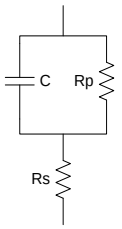

Figure 36: Circuit selected for the analysis and development of a model

Where R_s is the impedance value at the highest frequency (R_s is equivalent to R_∞), R_p is the distance in the real axis from R_∞ to R_0, and C is the capacitance part of the membrane.

The following graphs (Figure 37 and Figure 39) show the values for the 3 components of the circuit: R_s, R_p and C.

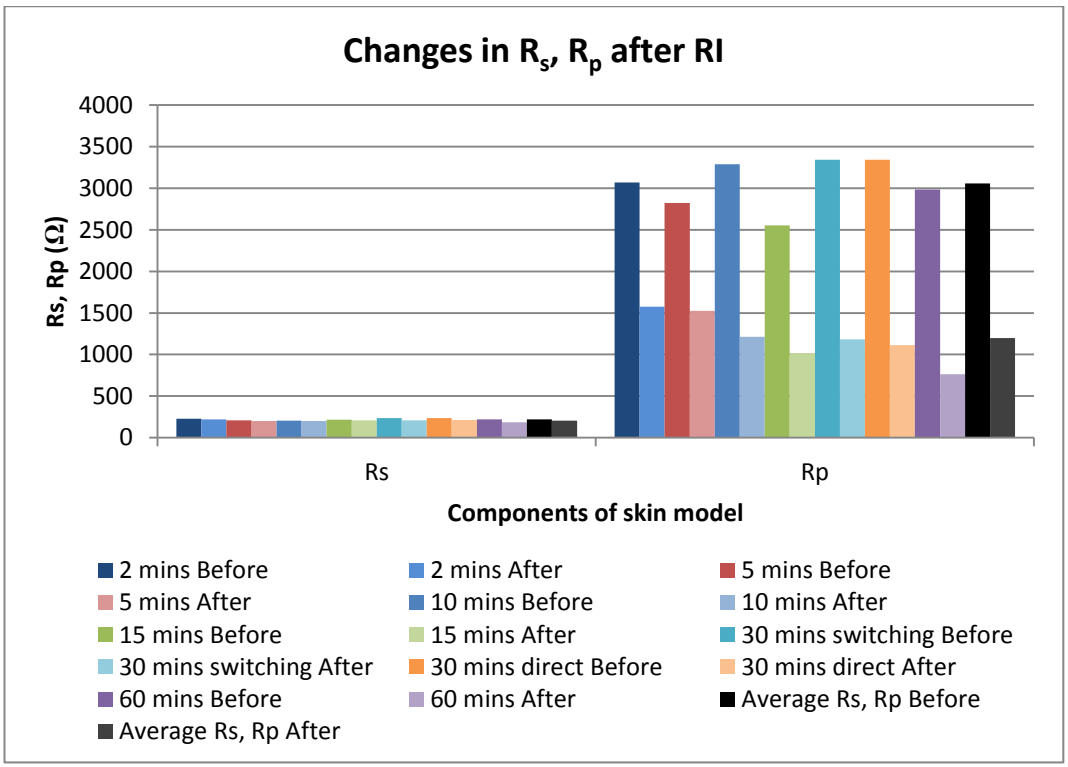

Figure 37: In vitro R_s and R_p values before and after experiments

As it can be noticed in Figure 37 R_s keeps almost constant through the experiments. It is independent of the application of reverse iontophoresis to the membrane or to the extraction time. Its average value before is 221.0 Ω and its average value after performing the experiments is 205.0 Ω, which represents a decrease of a 7% approximately.

On the right side of the graph R_p shows marked variations within each experiment. Therefore the application of reverse iontophoresis to the membrane makes changes in the value of the parallel resistance of the circuit model. Its value decreases up to a 54%. However the dependence with time of extraction is not quite clear from the graph (Figure 37). In order to see the relationship more clearly a new graph has been plotted calculating the ratio of decrease after RI. This is shown in Figure 38.

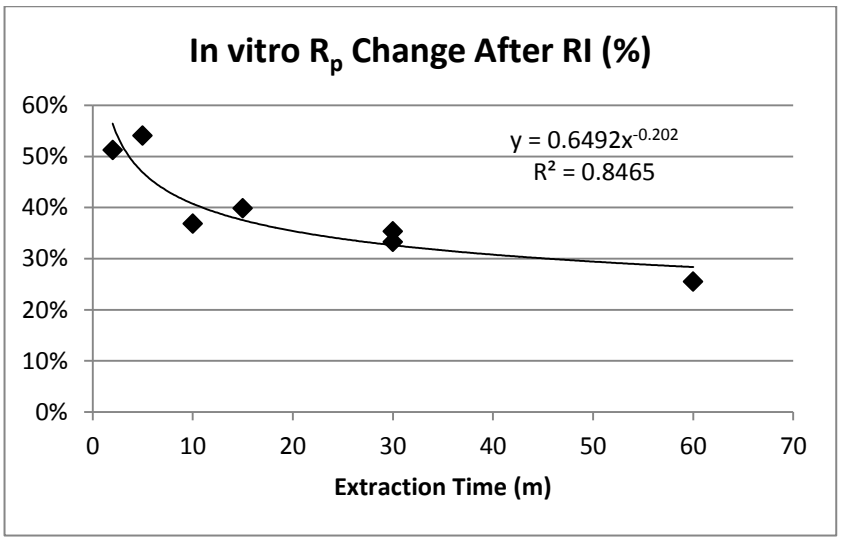

Figure 38: In vitro R_p change with RI in %

The points observed in Figure 38 from left to right are 2, 5, 10, 15, 30, 30 and 60 minutes. They show the percentage of the original resistance value (R_p) after RI has been applied. As it can be observed it decreases exponentially in the first 10 minutes. After 10 minutes it decreases slowly and more linearly until 60 minutes.

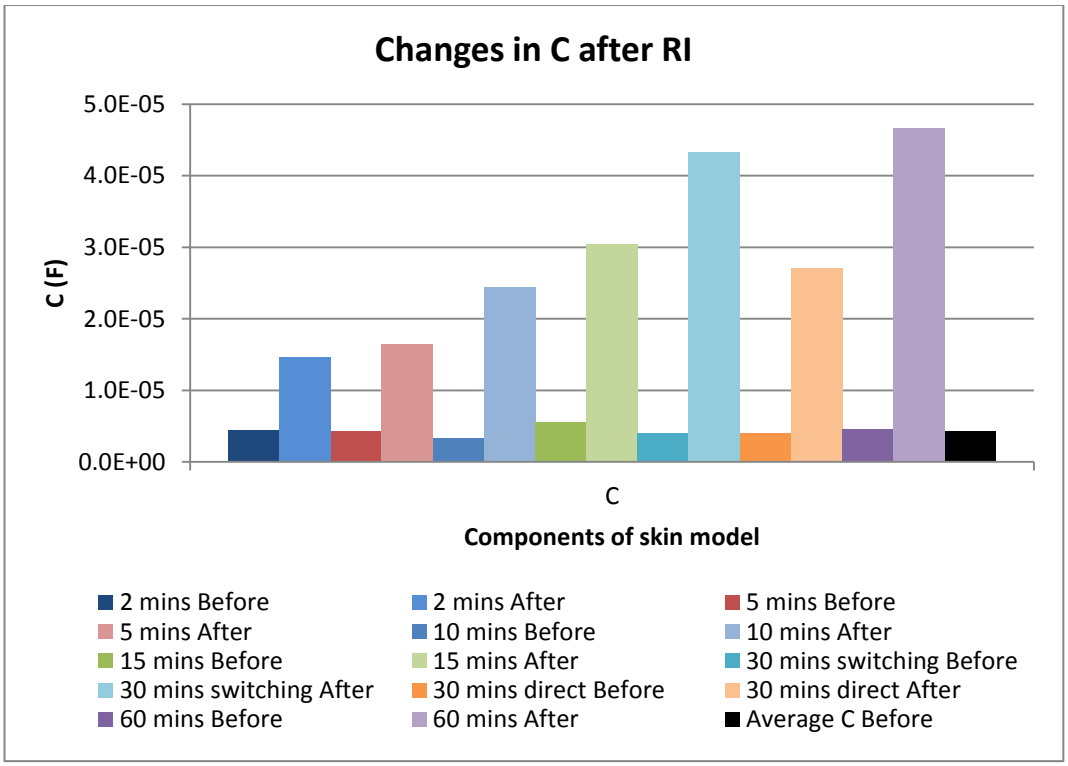

Figure 39: In vitro C values before and after experiments

The capacitance part of the membrane before performing RI shows an average value of 4.3 μF. In addition, it is clearly visible how it is dependant with the duration of extraction. The longer the time of extraction the higher the capacitance.

4.1.5. Time Constant of the membrane

	Time constant τ (ms)	
Extraction Time (m)	**Before**	**After**
2	13.7	23.1
5	12.1	25.1
10	11.0	29.6
15	13.9	30.9
30 switching	13.2	51.1
30 direct	13.2	30.1
60	13.7	35.5
Average	13.1	

Table 12: Time constant of the membrane

The average time constant of the membrane before the experiments is 13.1 ms. After performing the experiments there is an increase in value in all cases, with a maximum increase of 388% in the experiment of 30 minutes switching polarity. However, the relationship, if any, between time constant and extraction time is unclear from those results.

4.1.6. Potassium-Impedance relationship

The last step in the project is to investigate any relationship between the potassium concentration and the impedance measured for the given experiments.

The serial component of the model, R_s, does not show any change with the application of the experiments, so it is unlikely to be useful in linking membrane impedance and potassium extraction. Values before the experiment are not useful either as no change exists. However, R_p and C after performing the reverse iontophoresis do show some correlation with the potassium extracted.

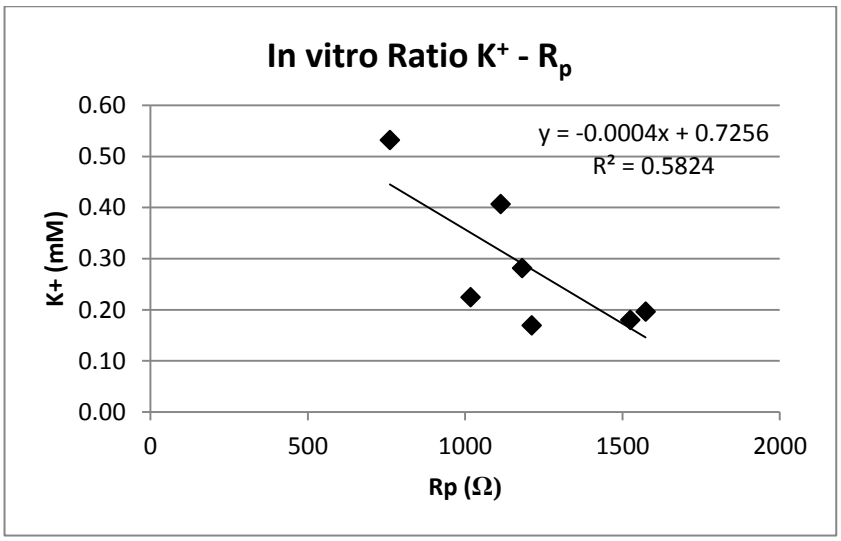

Figure 40: In vitro relationship between potassium concentration and R_p of the membrane

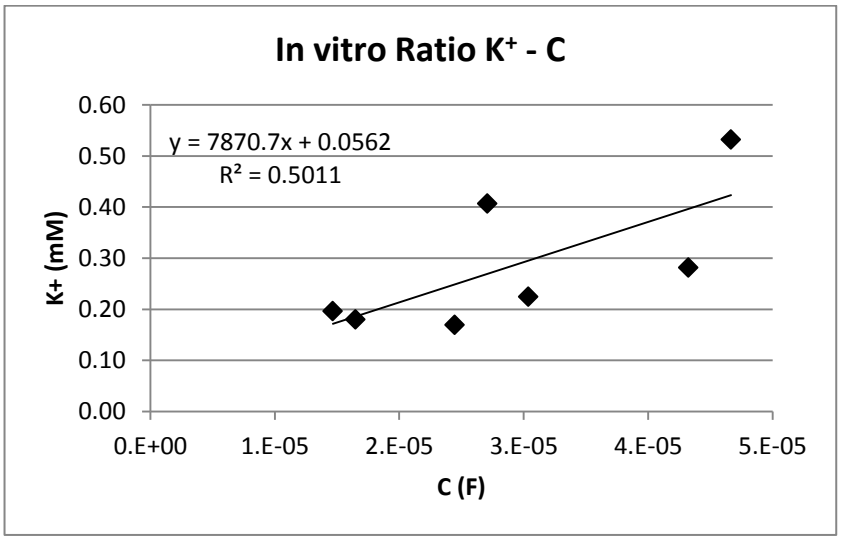

Figure 41: In vitro relationship between potassium concentration and capacitance of the membrane

Both graphs (Figure 40 and Figure 41) show correlations of 58 and 50% respectively. Potassium concentration against resistance and potassium concentration against capacitance relationships seem to be inversed; as resistance increases the amount of potassium extracted decreases, as would be expected, and as capacitance increases the amount of potassium extracted increases as well.

4.2. *In vivo* results and analysis

Data from *in vivo* experiments, performed under University ethics and in accordance with approved procedures, was given so as to compare results carried out on an artificial membrane and results performed on people. The *in vivo* experiments were divided into 2, 5, 10 minutes of RI extraction with no change in polarity and 60 minutes of RI extraction changing polarity every 15 minutes.

Two sets of *in vivo* experiments were obtained. The first one consisting on the application of reverse iontophoresis to 9 participants and the second set made up of 5 experiments performed on the same person along different days.

For comparison purpose all *in vivo* data will be presented, although the second set of experiment consisting of 5 repetitions on the same person would be more approximate to the *in vitro* experiments carried out. In the *in vitro* experiments the same type of membrane was used for all experiments. That would account for the same type of skin.

4.2.1. Potassium results

The first results shown are the short duration ones (2, 5 and 10 minutes) for 9 different participants. The average value of the 9 participants for each of the electrodes is shown in Figure 42. The error bars denote the standard error of the mean.

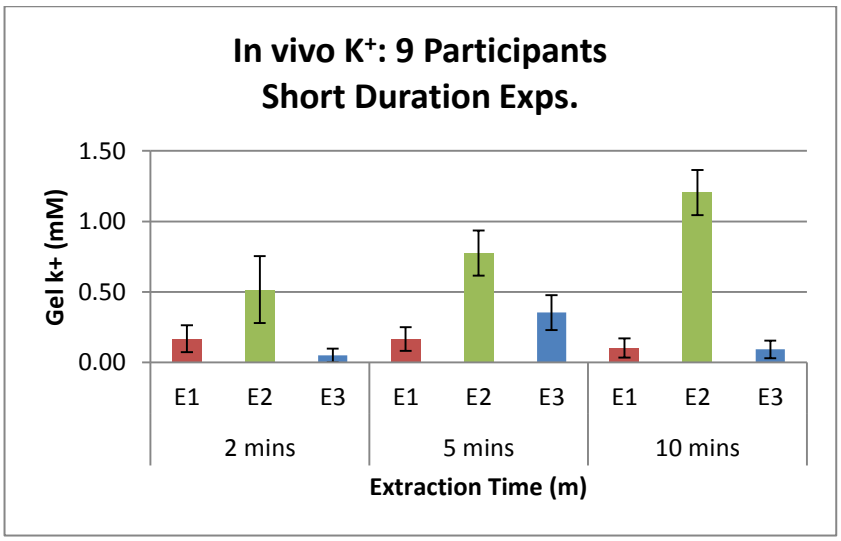

Figure 42: In vivo results for potassium concentration of 9 participants. Experiments of 2, 5 and 10 minutes

Electrode 2 reaches higher potassium concentrations than electrodes 1 and 3 in all cases up to 1.21 mM. Electrode 1 at first sight seems to decrease with increasing duration of the experiment, but once the error bars are analysed it can be cleared that they are within the same range (between 0.1 and 0.17 mM), so no clear variation exists. The two sample t-test statistical analysis shown in Table 13 proves that there is no statistical difference between the means of the 3 experiments as the p-value is always greater than 0.05.

	Pair of experiments	**95% confidence interval P-value**
Electrode 1	2,5	0.985
	2,10	0.578
	5,10	0.562

Table 13: P-value at 95% CI of in vivo potassium analysis for Electrode 1

Electrode 3, however, seems to follow a different pattern, increasing and decreasing. It will be easier to analyse them together with long duration experiments.

Next results (Figure 43) show the average of potassium concentration extracted from the same patient during 5 experiments.

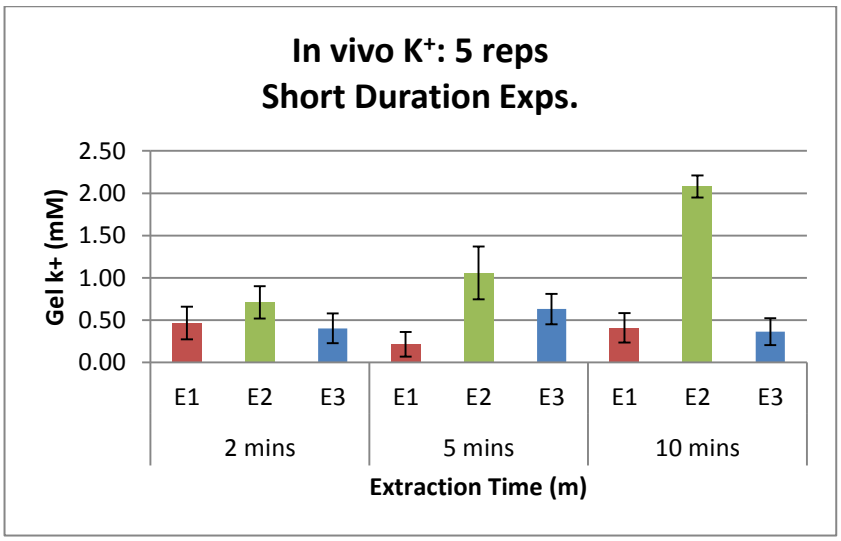

Figure 43: In vivo results for potassium concentration of the same participant during 5 different days. Experiments of 2, 5 and 10 minutes

As in the previous case, electrode 2 rises up markedly with increasing duration of experiment up to 2.08 mM in 10 minutes experiment. Electrode 1, as well, follows the same variations possibly repelling potassium ions. The pattern observed in electrode 3 seems to have no dependency with time over these short time periods. As it is the diffusion electrode reverse iontophoresis has no effect on it.

Long-time duration experiments are of 60 minutes of duration. The complete series of values can then be observed together in Figure 44.

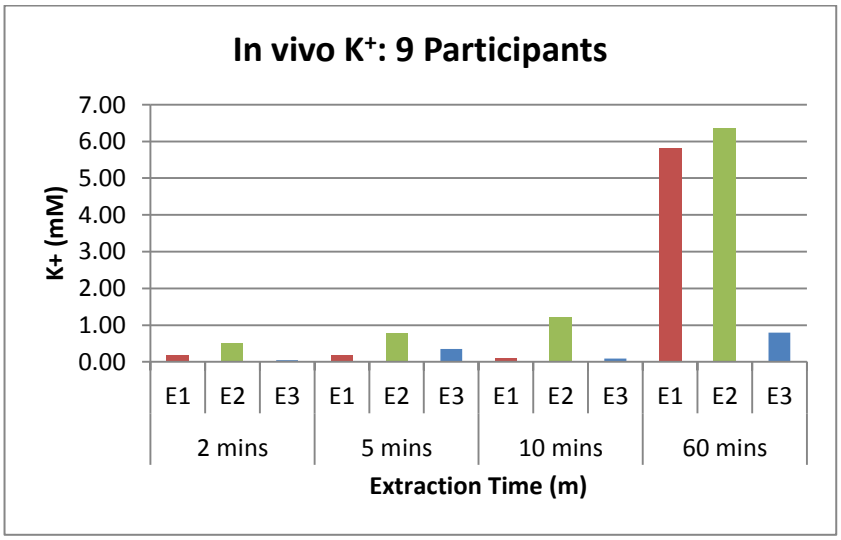

Figure 44: Comparison of potassium results for in vivo experiments

As expected, in 60 minutes experiment, electrode 2 shows the highest concentration (6.35 mM). Electrode 1 reaches a similar value to electrode 2 (5.80 mM) as the polarity has switched for half of the time in the 60 minute experiment so electrode 1 and 2 are expected to show similar results here. On the other hand, electrode 3 is notably much lower and reaches a value of just 12.5% of electrode 2 (0.80 mM).

Detailed views of electrodes for 60 minutes are available in Appendix K.

A mathematical modelling was also performed for electrode 2 on *in vivo* experiments showing the following relationship (Figure 45).

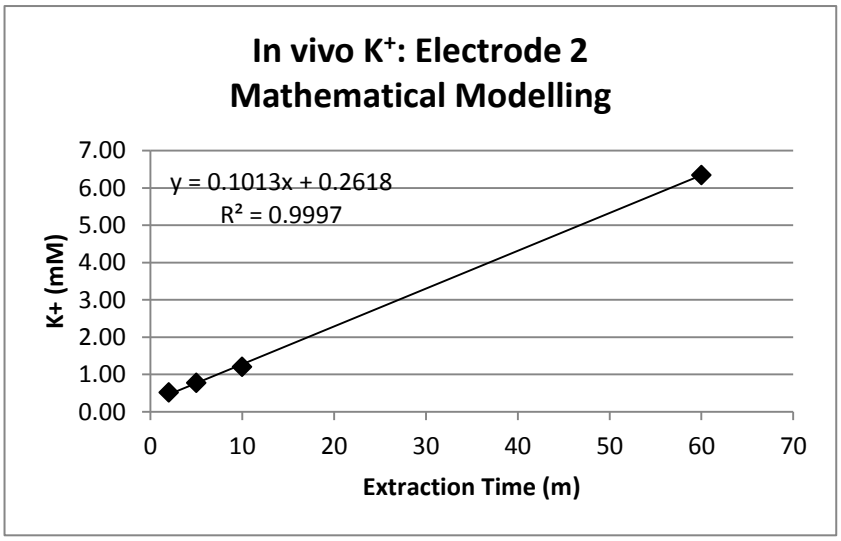

Figure 45: Mathematical modelling of potassium extracted on electrode 2 in vivo

A very linear relationship of potassium with extraction time is observed. The coefficient of correlation reaches 99.9%.

4.2.2. Glucose results

The average values of glucose levels measured are shown in Figure 46 and the calibration curves used to generate the data in concentration units (μM) is shown in Appendix L:

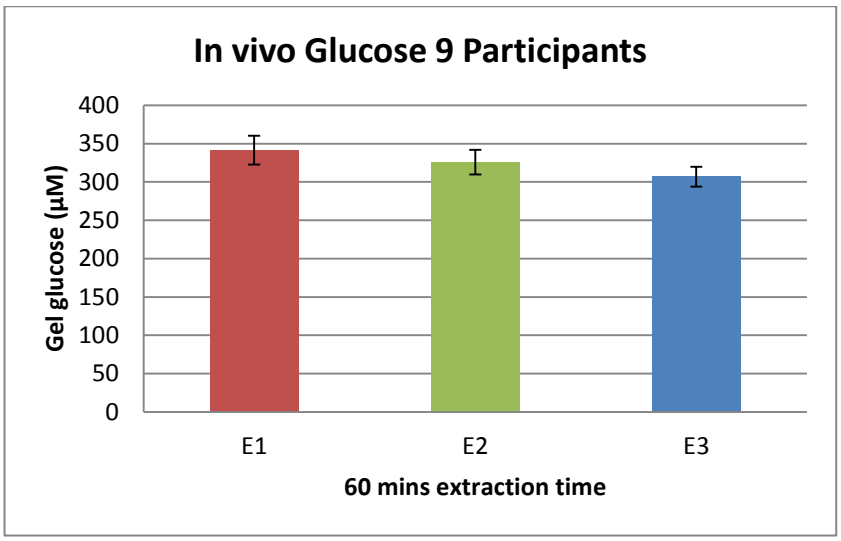

Figure 46: In vivo glucose concentration for 60 min extraction time

From the values shown no clear observation can be made. Values seem to decrease from electrode 1 (342 µM) to electrode 3 (307 µM) as also seen in the *in vitro* case, but because of the error bars they all lie within the same range.

4.2.3. Impedance results

Impedance analysis *in vivo* was carried out both in a group of 9 different participants and also 5 times on the same participants. For the former group the experiments were of 2, 5, 10 and 60 minutes of duration. For the latter group only short range duration experiments (2, 5 and 10 minutes) were carried out as 5 repetitions on one participant had not been performed at 60 minutes of extraction.

For comparison and clarity purposes only data from the pair of electrode 1 and 2 will be presented.

As in the case of *in vitro* results, *in vivo* results also show numbers which do not seem to agree with theory, especially those showing the imaginary part which changes to a positive value. Real part of impedance at 1 MHz has been discarded because of reliability and the maximum frequency considered has been set up at 100 KHz. For the calculation of R_p only the real part is necessary, therefore the lowest frequency was set at 1 Hz, however for the calculation of C the imaginary part is

used, and again, it shows positives numbers. Thus, for the calculation of C the lowest frequency was set at 100 Hz.

4.2.3.1. Results for 9 participants

As in the *in vitro* case the first graph (Figure 47) shows the real part of the impedance at several frequencies for the set of short time duration experiments.

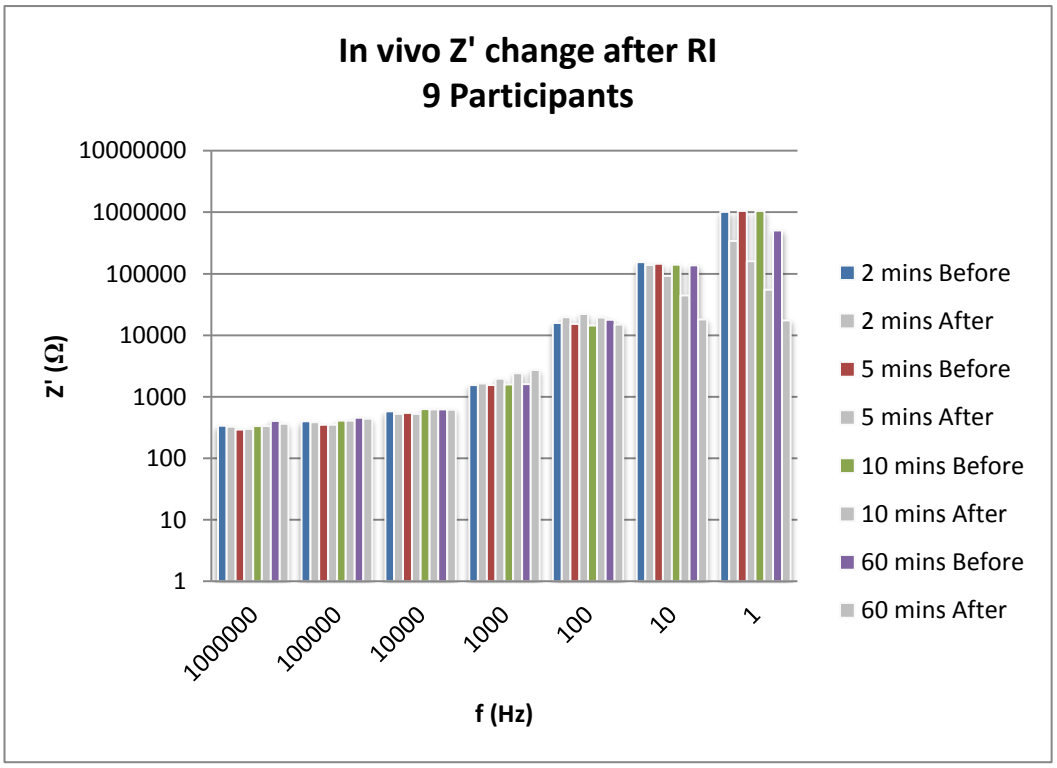

Figure 47: In vivo Z' results of 9 participants

From the graph, several remarks can be made. Firstly, as frequency decreases the real part of the impedance increases either before or after applying reverse iontophoresis. Before RI, impedance increases up to 3 orders of magnitude (from 341 Ω to 1 MΩ). Secondly, looking at just one experiment before and after, e.g. 60 minutes, the value decreases as the experiment is performed up to 97% at 1Hz. Thirdly, focusing at one frequency, e.g. 1 Hz, it can be noticed that the values after carrying out the experiment decreases up to 85%, so there is a dependency with the duration of the experiment. Therefore the real part of the impedance has a dependency with the frequency and with the duration of RI.

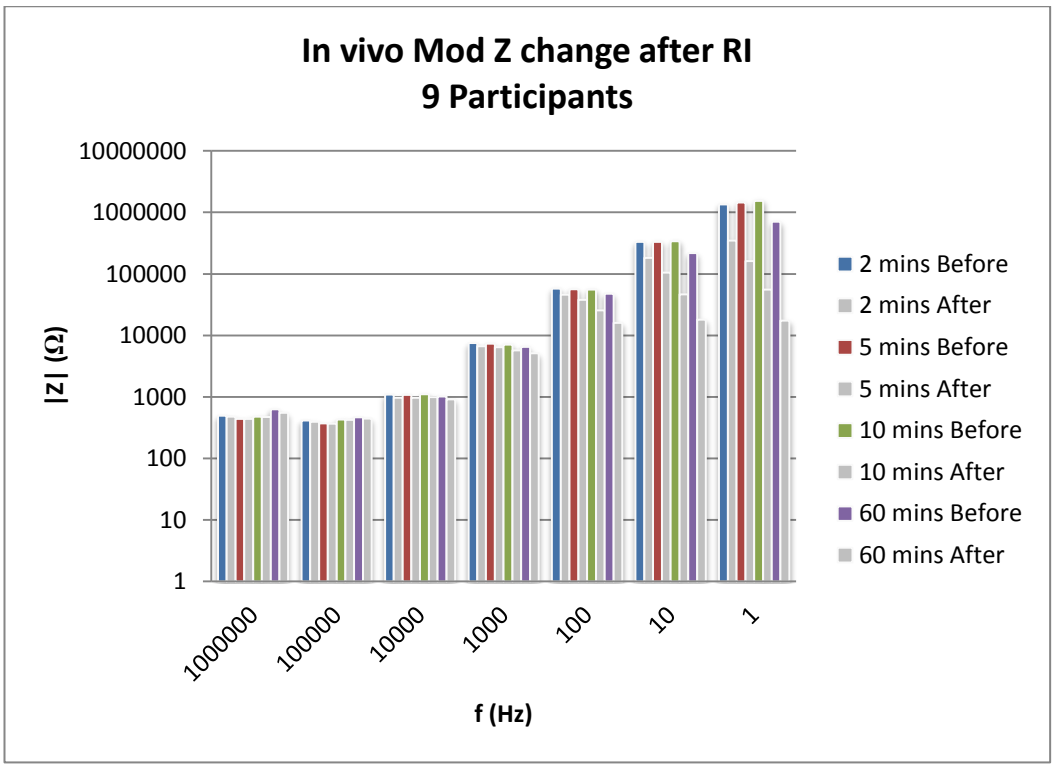

Figure 48: In vivo modulus of Z results of 9 participants

Similar results as for the real part of the impedance can be expected for the modulus. There is one extra observation at high frequencies (1 MHz – 100 KHz), the values in that range are lower than at 1 MHz. That means that the imaginary part of the impedance has a higher absolute value at 1 MHz. That is in accordance with the *in vitro* cases in which it was explained that data at 1 MHz is not used for calculations due to the reliability of the results.

4.2.3.2. Results for 5 repetitions on the same participant

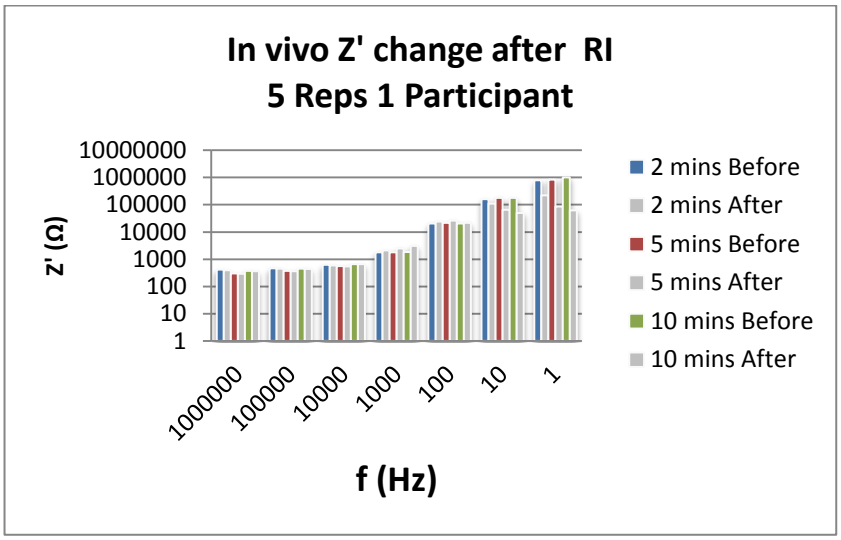

Figure 49: In vivo Z' results of 5 repetitions on 1 participant

The tendency of the series in Figure 50 corresponds to that explained for the 9 participants. The real part of the impedance shows a dependency with the frequency, the application of the experiment and the duration of extraction.

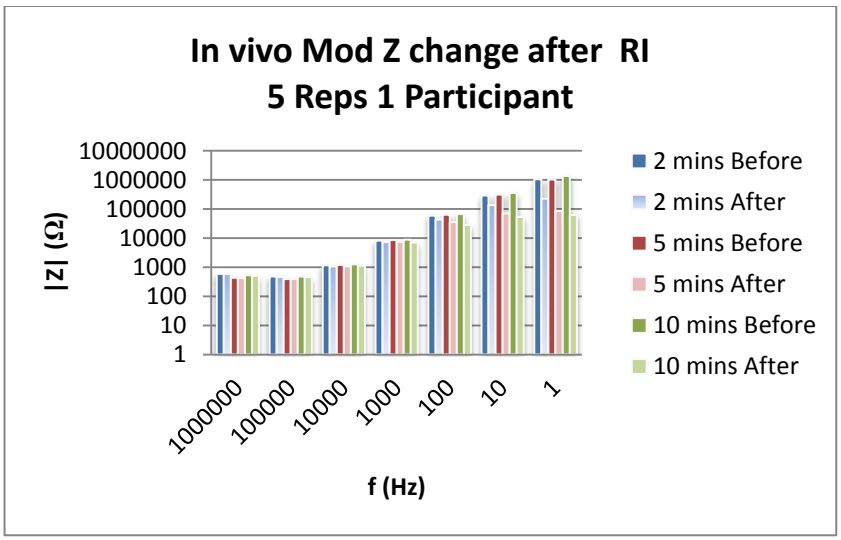

Figure 50: In vivo modulus of Z results of 5 repetitions on 1 participant

The modulus also shows the same tendency as for the 9 participants' case including the detail on high frequencies with a decreasing slope.

4.2.4. Electrical Skin model

As in the case of impedance results, the same model can be presented and the same electrical components used as shown in Figure 7.

The values are divided into the two sets of experiments, first for 9 participants it was performed for 2, 5, 10 and 60 minutes and then for 5 repetitions on 1 participant of 2, 5 and 10 minutes of duration.

4.2.4.1. Results for 9 participants

Results for the components of the equivalent circuit (R_s, R_p and C) are shown in the next few graphs (Figure 51, Figure 52 and Figure 54).

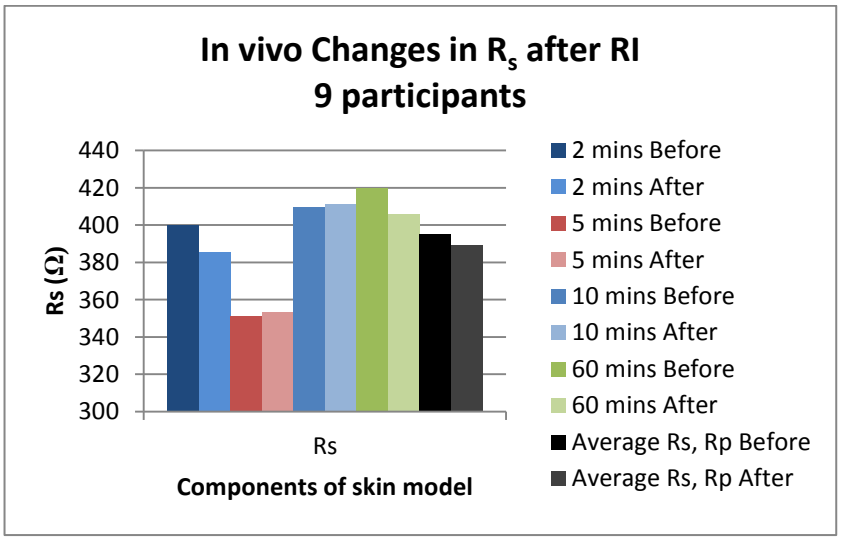

Figure 51: In vivo R_s values before and after RI of 9 participants

The first *in vivo* results show R_s for 9 participants. Although the graph (Figure 51) shows variations in values up to 18% they can be considered almost constant through all experiments. Furthermore, it shows a similar average value before (395 Ω) RI and after (389 Ω) RI, which is a decrease of just 2%.

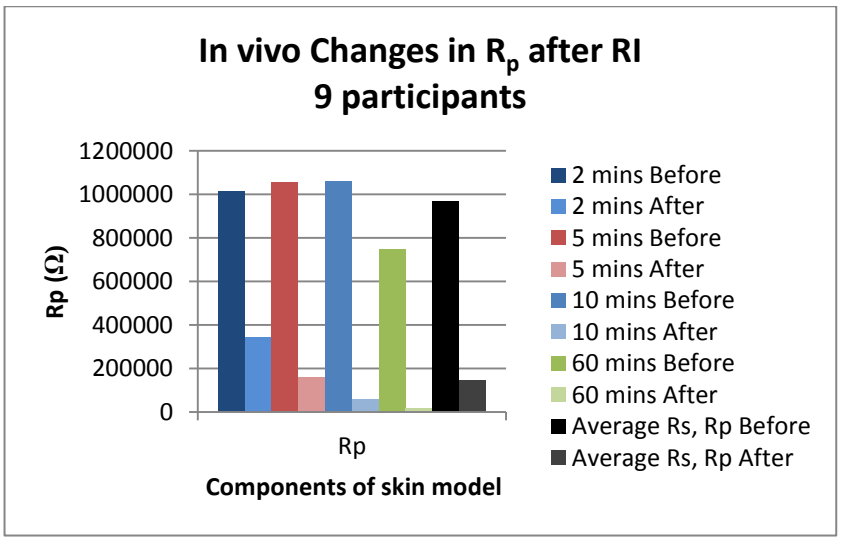

Figure 52: In vivo R_p values before and after RI of 9 participants

The second component, R_p, shows notable differences before and after performing RI. Average values before (968 KΩ) and after (143 K Ω) show a decrease of 85%. Through experiments it seems R_p after the experiment seems to decrease with time of extraction, but it is not clear from the graph. In order to see that relationship more clearly a graph showing the percentage decreased after the experiments is shown in Figure 53.

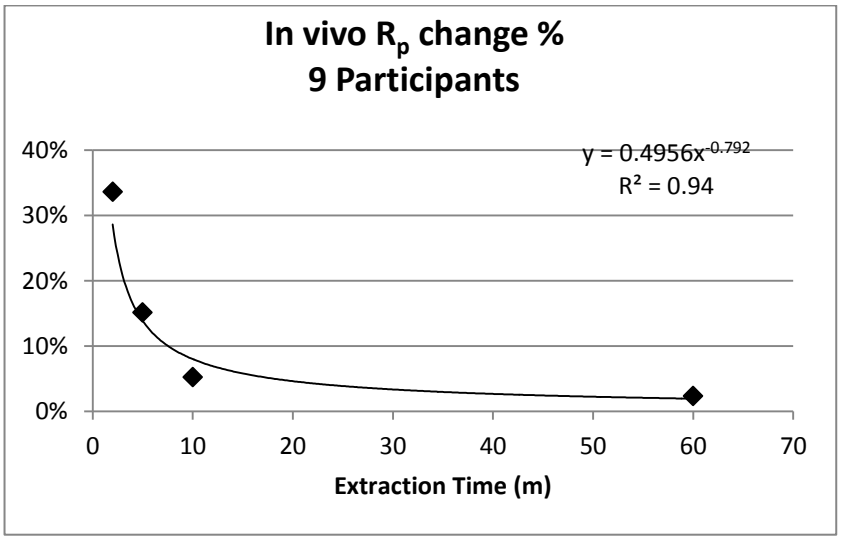

Figure 53: In vivo R_p change in percentage for 9 participants

The points in the graph, from left to right, show the percentage of R_p after applying RI. In the first 10 minutes there is a notable decrease. At 10 minutes the R_p is just 5%

of the original value. From 10 minutes upward it decreases slowly until 60 minutes where the R_p value is just 2% of the original value of R_p. This suggests that from 10 minutes, the skin resistance R_p is approximately constant.

Figure 54 shows values for C.

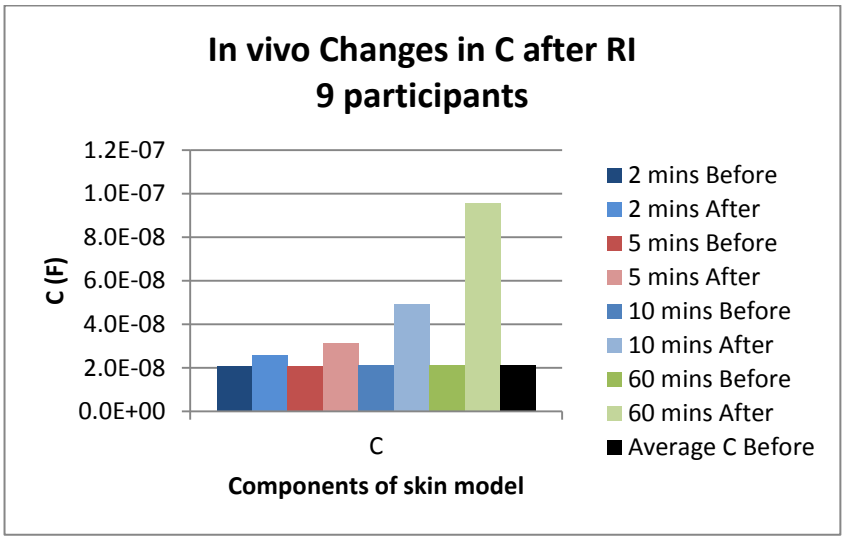

Figure 54: In vivo C values before and after RI of 9 participants

In the case of the capacitor values, C before performing the experiments shows an almost constant value (210 nF). The results suggest that after RI, the skin capacitance either increases with the application of current and is proportional to the duration of RI. The increase reaches up to 457% for 60 minutes.

4.2.4.2. Results for 5 repetitions on the same participant

Figure 55, Figure 56 and Figure 58 show the values of the component of the circuit model for the experiments performed on 1 participant during 5 repetitions.

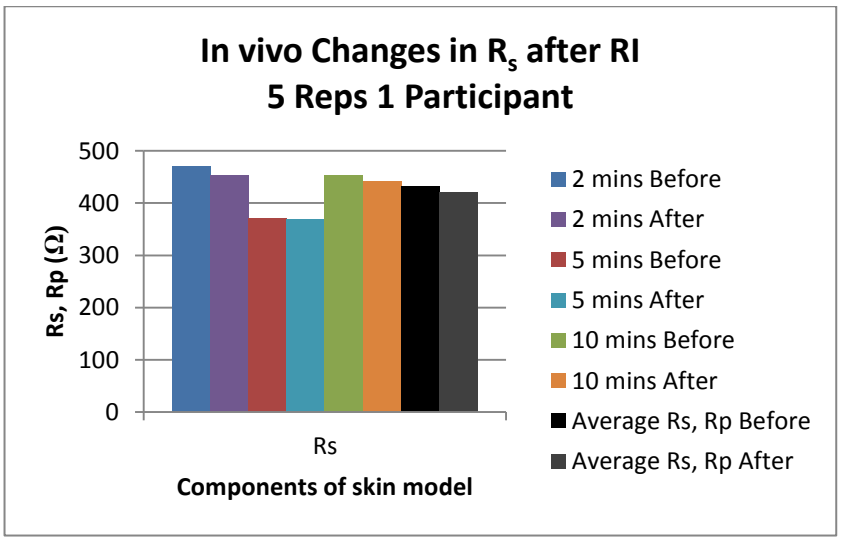

Figure 55: In vivo R_s before and after RI of 5 reps on 1 participant

Again, R_s seems to keep constant through experiments, either before (431 Ω) or after (421 Ω) RI.

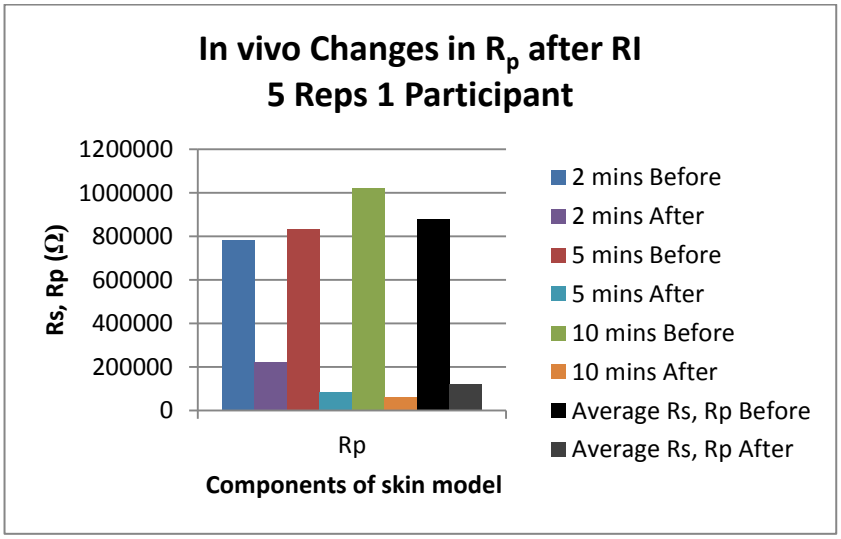

Figure 56: In vivo R_p before and after RI of 5 reps on 1 participant

R_p shows a similar value before the application of reverse iontophoresis (881 KΩ) and after there is a decrease of the value (average 122 KΩ), and it seems to depend also on the duration of extraction. That dependency is shown in Figure 57. The same rapid reduction in the value of R_p can be seen in the first 10 minutes.

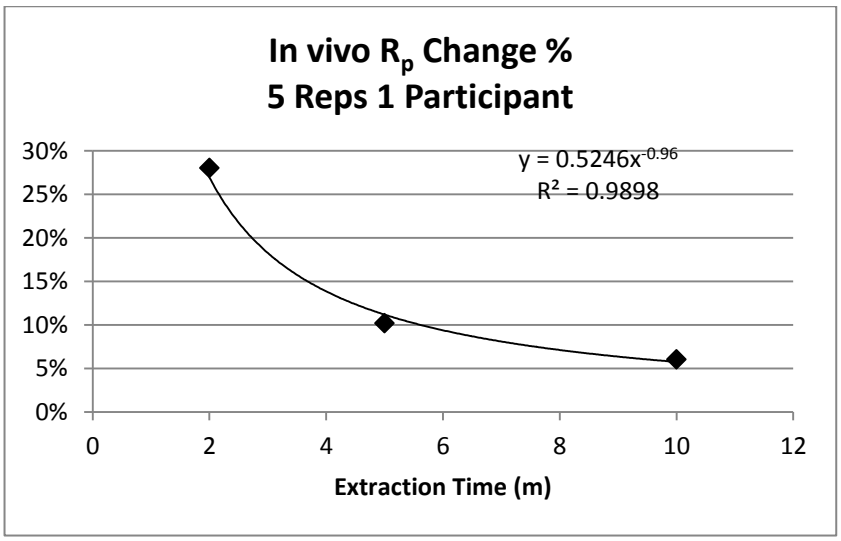

Figure 57: In vivo R_p change % for 5 reps on 1 participant

The following graph (Figure 58) shows results for the capacitance for 5 repetitions on 1 participant.

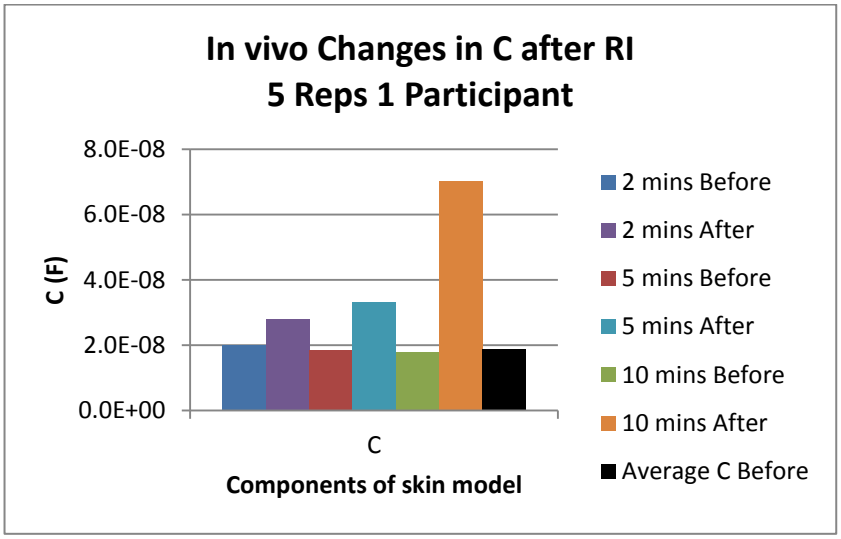

Figure 58: In vivo C before and after RI of 5 reps on 1 participant

Finally, C shows a constant value for the skin along the different experiments (20 nF) and after the experiments the value increases. It seems to have a dependency with the duration of the extraction.

4.2.5. Time Constant of the skin

The time constant of the skin was calculated using Equation 6. The values for time constant before and after RI are shown in Table 14 for the 9 participants' case and in Table 15 for the 1 participant's case.

	Time constant τ (ms)	
Extraction Time (m)	**Before**	**After**
2	20	8.3
5	21	4.3
10	22	2.2
60	14	1.5
Average	19	

Table 14: Time constant of the skin of 9 participants

Before applying reverse iontophoresis, the average time constant of 9 participants has been calculated as 19 ms. After carrying out the experiment the time constant of the skin decreases up to 90% at 60 minutes. From the numbers another observation can be made, the time constant decreases not only with RI but also with extraction time. These results are similar to values of skin time constants reported in literature (Coston and Li 2001).

For the case of 5 repetitions on 1 participant similar observations can be made.

	Time constant τ (ms)	
Extraction Time (m)	**Before**	**After**
2	16	5.4
5	15	2.5
10	18	2.5
Average	16	

Table 15: Time constant of the skin of 5 reps on 1 participant

The average value before RI is 16 ms and after decreases up to 86% at 10 minutes.

It can be concluded that the time constant of the skin depends on the duration of RI application.

4.2.6. Potassium-Impedance relationship

In order to obtain a good skin model the rate between the extracted potassium and impedance can be graphed.

Two rates are shown, the first one for the group consisting of 9 participants and the second one consisting of 5 repetitions on 1 participant.

The results for 9 participants include data from experiments of 2, 5, 10 and 60 minutes of extraction time.

Extraction Time (m)	**R_p (Ω)**	**C (F)**	**K^+ E2 (mM)**
2	340512	2.6E-08	0.52
5	159563	3.1E-08	0.78
10	55164	4.9E-08	1.21
60	17341	9.6E-08	6.35

Table 16: R_p, C and K^+ data for 9 participants in vivo

It is shown in Figure 59 and Figure 60.

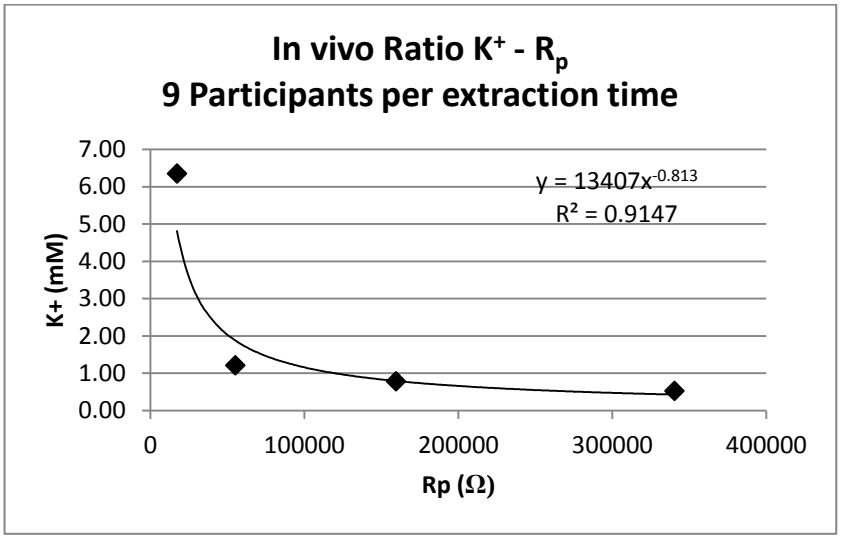

Figure 59: In vivo relationship between K^+ and R_p for 9 participants

The rate between potassium and the parallel resistor in the model shows a correlation of 91% when performing an exponential regression curve. As resistance increases the potassium extracted decreases, so the slope of the equation that relates them has a negative sign.

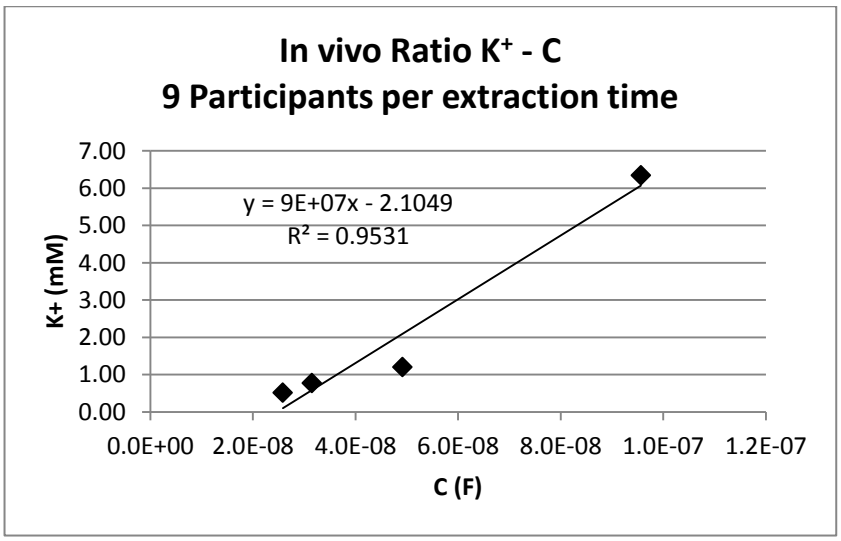

Figure 60: In vivo relationship between K^+ and C for 9 participants

The rate between potassium extracted and capacitance is opposite to the resistance. As the capacitance increase so does the amount of potassium extracted. The rate between them is 88%. In this case the slope is positive.

In the case of 5 repetitions on 1 participant only 3 sets of experiments are included: 2, 5 and 10 minutes.

Extraction Time (m)	**R_p (Ω)**	**C (F)**	**K^+ E2 (mM)**
2	220239	3.E-08	0.71
5	85296	3.E-08	1.06
10	61956	7.E-08	2.08

Table 17: R_p, C and K^+ values for 5 reps on 1 participant in vivo

The results are shown in Figure 61 and Figure 62.

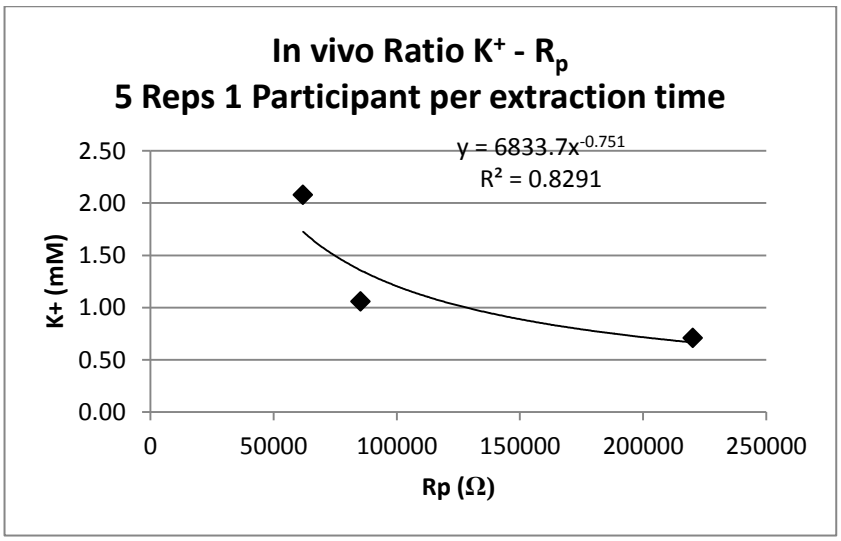

Figure 61: In vivo relationship between K^+ and R_p for 5 reps on 1 participant

Results from only 3 numbers cannot be used to make firm conclusion. However, the regression line appears to follow the same pattern as in the previous results with a coefficient factor of 83%.

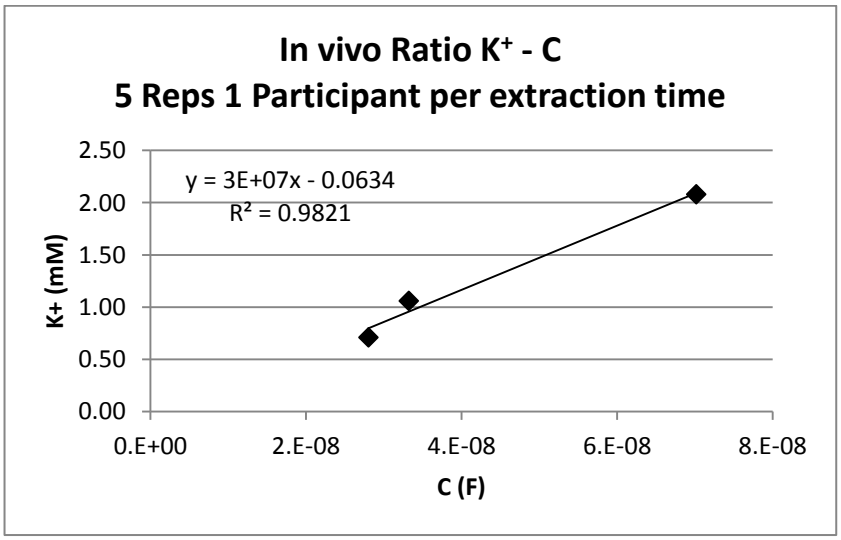

Figure 62: In vivo relationship between K^+ and C for 5 reps on 1 participant

Again, even though only 3 experiments are used for the ration capacitance-potassium extracted, it seems to be very well correlated (97%). The pattern it follows is as the one expected, the higher the capacitance, the higher the amount of potassium extracted.

Ideally it would be desirable to use parameters, such as skin impedance values, to account for the skin variation observed from person to person or between people day to day with an aim of calibrating for potassium extraction *in vivo*. To investigate this, R_p and C were calculated for the skin of each of the 9 participants and were plotted against the potassium extraction for each of the participants. In the following graphs (Figure 63 and Figure 64) the relationship between R_p and C with the quantity of potassium extracted is plotted per each of the participants.

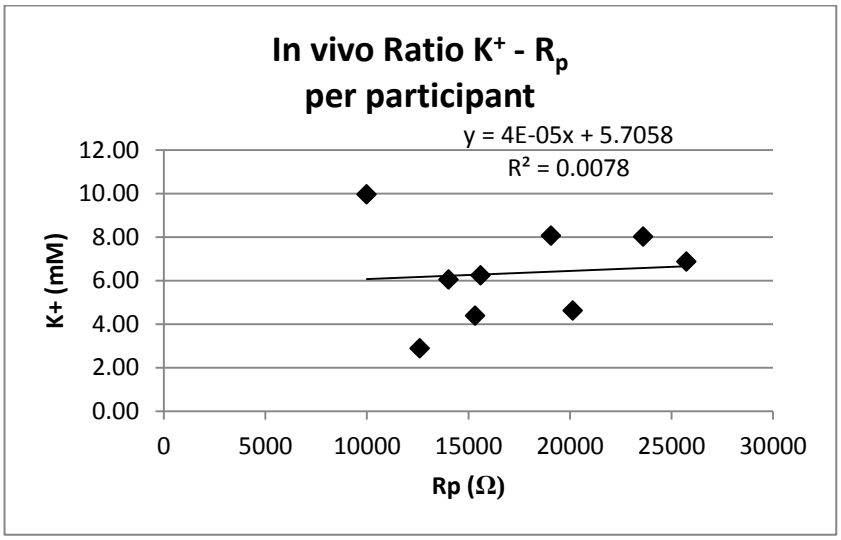

Figure 63: *In vivo* ratio K^+ with R_p per participant

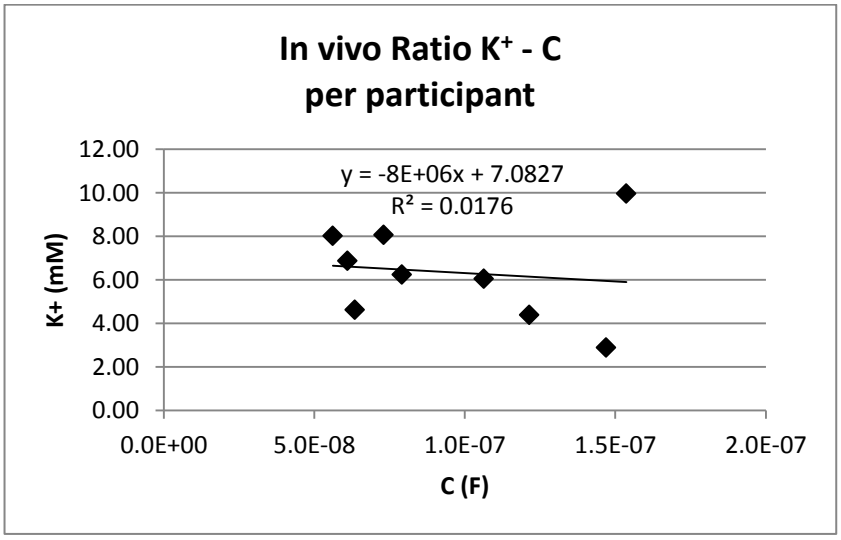

Figure 64: *In vivo* ratio K^+ with C per participant

Both ratios do no show a clear relationship between the potassium extracted and the resistance or capacitance components of the skin. A single parameter may be insufficient to establish a calibration algorithm to account for individual participant's skin permeability *in vivo*. However, the work carried out in this project has shown that mathematical modelling from experimental observations and electrical equivalent modelling from accompanying impedance data can provide valuable information in describing skin permeability that may contribute to a future calibration algorithm.

Chapter 5: Discussion

The experiments carried out on the *in vitro* cell together with those provided from *in vivo* experiments have shown some very interesting findings. As it will be seen the *in vitro* model chosen with the dialysis membrane approximates the skin well up to a certain limit. The extraction of either potassium ions or glucose can be modelled and the correlation with the impedance seems to be successful. *In vitro* results will be firstly discussed and then compared with *in vivo* results.

5.1. Potassium results

Before discussing the results in detail, it must be remembered that extraction of molecules into the electrodes are governed by three forces during reverse iontophoresis: passive diffusion, electromigration (active diffusion) and electro-osmotic flow. The details of these forces and accompanying equations are discussed in Chapter 2:, section 2.6.2. Extraction into all three electrodes, as discussed in section 2.6.2.1 are governed by passive diffusion (Equation 13), because the concentration in the solution is higher than in the gel the ions will be forced to cross the membrane towards the electrodes. Furthermore electrodes 1 and 2 will be also controlled by electromigration (Equation 15) and electro-osmotic solvent flow (Equation 16) which add the total of these forces give the final amount of potassium extracted.

The potassium concentration measured from *in vitro* experiments changed with extraction time. Firstly, it maintained at the same level for 2, 5 and 10 minutes in all 3 electrodes (because error bars made them lie within the same range) and then it increased again from 15 up to 60 minutes. Short extraction time's results vary slightly from those expected, as the amount of potassium extracted should increase gradually from the beginning. That difference could be due to the sensitivity of the sensor or any parameter in the method of extraction chosen. Between 2, 5 and 10 minutes there is not enough time difference to see the variation in potassium extracted and the difference cannot be measured. It should be remembered that the in

vitro experiment was constructed to mimic fasting conditions so low potassium and low glucose concentration was chosen. From 15 minutes upward the amount of potassium extracted lay within the capability of the technique, so results seems to be clearer. That observation is also in line with theory, which can be easily explained having a look at the electromigration equation (Equation 15) which depends on the time of extraction; the longer the time of extraction the more movement of ions there is.

Polarity on the electrodes also makes variations in the potassium extracted. When polarity is switched, electrodes 1 and 2 show the same amount of potassium extracted as would be expected.

Electrode 1 was the anode at all times for experiments 2, 5, 10, 15 and 30 → and half the time for experiments 30 ↔ and 60 ↔. The latter experiments change polarity every 15 minutes. Because of the polarity in electrode 1, in the first batch of experiments ions were discouraged to cross the membrane towards it and thus the concentration of potassium was lower; however experiments 30 ↔ and 60 ↔ present a similar result for electrodes 1 and 2 since half the time they changed polarity.

Electrode 2 was always the cathode in experiments 2, 5, 10, 15 and 30 →, and it was half the time cathode and half the time anode in experiments 30 ↔ and 60 ↔. The cathode attracts the positive ions, thus it attracted the potassium ions towards itself. As it was expected the potassium concentration in this electrode was higher than in any others. The phenomenon of attraction can also be seen when looking at experiments 30 → and 30 ↔ in Figure 23 *in vitro* results of potassium, the former extracted twice the amount of potassium than the latter as it maintained the polarity through the experiment.

However, electrode 3 is the diffusion electrode. The gel from this electrode collected the ions diffused passively across the membrane. The amount extracted in this electrode is the lowest since only one force out of three is acting.

These results confirm that the potassium is attracted to the cathode and repelled from anode as it was expected from theory. Besides, they confirm that it is field dependant, i.e., the active diffusion force is much stronger than the passive diffusion.

Also the difference in the amount of potassium extracted between electrodes shows the effects produced by adding the electromigration force to the existing passive diffusion.

The mathematical model fitted for electrode 2 which was shown to be linear, suggests that the potassium extracted depends on the extraction time and its behaviour becomes very predictable. The linearity of this model could be used for calibrating devices. Even, if any of the variables fixed to perform the experiments (potassium concentration in liquid or type of membrane) were changed the linear relationship would not be affected; those changes would affect the slope.

In vivo results show a similar behaviour to *in vitro* results. Electrode 2 shows a higher concentration than electrode 1 and 3, and increases with extraction time. Thus *in vitro* membrane seems to be a suitable representative of skin for the extraction of potassium. However, the difference of potassium extracted in electrode 3 in *in vivo* experiments is more pronounced than *in vitro*. Also the mathematical model of the membrane can be extended to *in vivo* cases with confidence. It can be observed in Figure 45 that the gradient is steeper (0.101 *in vivo* compared with 0.0059 *in vitro*), what suggests that the skin is more permeable than the membrane. However, electrodes 1 and 3 do not clearly show any pattern or dependency with time. Electrode 1 is governed by passive diffusion and electromigration. Passive diffusion will bring ions to the electrode, but electromigration will repel them. Electrode 3 is governed only by passive diffusion. Again, as in the *in vitro* case, the method chosen could not detect the difference of amount of potassium extracted within 2, 5 and 10 minutes experiments properly, but at 60 minutes the statistical increase clearly shows that it can be detected.

5.2. Glucose results

Results from glucose show less information than potassium. At first sight, each experiment followed the same pattern: concentration of glucose on electrode 1 was higher than on electrode 2 and the concentration on electrode 2 was higher than that on electrode 3. It must be reminded that glucose is a neutral molecule which is not

influenced by electromigration, thus there are 2 forces acting on it: passive diffusion and electroosmotic flow. Passive diffusion, which governs electrode 3, is consistent with the results as the results are lower on that electrode. However, electrode 2 (cathodal chamber), which is governed by electromigration and passive diffusion, should reach a higher concentration than electrode 1 (anodal chamber), but the results show the opposite, as it can be seen in Figure 26, which is unexpected. Despite the results being different from those expected, there seems to be consistency in the results. All experiments follow the same pattern so it was not random.

Having a look at the experiments through extraction times, experiments 2, 5 and 10 do not show an expected behaviour. From 15 minutes upward they increase slightly with duration of RI. That glucose pattern is similar to potassium in which results for 2, 5 and 10 minutes do now show any difference because they could not be detected through the methods chosen or with the equipment used. However, from 15 to 60 minutes there is an increase with extraction time which is expected. From that observation it could be suggested that when using RI with the chosen membrane, the experiments should be longer than 10 minutes in order to observe the correct behaviour of the extraction.

Glucose results *in vivo* were not available for 2, 5, 10, 15 and 30 minutes, so no comparative can be made. However, results for 60 minutes on 9 participants were available and show the same pattern as *in vitro* results, being glucose extracted higher in electrode 1 than in electrode 2 and 3. Taking into account that observation it could be confirmed that the membrane simulates the skin well. Again, results for glucose are unexpected according to the theory. The reason for this finding would need to be further investigated.

5.3. Impedance results

Impedance results for the *in vitro* cell seem to follow biological tissue patterns as it was expected from a membrane chosen to simulate skin.

Firstly, *Z*’ decreases with frequency. It has been suggested that the impedance at lower frequencies reflects the outermost layers of the skin like the epidermis and

higher frequencies reflect deeper tissue (Pang and DaPeng 2009). The differences in the results are according to theory.

Secondly, impedance decreases significantly after RI. The change of impedance suggests that RI changes the properties of the membrane and the skin making them more permeable and facilitating transport through the existing channels.

Thirdly, the difference in impedance before and after RI is greater at lower frequencies for a fixed time. The higher changes at low frequencies reflect the property changes of the outermost layers than the inner layers. The results suggest that the differences in impedance across the frequencies simulate the different layers of the skin. That could be due to the hydration of the membrane, being higher at the liquid interface than at the electrode interface.

Fourthly, the impedance trace is semi-circular curve. The Cole-Cole plot is representative of the biological tissue behaviour of the skin. And the membrane's trace displays the same graph what seems to reflect a good simulation of skin.

Fifthly, Z' decreases after RI and it is more pronounced with longer durations for a fixed frequency. That is also expected as the longer the experiment is applied the more pronounced the effect on the skin and the membrane.

Finally, *in vivo* results show the same behaviour as *in vitro* results, but values are much higher *in vivo*. E.g., at 1 Hz *in vitro* is in the order of 1 KΩ while *in vivo* it is in the order of 1 MΩ.

5.4. Electrical skin model

The results obtained for the components of the model proposed (Figure 7 model A) also agree with the theory of the circuit and the graphical representation of the Cole-Cole plot. The membrane represents the outermost layers of the skin and the solution underneath internal layers. As the solution will not change significantly over time it will be represented by a fixed component. That was calculated as R_s which can be seen in Figure 37 and does not change. On the other hand, the membrane, whose properties are disturbed with the application of reverse iontophoresis during a fixed

time, shows variation in both components R_p and C. That is represented in Figure 37 and Figure 39. R_p decreases exponentially along time with the application of RI. Up to 10 minutes it decreases sharply, reaching 5% of the original value, and then it decreases slowly in a linear fashion, reaching 2% of the original value at 60 minutes. That makes one think that RI have a huge impact during the first 10 minutes in permeability (decreases 95%), but after that the changes it produces are hardly noticeable. Therefore, short durations of RI (up to 10 minutes) might be sufficient to enhance transport of molecules across skin. In that situation it would be desirable to know the time of recovery of skin in order to maintain such permeability. The calculated value for capacitance, C, not only reflects the variation produced by the reverse iontophoresis but also the changes produced between different extraction times. The value of C increases with increasing extraction times. This suggests that the capacitance properties of the membrane are altered due to the application of a DC current.

5.5. Time constant

The values of R_p and C were used to calculate the time constant for the membrane and for skin. The data shown in Table 12 (Chapter 4:) are the calculated time constants for the membrane experiments. The value of the time constant changes with the application of RI. This suggests that the time constant may reflect changes in the membrane's properties due to the application of the reverse iontophoresis. A low time constant means a short capacitance. Thus an increase in capacitance will increase the time constant of the membrane too. It can be calculated using Equation 6.

The time constant values calculated for human skin *in vivo* are different from those *in vitro*. In the *in vivo* case the time constant decreases after the application of RI. It is unclear why the apparent behaviour of the time constant is different in the *in vitro* and *in vivo* case.

5.6. Potassium – Impedance relationship

Finally, the relationship between the potassium extracted and R_p or C confirms the analysis performed. Figure 40, Figure 59 and Figure 61 show that the resistive part opposes the flow of ions, impeding the passage, while Figure 41, Figure 60 and Figure 62 show that the capacitive part appears to facilitate the flow of ions. These results merit further work to further refine the relationship between skin and membrane resistance and the extraction rate of potassium. This result is likely to make an important contribution in calibrating ion flux though human skin *in vivo* to account for the high degree of variation observed.

Chapter 6: Conclusions

The study sought to construct an in vitro experiment for the extraction of potassium and glucose to accompany an existing in vivo experimental data set previously gathered. The aims of the project were as follows:

- Construct and carry out an *in vitro* study for comparison with the existing *in vivo* studies.
- Determine, if any, and model the extraction behaviour of potassium and glucose *in vitro* and *in vivo.*
- Compare the extraction behaviour *in vitro* and *in vivo* for potassium and glucose and comment on the suitability of the *in vitro* synthetic membrane as an artificial skin membrane.
- Analyse the impedance of the *in vitro* synthetic membrane and analyse the impedance of the skin *in vivo* in response to reverse iontophoresis, comparing and contrasting the results.
- Use the impedance data to model the characteristics of the *in vitro* synthetic membrane and human skin *in vivo.*
- Use modelled parameters, or other parameters, to describe the extraction rate of potassium and glucose *in vivo* and *in vitro.*

The results of this project have successfully investigated these aims and have produced some very interesting and worthwhile results as has been discussed. The main conclusions of the study can be summarised as follows:

The *in vitro* arrangement constructed mimicked the *in vivo* study well. The synthetic membrane chosen appeared to possess many of the characteristics of human skin. This was shown when the potassium extraction behaviour was modelled across the membrane and the skin, in both cases the potassium extraction could be well approximated by a linear relationship with time. The quantity of potassium extracted through the membrane by diffusion was very similar to that extracted through the skin for a given time period. However, there was almost ten times the amount of

potassium extracted across skin by reverse iontophoresis compared with the membrane. This demonstrates a potential limit to the *in vitro* arrangement.

Similarly the extraction behaviour of glucose across the membrane was very similar to the extraction of glucose across skin. This supports the use of the membrane as an artificial skin substitute for future in vitro experiments.

The extraction behaviour of potassium across the membrane and across skin was successfully modelled and a linear relationship with time is suggested as a suitable approximation for extraction times up to 60 minutes.

The impedance data was analysed and the trends in impedance data with respect to frequency were noted. In particular the decrease in impedance with increasing frequency was identified as important as higher frequencies may represent deeper layers of tissue. Again, the synthetic membrane and human skin exhibited a similar frequency dependence, although the absolute impedance values for skin were always much higher than the membrane.

An electrical equivalent circuit model was successfully used to model both the membrane and the skin. The components of this model were extracted and analysed. The behaviour of these components operated in accordance with what would be expected in theory.

Impedance measurements were used to demonstrate the impact of iontophoresis on the membrane and skin. This impact shows a rapid decrease in the skin (and membrane) resistance in the first 10 minutes of application reducing to approximately 95% of the original value in the case of human skin. This is an important result as this suggests that the skin resistance stabilises after this point.

Skin (and membrane) resistance were linked to potassium extraction with a linear correlation. Although the coefficient of correlation was not strong, the relationship between skin resistance and potassium extraction is as would be expected in theory. This result strongly suggests that skin resistance may be a good indicator of skin permeability.

Chapter 7: Future work

The results from this study have produced some very interesting findings and have largely addressed the objectives of the study. However, given the large data set and limited time, there is scope to extend this study in many directions. Firstly, further analysis could be performed to examine more advanced modelling techniques or investigating additional parameters to use in conjunction with skin resistance when establishing a basic calibration algorithm for human skin.

Experimentally, the *in vitro* experimental arrangement could be further refined. For instance several types of membranes could be used to simulate the different kind of skins. This could account for the variability along the body or reproduce the difference between races, gender, age or healthy state of the skin. A second variable could be the temperature under which the tests are performed. As materials dilate under higher temperatures so do the pores in the membranes and thus reproduces the physiological changes in the skin. The use of different concentrations is a very reasonable parameter to consider. In particular using higher concentration in the *in vitro* cell may allow the extraction at short time points (2, 5 and 10 minutes) to be characterised. Interstitial fluid in any human is in constant change due to the metabolism of the cells. So the variation in concentrations not only would account for the metabolism but also would help to relate the effects on the concentration of ions and molecules.

Other part of the future work is closer to the measurement devices used. A self-contained sensor capable of measuring potassium concentration or other ion concentration would help to avoid introduction of error during the stages of the experiment. A self-contained multi sensor would introduce a very suitable advance into the development of the process.

The properties of the membrane should be further analysed in order to find out why the concentration of potassium ions diffused is higher through the membrane than through the skin. As well as the method used to measure the glucose. It may need to be reviewed for future analysis.

References

Amir, O., D. Weinstein, et al. (2007). "Continuous noninvasive glucose monitoring technology based on "occlusion spectroscopy"." J Diabetes Sci Technol **1**(4): 463-469.

Ballerstadt, R., A. Gowda, et al. (2004). "Fluorescence resonance energy transfer-based near-infrared fluorescence sensor for glucose monitoring." Diabetes Technol Ther **6**(2): 191-200.

Barbero, A. M. and H. F. Frasch (2009). "Pig and guinea pig skin as surrogates for human in vitro penetration studies: a quantitative review." Toxicol In Vitro **23**(1): 1-13.

CalistoMedical. (2011). "Glucoband." from http://www.calistomedical.com/.

Chang, D. C. (1989). "Cell poration and cell fusion using an oscillating electric field." Biophysical journal **56**(4): 641-652.

Chen, B., J. Wei, et al. (2010). "Sonophoretic enhanced microneedles array (SEMA)--Improving the efficiency of transdermal drug delivery." Sensors and Actuators B: Chemical **145**(1): 54-60.

Ching, T. S. and P. Connolly (2008). "Simultaneous transdermal extraction of glucose and lactate from human subjects by reverse iontophoresis." Int J Nanomedicine **3**(2): 211-223.

Chizmadzhev, Y. A., A. V. Indenbom, et al. (1998). "Electrical properties of skin at moderate voltages: contribution of appendageal macropores." Biophys J **74**(2 Pt 1): 843-856.

Chu, M. and N. Kollias (2011). "Documentation of normal stratum corneum scaling in an average population: features of differences among age, ethnicity and body site." Br J Dermatol **164**(3): 497-507.

Cook, C. J. (1997). "Real-time measurements of corticosteroids in conscious animals using an antibody-based electrode." Nat Biotechnol **15**(5): 467-471.

Cook, C. J. (2002). "Rapid noninvasive measurement of hormones in transdermal exudate and saliva." Physiology & Behavior **75**(1-2): 169-181.

Costello, C. T. and A. H. Jeske (1995). "Iontophoresis: applications in transdermal medication delivery." Phys Ther **75**(6): 554-563.

Coston, A. F. and J. K. J. Li (2001). "Iontophoresis: Modeling, Methodology, and Evaluation." Cardiovascular Engineering **1**(3): 127-136.

Cox, M. "An Overview of Continuous Glucose Monitoring Systems." Journal of Pediatric Health Care **23**(5): 344-347.

Curdy, C., Y. N. Kalia, et al. (2001). "Non-invasive assessment of the effects of iontophoresis on human skin in-vivo." J Pharm Pharmacol **53**(6): 769-777.

Das, D. (1978). Biochemistry, Academic Publishers.

Davies, D. J., R. J. Ward, et al. (2004). "Multi-species assessment of electrical resistance as a skin integrity marker for in vitro percutaneous absorption studies." Toxicol In Vitro **18**(3): 351-358.

Degim, I. T., S. Ilbasmis, et al. (2003). "Reverse iontophoresis: a non-invasive technique for measuring blood urea level." Pediatr Nephrol **18**(10): 1032-1037.

Diridollou, S., D. Black, et al. (2000). "Sex- and site-dependent variations in the thickness and mechanical properties of human skin in vivo." International Journal of Cosmetic Science **22**(6): 421-435.

Elden, H. R. e. (1971). A treatise of skin vol 1 biophysical properties of the skin. [S.l.], Wiley interscience.

Elias, P. M. (1983). "Epidermal lipids, barrier function, and desquamation." J Invest Dermatol **80**(1 Suppl): 44s-49s.
Elias, P. M., N. S. McNutt, et al. (1977). "Membrane alterations during cornification of mammalian squamous epithelia: a freeze-fracture, tracer, and thin-section study." Anat Rec **189**(4): 577-594.
Escobar-Chavez, J. J., D. Bonilla-Martinez, et al. (2009). "The use of sonophoresis in the administration of drugs throughout the skin." J Pharm Pharm Sci **12**(1): 88-115.
FDA (2001). GlucoWatch Automatic Glucose Biographer. D. o. H. H. Services. Rockville, Food and Drug Administration.
Frances, C., M. C. Branchet, et al. (1990). "Elastic fibers in normal human skin. Variations with age: a morphometric analysis." Arch Gerontol Geriatr **10**(1): 57-67.
Gabriely, I., R. Wozniak, et al. (1999). "Transcutaneous glucose measurement using near-infrared spectroscopy during hypoglycemia." Diabetes Care **22**(12): 2026-2032.
Giacomoni, P. U., T. Mammone, et al. (2010). "Gender-linked differences in human skin." Journal of dermatological science.
Gioia, F. and L. Celleno (2002). "The dynamics of transepidermal water loss (TEWL) from hydrated skin." Skin Research and Technology **8**(3): 178-186.
Glickman, Y. A., O. Filo, et al. (2003). "Electrical impedance scanning: a new approach to skin cancer diagnosis." Skin Res Technol **9**(3): 262-268.
Goldsmith, L. A. (1983). Biochemistry and physiology of the skin. New York ; Oxford, Oxford University Press.
Hadgraft, J. (2004). "Skin deep." Eur J Pharm Biopharm **58**(2): 291-299.
Harding, C. R. (2004). "The stratum corneum: structure and function in health and disease." Dermatol Ther **17 Suppl 1**: 6-15.
Howard, J. P., T. R. Drake, et al. (1995). "Effects of alternating current iontophoresis on drug delivery." Arch Phys Med Rehabil **76**(5): 463-466.
Hui, S. W. (1998). "Low voltage electroporation of the skin, or is it iontophoresis?" Biophys J **74**(2 Pt 1): 679-680.
IDF. (2011). "International Diabetes Federation." from http://www.idf.org.
Kost, J., S. Mitragotri, et al. (2000). "Transdermal monitoring of glucose and other analytes using ultrasound." Nat Med **6**(3): 347-350.
Kyle, U. G., I. Bosaeus, et al. (2004). "Bioelectrical impedance analysis--part I: review of principles and methods." Clinical Nutrition **23**(5): 1226-1243.
Lavon, I. and J. Kost (2004). "Ultrasound and transdermal drug delivery." Drug Discov Today **9**(15): 670-676.
Leboulanger, B., R. H. Guy, et al. (2004). "Non-invasive monitoring of phenytoin by reverse iontophoresis." Eur J Pharm Sci **22**(5): 427-433.
Leboulanger, B., R. H. Guy, et al. (2004). "Reverse iontophoresis for non-invasive transdermal monitoring." Physiol Meas **25**(3): R35-50.
Lykken, D. T. (1970). "Square-wave analysis of skin impedance." Psychophysiology **7**(2): 262-275.
Madison, K. C., D. C. Swartzendruber, et al. (1987). "Presence of intact intercellular lipid lamellae in the upper layers of the stratum corneum." J Invest Dermatol **88**(6): 714-718.
Martini, F., J. L. Nath, et al. (2009). Fundamentals of anatomy & physiology. San Francisco ; London, Pearson/Benjamin Cummings.
Martinsen, O. G. and S. Grimnes (2001). "Facts and myths about electrical measurement of stratum corneum hydration state." Dermatology **202**(2): 87-89.
Martinsen, O. G., S. Grimnes, et al. (2002). Interface Phenomena and Dielectric Properties of Biological Tissue. Encyclopedia of Surface and Colloid Science.

McShane, M. J. (2002). "Potential for glucose monitoring with nanoengineered fluorescent biosensors." Diabetes Technol Ther **4**(4): 533-538.
Michaels, A. S., S. K. Chandrasekaran, et al. (1975). "Drug permeation through human skin: Theory and invitro experimental measurement." AIChE Journal **21**(5): 985-996.
Mitragotri, S., D. Blankschtein, et al. (1996). "Transdermal drug delivery using low-frequency sonophoresis." Pharm Res **13**(3): 411-420.
Mize, N. K., M. Buttery, et al. (1997). "Reverse iontophoresis: monitoring prostaglandin E2 associated with cutaneous inflammation in vivo." Exp Dermatol **6**(6): 298-302.
Morganti, P., E. Ruocco, et al. (2001). "Percutaneous absorption and delivery systems." Clin Dermatol **19**(4): 489-501.
Nicander, I. and S. Ollmar (2004). "Clinically normal atopic skin vs. non-atopic skin as seen through electrical impedance." Skin Res Technol **10**(3): 178-183.
Orsense. (2011). "NBM-200G." from http://www.orsense.com/Glucose.
Pang, G. K. H. and Q. DaPeng (2009). Skin impedance models for transdermal drug delivery. Mechatronics and Automation, 2009. ICMA 2009. International Conference on.
Phillips, M., J. Greenberg, et al. (1995). "Evaluation of the Alcopatch, a Transdermal Dosimeter for Monitoring Alcohol Consumption." Alcoholism: Clinical and Experimental Research **19**(6): 1547-1549.
Pliquett, U., R. Langer, et al. (1995). "Changes in the passive electrical properties of human stratum corneum due to electroporation." Biochim Biophys Acta **1239**(2): 111-121.
Potts, R. O. and R. H. Guy (1995). "A predictive algorithm for skin permeability: the effects of molecular size and hydrogen bond activity." Pharm Res **12**(11): 1628-1633.
Prausnitz, M. R. (2004). "Microneedles for transdermal drug delivery." Adv Drug Deliv Rev **56**(5): 581-587.
Prausnitz, M. R., E. R. Edelman, et al. (1995). "Transdermal delivery of heparin by skin electroporation." Biotechnology (N Y) **13**(11): 1205-1209.
Sieg, A., R. H. Guy, et al. (2004). "Electroosmosis in transdermal iontophoresis: implications for noninvasive and calibration-free glucose monitoring." Biophys J **87**(5): 3344-3350.
Solartron. (2011). from www.solartronanalytical.com.
Timm, U., E. Lewis, et al. (2009). "Sensor System Concept for Non-Invasive Blood Diagnosis." Procedia Chemistry **1**(1): 493-496.
Tregear, R. T. (1966). Physical functions of skin. London ; New York, Academic Press.
Wang, P. M., M. Cornwell, et al. (2005). "Minimally invasive extraction of dermal interstitial fluid for glucose monitoring using microneedles." Diabetes Technol Ther **7**(1): 131-141.
Wascotte, V., M. B. Delgado-Charro, et al. (2007). "Monitoring of urea and potassium by reverse iontophoresis in vitro." Pharm Res **24**(6): 1131-1137.
Yamamoto, T. and Y. Yamamoto (1977). "Analysis for the change of skin impedance." Med Biol Eng Comput **15**(3): 219-227.
Yan, G., Q. Xu, et al. (2008). "Alternating current (AC) iontophoretic transport across human epidermal membrane: effects of AC frequency and amplitude." Pharm Res **25**(3): 616-624.

Appendices

Appendix A. List of materials used for the experiments

Experiments *In vitro*

Material/Device	Manufacturer	Model
½ L Airtight glass flask	Fisherbrand	FB33146
½ L Beaker	Fisherbrand	FB33113
½ L Measuring cylinder	Fisherbrand	FB55213
1 L Airtight glass flask	Fisherbrand	FB33147
1 L Beaker	Fisherbrand	FB33115
1 L Cylinder	Fisherbrand	1000:10 ml
10 ml Measuring cylinder	Fisherbrand	FB55203
100 ml Measuring cylinder	Azlon	100:1
10, 100, 5000 µl, 10 ml tips	epT.I.P.S.	Eppendorf Tips
250 ml beaker	Kartell	250 ml
50 ml Measuring cylinder	Fisherbrand	FB55207
500-5000µL Pipette	Eppendorf	Research
7 ml Bijou container	Greiner Bio-one	7 ml Bijou tube
96-well plate	Sterilin	Single *in vitro* use
96-well plate reader	Labsystem	Multiskan Ascent
Acetate (Acetyl sheet)	Niceday, UK	MA10
Alarm clock	-----	-----
Allen key	-----	4 mm
Anisotropic dialysis membrane	SPECTRUM	Spectra/Por
Battery operated power stirrer	Stuart Scientific	-----
BNC cables	-----	-----
BNC-banana connector cables	-----	-----
Carbon ink	Electrodag	PF-407A
Conical base tube	Fisher Scientific	30 ml
Deionized water	ELGA	Purelab Option
DEK Screen Printing Machine	DEK	Model 247
Dielectric paste	Creative Materials	113-35
Driller with adaptor for holes	RS	254844
Dropper	-----	-----
Electrode Mask	-----	-----
ELIT interface	ELIT	9801

Extracting pipette	Gilson Distriman	CL10010
Face mask	Sundstrom	SR 90-2 Type S/M
Face mask filter	Sundstrom	Ax SR 298
Gloves	Semperguard	Nitrile powder free
Glucose (MW = 180.2)	SIGMA	G-8270
Glucose oxidase enzyme reagent	Randox	GOD-PAP GL2623
Goggles	-----	------
HEPES (2 Hydroxyethylpiperazine 2ethanesulfonic acid)	SIGMA	H3375
Impedance interface	Solartron	1294
Impedance/gain-phase analyser	Solartron	SI1260
In vitro cell	-----	Custom
Ion Selective Electrode (ISE) software	ISE pH Ion Analyser	-----
Magnetic stirrer	Fisher Scientific	
Methocel methylcellulose powder	Dow	A4M PREM
Multipipette	Eppendorf	Multipippette plus
Pace 250 filter unit	-----	-----
Para-film	Pechiney Plastic Packaging	Parafilm “M”
pH meter	Fisherbrand	Hydros300
Plastic gasket	-----	-----
Potassium chloride (KCl) (MW = 74.56)	Fisher BioReagents	BPE366-500
Potassium Ion Selective Electrode	-----	Potassium K^+
PTFE	Gilbert Curry Ind.	-----
Reverse iontophoresis device	Crombie Anderson	Custom made
Rubber gloves	Mariglod Industrial	Type 12M, BS 164:1986
Scale	Mettler Toledo	AB104-S/Fact
Scissors	-----	-----
Screwdriver	-----	-----
Silver ink	Electrodag	PF-410
Silver/Silver chloride ink	Electrodag	6037 S
Sodium chloride (NaCl) (MW = 58.42)	SIGMA-ALDRICH	S7653
Sodium hydroxide (NaOH)	-----	-----
Sodium phosphate	SIGMA	S-2554

monobasic, USP (NaH_2PO_4) (MW = 119.98)		
Solution to keep membrane	0.1% sodium azide	-----
Syringe with adaptor lead	BD Plastipak	60 ml
Tissue paper	-----	-----
Toupe tape	Sensi-TAK	-----
Vortex mixer	Fisons	WhirliMixer
Wash bottle filled with acetone	-----	-----
Water bath	Omega Media	Prestige Medical
ZPlot	Solartron	-----
ZView2	Solartron	-----

Table 18: Materials used for in vitro experiments

Note:

- ----- stands for a generic manufacturer/model. Any manufacturer or model could be used.

Appendix B. Preparation of materials

Electrodes

Equipment and material used to screen print single electrodes using the DEK semi-automated printing machine:

Description	**Quantity**
DEK Screen Printing Machine	1
Electrode Mask	1
Wash bottle filled with acetone	1
Rubber gloves	2
Face mask	1
Face mask filter	1
Goggles	1
Pace 250 filter unit	1
Acetate	As many as required
Silver ink	1
Silver/Silver chloride ink	1
Carbon ink	1
Dielectric paste	1
Screwdriver	1
Drill with adaptor	1
PTFE	As necessary
Toupee tape	As necessary
Scissors	1

Table 19: Materials used for preparation of electrodes

Method:

Part 1: screen printing of electrodes

1. Secure the machine making sure the wheels are up and the foot switch is accessible but unlikely to be stood on accidentally.
2. Prepare the mask by screwing the 4 spacers onto the metal mask frame. Then push the screen into the screen mount. To do this clip the right hand side in first as it is spring loaded. Once the screen has been clipped and pushed in fully, pull down the screen lock to hold the screen in place.
3. Prepare the machine. Lift the viewing window and unclip the rod (strut) from under the left hand side of the lid and place the end in the hole below to

support the lid in an open position. After this, put on the flood blade onto the mount (this clips on either side). Then screw the squeegee on to the mount over the flood blade. Shut the lid. Use the height adjust screw for the plate (located on the left hand side of the machine) left hand screw to move the plate down so it can move under the screen without colliding with the screen or housing. Turn on the power.

4. Set height and perform a practice run. Flood mode should always be selected. The pressure level should be set to a low number (<8) when the practice sun is done dry. Select jog mode. This performs the movements in sections. Press the front JOG button to move the plate under the screen. Use the plate height adjust screw to move the plate up under the screen until it almost touches. Zero the measuring display by pressing ON and MODE. Move the plate back down by 1mm using the plate height screw adjuster. Press the front JOG button to perform a complete test run. During this check that the area that the squeegee covers over the mask prints and that theses coincide with the area of the plate that the acetate will be held.
5. Printing the first layer. Put an acetate on the plate (set reference corner if doing more than one layer to ease lining up later). All other air holes should be covered with black electrical insulation tape to provide a maximum amount of negative pressure. Take off the squeegee. Transfer some ink (e.g. Ag/AgCl) onto the screen in front of the flood blade and spread it the width of the mask pattern. Put the squeegee back on. Set the pressure to the level required. Close the lid. Turn off the JOG button on the main panel. Press the foot pedal to start the automatic process. Load a new acetate and repeat the print as many times as required.
6. Cleaning the mask. When printing is finished, the excess ink on the screen can be gathered and returned to the ink tub. The mask, squeegee, flood blade and other equipment undesirably coated in ink should be cleaned with acetone. It is important to ensure that the holes in the mask are completely cleared of ink if the mask is to be used again. When cleaning the mask the door to the adjacent lab should be shut and the window leading outside

should be open. A face mask should be worn with an appropriate filter. A form of air filtration or extraction should be used with appropriate filter.

Notes:

- Inks should be stored as per manufacturer instructions.
- Electrodes should be kept in sealed bag or box and kept in the dark.

Part 2: Mounting of electrodes

1. Cut a stripe of PTFE, widen enough to cover the electrode (~2.5 cm).
2. Stick toupee tape on both sides of the stripe of PTFE.
3. Makes holes in the stripe using the drill with the adaptor every 3 cm.
4. Cut the stripe into bits so there is a hole for each electrode.
5. Cut the electrodes from the acetate and stick them to the bits of PTFE with toupee tape.
6. Keep the electrodes in a sealed bag for later use.

Phosphate Buffer

Equipment and material used to prepare 1 litre of 0.1 M sodium phosphate buffer solution pH 7.4 for use in reverse iontophoresis experiments:

Description	**Quantity**
1 L Beaker	1
1 L Measuring cylinder	1
Magnetic stirrer	1
pH meter	1
Dropper	1
1 L Airtight glass flask	1
Gloves	2
Scale	1
Sodium phosphate monobasic, USP (NaH_2PO_4)	11.99g
Deionised water	Sufficient to rinse containers
Sodium hydroxide (NaOH)	As required

Table 20: Materials used for preparation of phosphate buffer

Method

1. Weigh 11.99 g of sodium phosphate with the help of the scale
2. Add the sodium phosphate monobasic (USP grade) powder to about 750 ml deionised water in beaker, whilst stirring with magnetic stirrer.
3. Add sodium hydroxide, using a dropper, to the beaker until a pH of 7.4 has been reached.
4. Add deionised water to the buffer solution to make it up to a volume of 1 litre. Store into a sterile, 1L airtight glass flask and keep in the fridge.

Notes:

- Store at 4 ºC in sealed glass flask
- Avoid contact of sodium hydroxide with skin and eyes. In case of contact, wash with ample volume of water.
- Discard remaining solution after 5 days.

Hydrogel

Equipment and material used to prepare 100 mg of 4% (w/v) Methylcellulose hydrogel:

Description	**Quantity**
250 ml Beaker	1
100 ml Measuring cylinder	1
Battery operated power stirrer	1
Water bath set to 80 ºC	1
Para-film	Sufficient to cover the beaker
0.1 M Phosphate buffer solution pH 7.4	100 ml
Methocel methylcellulose powder	4 g
Gloves	2
Scale	1

Table 21: Materials used for preparation of hydrogel

Method

1. Heat 30 ml of 0.1 M phosphate buffer solution to 80 ºC using water bath.
2. Add 80 ºC 0.1 M phosphate buffer solution to a beaker containing 4 g of methylcellulose powder.

3. Stir using battery-operated power stirrer until all of the powder has been wetted thoroughly and an even consistency of paste is obtained
4. Add the remaining 70 ml of 0.1 M phosphate buffer solution at room temperature to the paste, whilst stirring.
5. Continue stirring until an even gel has been obtained and the gel has been brought down to room temperature.
6. Cover beaker in Para-film and store overnight at 4 ºC.
7. Transfer the hydrogel to syringes to improve shelf-life.

Note: in order to alter w/v of hydrogel, use the following mass of Methylcellulose powder:

w/v of hydrogel	**Methylcellulose powder**
2%	2.0 g
3%	3.0 g
4%	4.0 g
5%	5.0 g
6%	6.0 g

Table 22: Quantity of methylcellulose powder necessary to prepare hydrogel in different concentrations

Notes:

- Gel must be kept in fridge to increase its life. Discard after 6 weeks.
- Keep syringes as sealed as possible to prevent dehydration of the gel.

<u>HEPES Buffer</u>

Equipment and material to prepare 1 L of HEPES buffer pH 7.4 containing 25 mM HEPES, 133 mM NaCl, 4 mM of KCl and 5 mM of glucose:

Description	**Quantity**
1 L Cylinder	1
1 L Beaker	1
1 L Airtight glass flask	1
Magnetic stirrer	1
pH meter	1
Scale	1
HEPES (2 Hydroxyethylpiperazine 2ethanesulfonic acid)	5.96 gr
Sodium chloride (NaCl) (MW = 58.42)	7.77 gr

Sodium hydroxide (NaOH)	As necessary to get pH 7.4
Potassium chloride (KCl) (MW = 74.56)	0.298 gr
Glucose (MW = 180.2)	0.901 gr
Dropper	1

Table 23: Materials used for preparation of HEPES buffer

Method

1. Weigh out solutes: HEPES, sodium chloride, potassium chloride and glucose.
2. Add less than 1 litre of deionised water into beaker.
3. Pour solutes into the deionised water.
4. Place the beaker onto the magnetic stirrer to dissolve solutes.
5. Insert pH meter lead into the beaker.
6. While stirring add sodium hydroxide, drop wise, until pH 7.4.
7. With the aid of the 1 L cylinder add deionised water until 1L.
8. Pour the solution into a sterile, 1 L airtight glass flask.

Notes:

- The solution should be store at +4 ºC, in sealed, sterile glass flask and used within 5 days.
- Avoid any contact of sodium hydroxide with skin and eyes. It can be irritating. In case of contact wash immediately with copious amount of water.

Phosphate Buffer with 10 mM KCl

Equipment and material used to prepare ½ litre of 0.1 M sodium phosphate buffer solution pH 7.4 containing 10 mM of KCl for use in reverse iontophoresis experiments:

Description	**Quantity**
½ L Beaker	1
½ L Measuring cylinder	1
Magnetic stirrer	1
½ L Airtight glass flask	1
Gloves	2
Scale	1

Potassium chloride (KCl) (MW = 74.56)	0.3728 g

Table 24: Materials used for preparation of phosphate buffer with KCl

Method

1. Weigh out potassium chloride.
2. Pour ½ L of phosphate buffer into beaker.
3. Place beaker onto the magnetic stirrer and add potassium chloride.
4. Store in a sterile, ½ L airtight glass flask.

Notes:

- Store at 4 ºC in sealed glass flask and discard remaining solution after 5 days.

Membrane

Specifications of the membrane

Specification	**Value**
Membrane type	Symmetric Cellulose Ester
MWCO	100-500 Daltons
Physical appearance	Opaque, Rigid
Organic solvent tolerance	Fair
Packaging	Wet with 0.1% sodium azide
Flat width	31 mm
Diameter	20 mm
Vol/length	3.1 ml/cm
Length	10 m
Thickness	0.003 inches
Stable in pH range	5-9

Table 25: Specifications of the dialysis membrane used

Equipment and material used to prepare the membrane:

Description	**Quantity**
Membrane	Length enough to cover cell
0.1% Sodium azide	Enough to keep the membrane
Scissors	1
Deionised water	Sufficient to rinse the membrane
Gloves	2

Table 26: Materials used for preparation of the membrane

Method

1. Cut a length of membrane from the stock so that is sufficient to cover the *in vitro* cell.
2. Cut one of the edges of the membrane and unfold it with care.
3. Rinse the membrane with deionised water.
4. Stretch the membrane to cover the *in vitro* cell (see *In vitro* cell preparation for further details).

Note: once prepared keep membrane in deionised water if not used immediately as it dehydrates easily.

Notes:

- Discard the piece of membrane after use.

In vitro Cell

Equipment and material used to prepare the cell:

Description	**Quantity**
In vitro cell	1
Allen key 4 mm	1
Plastic gasket	2
Membrane	1
HEPES buffer	138 ml approx.
Syringe with adaptor lead	1
Deionised water	Sufficient to rinse the cell
Tissue paper	Sufficient to dry the cell
Gloves	2

Table 27: Materials used for preparation of the in vitro cell

Method

1. Rinse cell and all of its components with deionised water and dried it with tissue paper carefully.
2. Place one plastic gasket on top of the cell chamber.
3. Position the unfolded membrane on top of the gasket. The membrane must be kept as tense as possible to avoid any wrinkles.

4. Place another plastic gasket on top of the membrane.
5. Place the top frame of the cell chamber onto the upper plastic gasket.
6. Use both metallic sides to fix and tighten the cell chamber.
7. Use screws to create a tight seal.
8. Fill the cell with HEPES buffer using syringe and adaptor lead. Make sure there are no bubbles inside as they can interfere with the extracting process.
9. Rinse with deionised water to remove any possible particle and pat dry.

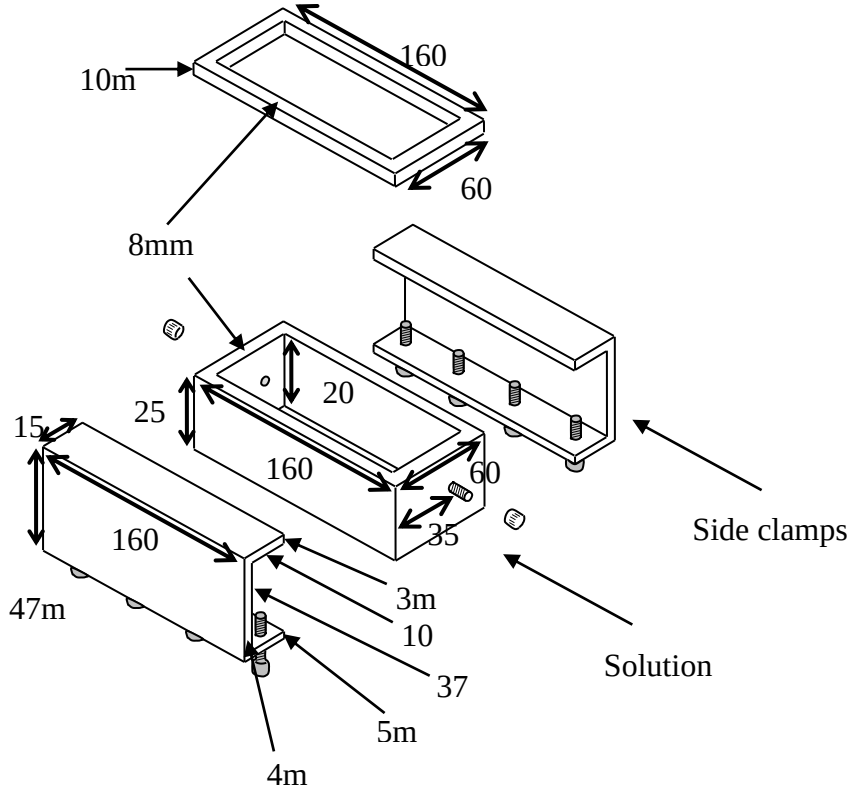

Figure 65: Diagram of in vitro cell with dimensions

Notes:

- *In vitro* cell must be kept clean and dried after use to prevent contamination and oxidation.

<u>1260/1294 Impedance Interface</u>

Equipment and material used to perform impedance measurements *in vitro* with the dialysis membrane.

Description	Quantity
Isolation Transformer to power all devices used	1
PC with Solartron SMART Software	1
Solartron 1260 Frequency Response Analyser	1
Solartron 1294 Human Interface	1
BNC – BNC cables	4
Standard male-female 25 pin parallel cable	1
Standard GPIB cable	1
1294 specialist loaded leads (BNC - banana plug) non-bio (non-current limited)	4
1294 specialist loaded leads (BNC - banana plug) bio (current limited)	4
12941 Test module	1
Custom built bridging box	1
Parallel cable sensor leads	1

Table 28: Materials used for performance of membrane impedance

Method:

1. With all unplugged devices, connect cables between the modules.
2. Use the standard GPIB cable to connect Solartron 1260 Frequency Response Analyser to PC.
3. Use the BNC – BNC cables to connect the 1260 to 1294 as indicated in the table below:

1260 front panel	1294 rear panel
Gen	Gen
V1 Hi	V1 Hi
V1 Lo	V1 Lo
V2 Hi	V2 Hi

Table 29: Configuration of BNC cables between 1260 unit and 1294 unit

4. Make sure the cables are connected to the current limited panel when performing *in vivo* experiments.
5. Use the standard male-female 25 pin parallel cable to connect PC to the 1294.
6. Use the specialist loaded leads to connect 1294 to custom built bridging box.
7. Use the parallel cable sensor leads to connect the bridging box to the sensor electrodes.
8. Plug PC, monitor, 1260 and 1294 to the isolation transformer.
9. Switch on the isolation transformer.

10. Run software and set properties to:
    a. Range of frequencies: 1 Hz to 1 MHz.
    b. Voltage: 200 mV
    c. Impedance interface: 1294
    d. Human interface: 1260

If the unit needs to be calibrated the 12941 Test module should be used.

1. Connect the test module to the non-biological panel of the 1294.
2. Configure software to perform a frequency sweep from 1 Hz to 1 MHz at amplitude of 0.1 mV.
3. Run the test.
4. A similar graph should be obtained:

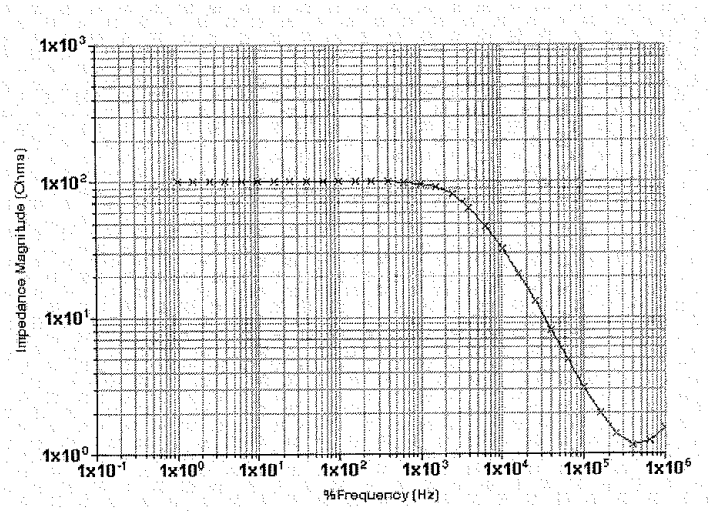

Figure 66: Typical bode plot expected if the 1294/1260 arrangement is used correctly with the 12941 test module as described in the 1294 manual

Notes:

- All main powered instrumentation used must be powered through an isolation transformer.
- When in use nothing should be connected to the non-biological panel.

Reverse Iontophoresis Device

Equipment and material needed for the usage of the reverse iontophoresis device

Description	Quantity
AA batteries	4
Reverse iontophoresis device	1
Alarm clock	1

Table 30: Material needed for the use of the reverse iontophoresis device

Method:

1. Program device for the correct timing (up to 60 minutes), polarity of operation (switched or direct) and intensity (~0.3 mA).
2. Insert charged batteries.
3. Connect cables.
4. Switch it on.
5. Once finished, switch it off.

Notes:

- An alarm clock is recommended to be used when operating the reverse iontophoresis device.

Potassium Flow Plus Ion Selective Electrode (ISE)

Equipment and material needed to prepare the potassium flow plus ion selective electrode for its usage:

Description	Quantity
Potassium Ion Selective Electrode	1
ELIT interface (conditioning + software)	1
Solutions for calibration	10
Vortex mixer	1

Table 31: Material used for preparation of Potassium ISE

Method:

1. Switch on the ELIT interface and start running the software.
2. Mix solutions using the vortex mixer.

3. Immerse the electrode into the highest potassium concentration solution for 10 minutes and write down the value.
4. Wash the electrode in deionised water.
5. Immerse electrode into the lowest potassium concentration solution prepared for the calibration. Keep for 3 minutes and write down the value.
6. Wash the electrode in deionised water to avoid cross-contamination.
7. Repeat steps 4 and 5 for the other increasing concentrations until the highest is reached again.
8. Repeat the calibration twice starting with the lowest concentration.
9. Once it has been calibrated it can be used to measure the samples.

Notes:

- Special attention must be paid to the tip of the electrode as the membrane that covers it is very fragile.
- Always keep tip of the sensor in a low potassium concentration solution when not in use.
- Clean electrode between uses to prevent cross-contamination.

Enzyme Assay Kit

Equipment and material used to quantify extracted glucose from gel samples using a standard enzyme assay kit:

Description	**Quantity**
Multipipette	1
100 µl tips	One tip for each sample
96-well plate	As necessary to measure all samples
Labsystem Multiskan Ascent	1
Eppendorf tubes	As necessary for each standard
Vortex mixer	1
0.1 M Phosphate buffer solution pH7.4	As necessary to prepare standards
Methylcellulose hydrogel	As necessary to prepare standards
Glucose powder for preparation of 1 l	0.9 g
Glucose oxidase enzyme reagent	As necessary to add to all wells
Container for the glucose oxidase	1

Table 32: Materials used for glucose measurements

Method:

1. Prepare standards as explained in appendix
2. To avoid cross-contamination use new tips for every solution.
3. Dispense 80 µl of each of the calibration solutions in 3 consecutive wells.
4. Dispense 80 µl of each of the samples in 3 consecutive wells until completing the plate.
5. Dispense 80 µl of the glucose oxidase enzyme reagent to each of the wells in the plate.
6. Place plate in Multiskan Ascent and apply the following program:
    a. Initial scan: single measurement in stepping mode at 492 nm
    b. Incubation: 90 minutes at 36.9 º
    c. Final scan: single measurement in stepping mode at 492 nm
7. Save the results with the appropriate name

Notes:

- The results given by the Multiskan are the absorbance.
- Glucose from samples can be read following a destructive method. After preparing the samples with and adding the enzyme they cannot longer be used for potassium measurements and they must be discarded.

Appendix C. In vivo study

Apart from the materials used in the *in vitro* experiments an additional list of further materials are needed.

Experiments *In vivo*

Material/Device	**Manufacturer**	**Model**
Glucose finger prick meter	Therasense	FreeStyle
Lancet Device	Roche	Accutrend
Lancets	Accu-Check	Softclix Pro
Glucose finger prick test strips	Therasense	FreeStyle
Sharp bins (suitable for biohazard material)	Frontier	Sharp Safe
Biohazard glass sheet working area	-----	-----
Alcohol swabs	Uhs	Alcotip Swab
Gloves	Semper Guard	Standard latex or nitrile
Tissues	-----	-----
Plasters	-----	-----
Contact-Activated Lancet	BD Microtainer	Blue ref 366594
Blade 2.0 mm x 1.5 mm	BD Microtainer	High Flow
175 µl plastic capillary tube	-----	-----
Receptacle for soiled material	-----	-----
Blood Gas analyser	-----	RapidLab

Table 33: Materials used in in vivo experiments

Note:

- ----- stands for a generic manufacturer/model. Any manufacturer or model could be used.

Preparation of materials

The materials used in the *in vivo* experiments are the same as in the *in vitro* part except for the *in vitro* cell and the impedance interface configuration. The *in vitro* cell is no longer used and instead the experiments are performed on a human forearm. An approved protocol exits to perform the measurements on the healthy volunteers under University ethics. The impedance interface is always used together with the 1294 human interface to avoid any potential harm to the participant.

Blood Glucose Extraction with a Lancet

In every experiment performed a control group is always advisable in order to compare the results and check if they are within the range expected. This is necessary when developing a new technology such as the case under study. The amount of glucose extracted with reverse iontophoresis has to be validated with that in the circulating blood. That will be useful to investigate correlations. Therefore a lancet is used to monitor the glucose levels. The volume of blood extracted for the measurement is less than 10 μl and uses standard blood glucose monitoring equipment used by diabetics in home monitoring of blood glucose.

Equipment and material used to take blood glucose using a home monitoring lancet and reader:

Description	**Quantity**
Glucose finger prick meter	1
Lancet Device	1
Lancets	A new one per test
Glucose finger prick test strips	A new one per test
Sharp bins (suitable for biohazard material)	1
Biohazard glass sheet working area	1
Alcohol swabs	As many as necessary to clean area
Gloves	2
Tissues	As many as necessary
Plasters	As many as necessary

Table 34: Material used to take blood glucose

Method:

1. Explain procedure to participant and obtain verbal written consent.
2. Select an appropriate site: avoid using index finger and thumb where possible.
3. Investigator must wash hands thoroughly and apply disposable gloves.
4. Investigator must instruct participant to wash the area to be used to obtain sample to remove any interfering substances.
5. Prime the spring mechanism, by turning the top of the lancet device clockwise.
6. Set the lancet device to the appropriate setting (1 is usually sufficient).

7. Insert a lancet into the lancet device and twist of the cover cap clockwise.
8. Position the lancet firmly against puncture site and press the trigger button. Do not remove the device from the site until an audible click is heard.
9. Discard used lancet into sharps disposal container by pointing the end of the lancet into the biohazard sharps bin and pressing the lancet release button at the end of the lancet device. The disposable needle will drop into the sharps bin.
10. Ensure all contaminated materials such as tissues and alcohol wipes containing blood are also disposed of in a Biohazard container. If a large amount of material is to be collected then a biohazard bag if preferable. However, if only a small amount of material is generated then the biohazard sharps bin is suitable.

Notes:

- In order to be able to use the system a programme of training must be undertaken.
- A risk assessment form must be signed prior to commencing the procedure.

<u>Blood Potassium Extraction with a Lancet</u>

As well as the glucose levels, the potassium levels in blood must be compared with those extracted using reverse iontophoresis. However, there are not such small portable devices to measure potassium on site and a gas analyser has to be used. Thus, the volume of blood is higher too, should be in excess of 400 µl, which is obtained with a neonatal heal prick lancet.

Equipment and material used to collect capillary blood via finger stick:

Description	**Quantity**
Contact-Activated Lancet Blade 2.0 mm x 1.5 mm	A new one for each sample
175 µl plastic capillary tube	A new one for each sample
Receptacle for soiled material	1
Sharp disposal container	1
Alcohol swabs	As many as necessary to clean area

Gloves	2
Tissues	As many as necessary
Plasters	As many as necessary
Blood Gas analyser	1

Table 35: Material used to take blood potassium

Method:

1. Explain procedure to participant and obtain written consent.
2. Select an appropriate site: avoid using index finger and thumb where possible.
3. Investigator must wash hands thoroughly and apply disposable gloves.
4. Investigator must instruct participant to wash the area to be used to obtain sample to remove any interfering substances and ask them to keep the identified area hanging down to aid blood flow.
5. Twist off the tab of the contact-activated lancet and discard. Never attempt to replace the tab once removed if required to break off during procedure discard and select a new lancet.
6. Position safety lancet firmly against puncture site. Hold safety lancet between fingers.
7. To activate, press safety lancet firmly against the puncture site. Do not remove the device from the site until an audible click is heard.
8. Discard used safety lancet into sharps disposal container. Ensure all contaminated materials are contained within the receptacle and disposed of according to the University waste policy.
9. To obtain sufficient blood flow, hold the puncture site downwards and gently apply intermittent pressure. Do not “milk” the site as this may cause haemolysis or tissue-fluid contamination.
10. Remove cap from collection device, and place tip under puncture site, allowing blood to flow from fingertip into the collection tube. Aim to allow a sphere of blood to form at the puncture site prior to collection to avoid loss of blood onto the surrounding skin surface. Once a sufficient volume of blood has been collected, replace cap on collection device.

11. Provide subject with tissues to absorb any remaining blood at the puncture site, and dispose of used tissues as per 4.8 above.

Notes:

- Blood samples to be used for potassium measurement have to be analysed within 30 minutes of sample collection.

Reverse Iontophoresis in Human participants

The human participant is the most valuable part within the *in vivo* experiments. The results give the most realistic values to assess the procedure.

Equipment and material used for the application of *in vivo* reverse iontophoresis in human subjects:

Description	**Quantity**
Electrodes	6
Reverse iontophoresis device	1
Connecting leads	3
Pipette	1
Alarm clock	1
Methyl Cellulose Gel	
Impedance monitor	1
Alcohol cleansing wipes	As necessary to clean area
Gloves	2
Tissues	As necessary
Plasters	As necessary

Table 36: Material used to perform reverse iontophoresis in human subjects

Method:

1. Obtain finger stick blood sample from subject using procedure described in Blood Potassium Extraction with a Lancet. For potassium experiments, samples should be obtained in a 175 µl capillary tube, and analysed using the RapidLab Blood Gas analyser.
2. Wipe inner forearm of subject using alcohol based hand wipe moved down the forearm in one constant motion. Leave for 30 seconds to allow arm to dry.
3. Add 300µl of methyl cellulose gel to each electrode pad.

4. Remove protective tape from electrodes and gently press electrodes onto surface of the subject's inner forearm.
5. Attach impedance monitor leads to each electrode pair in turn, and record the real and imaginary components of the impedance. Remove leads after use.
6. Attach each electrode pair to the constant current source using the leads and crocodile clips provided with the box. Apply current by switching on the box for periods according to experiments.
7. Switch current off and remove connecting leads from electrode pairs. Measure impedance across each pair as per step 5.
8. Carefully remove electrode pads from subject forearms. Extract the maximum volume of gel from each electrode pad into separate plastic 7 ml bijou bottles for potassium experiments using extracting pipette.
9. Obtain finger stick blood sample from subject.

Notes:

- No names from subjects are to be retained with samples. Names of subjects will be stored on a separate database with access limited to the study researchers.

Experimental arrangement and procedure

The procedure for the *in vivo* experiments is very similar to the *in vitro* experiment except for the first part in which the *in vitro* cell is replaced with a volunteer in fasting state. The *in vivo* procedure was conducted in accordance with a study procedure and accompanying ethics approved by the Ethics Committee at the University of Strathclyde.

Appendix D. Calculation of solutes for the HEPES buffer used in reverse iontophoresis experiments.

Any solution consists of solutes dissolved homogeneously in a solvent. And the solution is characterised with a concentration.

Each of the solutes has an associated molecular weight (MW). That molecular weight is the weight in grams of 1 mole of the solute. For example, sodium chloride (NaCl) has a molecular weight of 58.42.

A typical solvent is deionised water and that will be used for all solutions.

The concentration is defined as the amount of solute dissolved in a quantity of solvent. That is important and needs to be calculated. Any quantity of solvent can be used, but the proportional amount of solute has to be added in order to keep the concentration desired.

For example, if it is required 1 litre of 1 mol of NaCl, then 58.42 g of NaCl will be poured into 1 litre of deionised water.

In our case the concentrations are in mM so the weight in grams has to be divided by 1000.

The following quantities of solutes are necessary for the preparation of HEPES buffer:

Solute	**MW (g/mol)**	**Concentration desired (mM)**	**Weigh of solute needed (g)**
Sodium Chloride (NaCl)	58.42	133	7.77
Glucose	180.2	5	0.901
Potassium Chloride (KCl)	74.56	4	0.298
HEPES	238.30	25	5.96

Table 37: Quantity of solutes to prepare HEPES buffer

As the pH of the concentration has to be measured once the solutes have been poured into the solvent it is recommended to add the solutes in a quantity of solvent inferior to the desired one and complete up to the volume after the pH has been regulated.

Appendix E. Preparation of standards with different concentrations for the calibration of the potassium ion selective electrode.

An easy way to get a collection of scale concentrations is to prepare a high concentration solution, take a measured amount and add a measured amount of the same buffer without the solute. And then repeat the same operation from the new concentration.

The formula used to calculate the new concentration is:

$$Concentration\ new\ solution = \frac{Vas * Cas}{Vas + Vab}$$

Equation 25: Calculation of concentration of new solutions

Where Vas is the volume of the actual solution, Cas is the concentration of the actual solution and Vab is the volume of the buffer added to the volume of the actual concentration.

In the following table it is shown the volume of solutions taken and volume of buffer added.

Volume of actual solution (ml)	Concentration of actual solution (mM)	Volume of buffer added (ml)	Volume of new solution obtained (ml)	Concentration of new solution (mM)
10	10	90	100	1
10	1	90	100	0.1
10	0.1	90	100	0.01
90	0.01	10	100	0.009
80	0.009	10	90	0.008
70	0.008	10	80	0.007
60	0.007	10	70	0.006
50	0.006	10	60	0.005
40	0.005	10	50	0.004
30	0.004	10	40	0.003
20	0.003	10	30	0.002
10	0.002	10	20	0.001

Table 38: Preparation of solutions for the ISE calibration

In each step the remaining volume of concentration has to be kept into a labelled bottle.

Note that the volumes in each step are not the same, therefore special attention must be paid to that in order not to obtain a volume of solution inferior to the one needed.

Appendix F. *In vitro* Potassium calibration curves

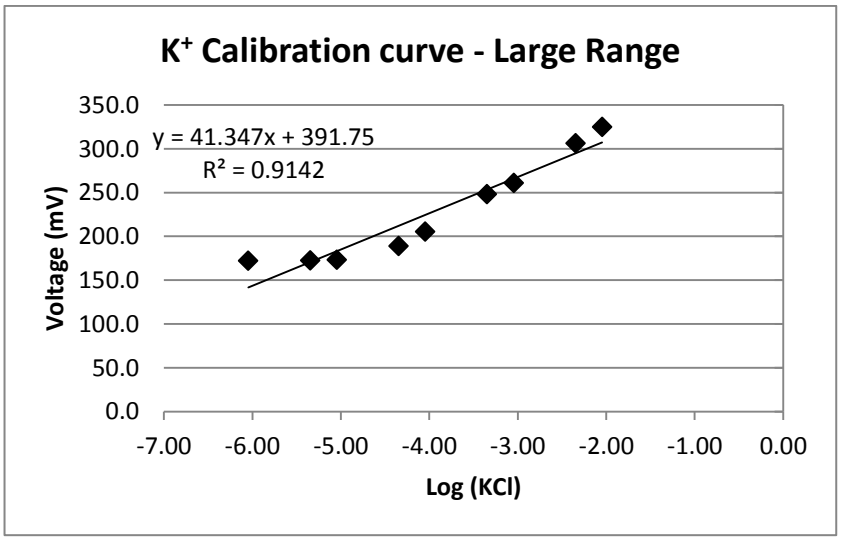

Figure 67: First attempt of potassium calibration curve

A part from the calibration points the calibration curve has also been calculated. Its associated regression line has a regression factor higher than 90%, what is very desirable because the higher the regression factor the more accurate the regression line is. The following calibration curves were used to calculate the concentration of potassium in the samples:

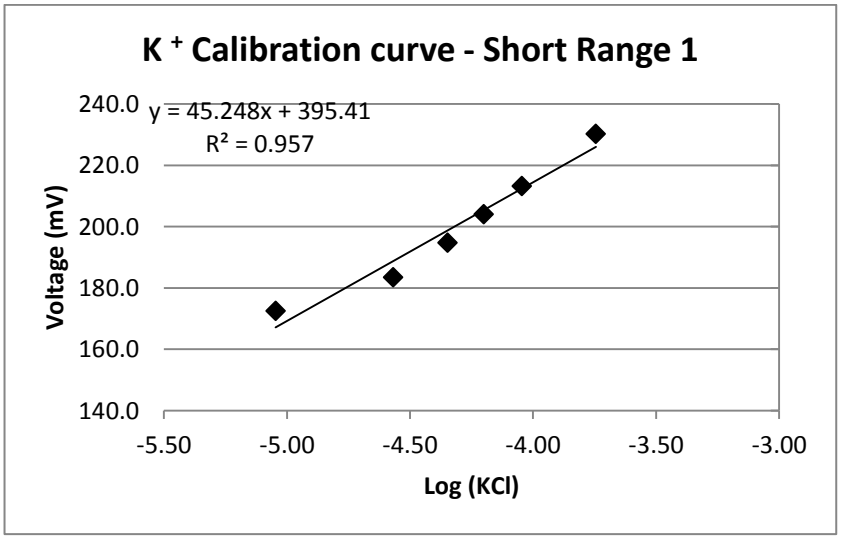

Figure 68: Potassium calibration curve used for experiments 1, 2 and 3 of 2, 5 and 10 min of duration

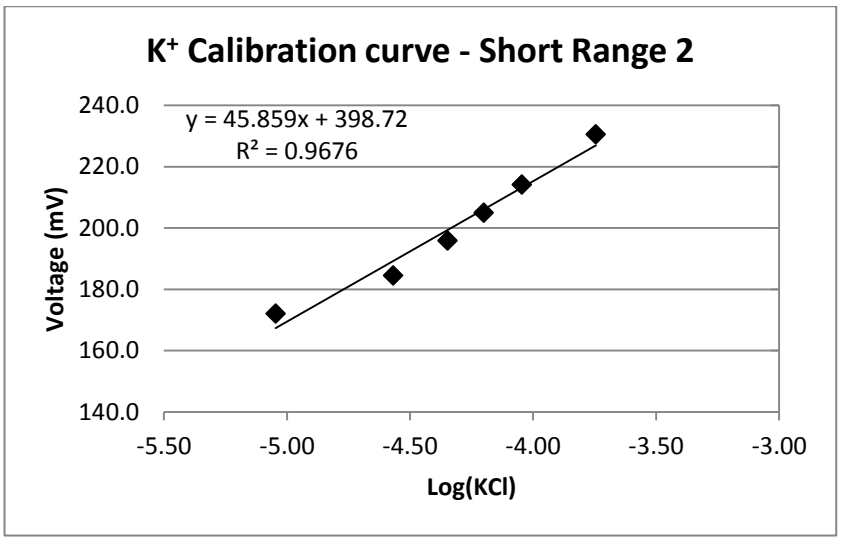

Figure 69: Potassium calibration curve used for experiments 1, 2 and 3 of 15 and 30 min of duration

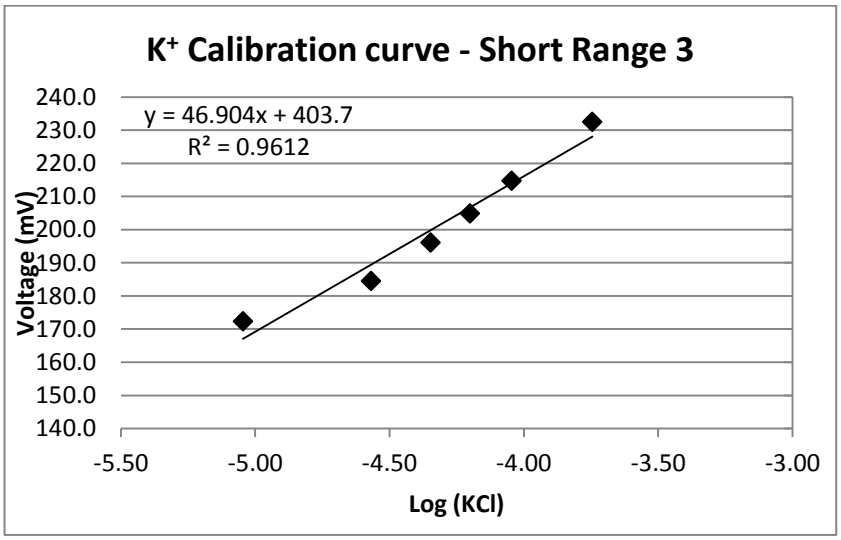

Figure 70: Potassium calibration curve used for experiment 4 of 2,5,10 and 15 min of duration

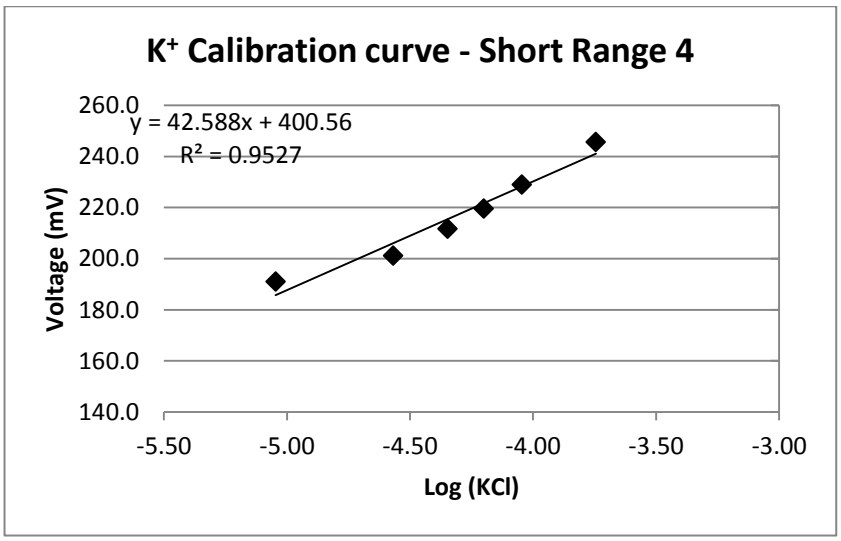

Figure 71: Potassium calibration curve used for experiments 1, 2, 3 and 4 of 60 min of duration

As it can be noticed, using the values within range from 0.01 to 0.2 mM gives a calibration curve with coefficient of correlation higher than 95%. That helps reducing the error of conversion significantly.

Appendix G. *In vitro* Glucose calibration curves

Linear regression lines used to calibrate the glucose measured from the *in vitro* samples.

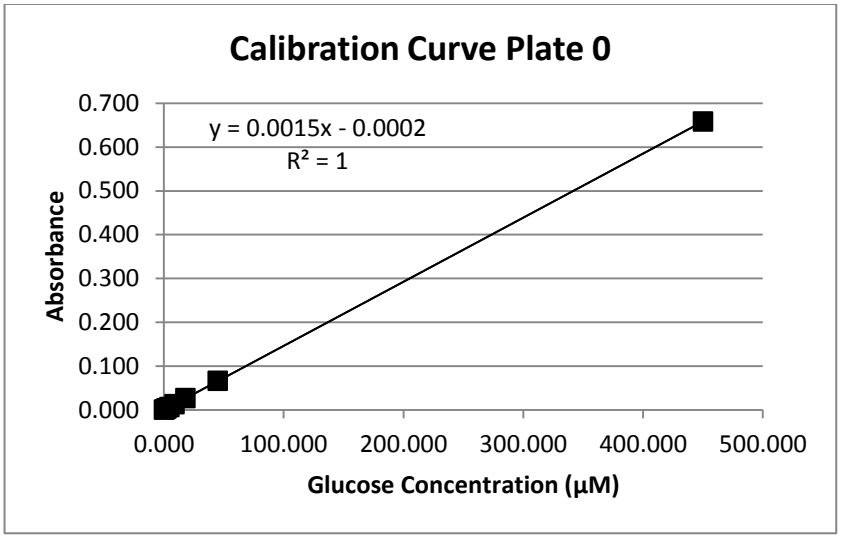

Figure 72: Complete range of calibration curve used for glucose analysis

The first one was used together with the average of the next two to calculate the samples in the second plate (10, 15 and experiments 1 and 2 in 30↔)

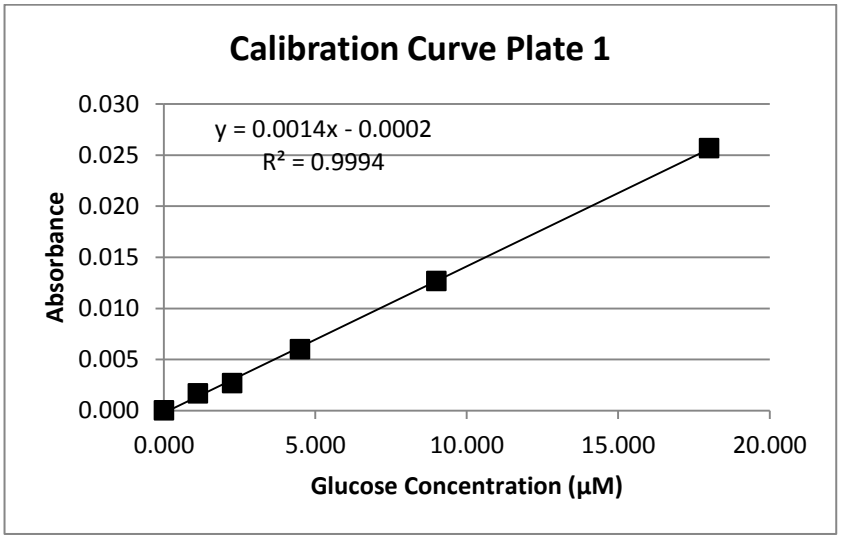

Figure 73: Calibration curve from plate 1 used in experiments of 2 and 5 minutes

The second one was used for the calculation of experiments of 2 and 5 minutes of duration.

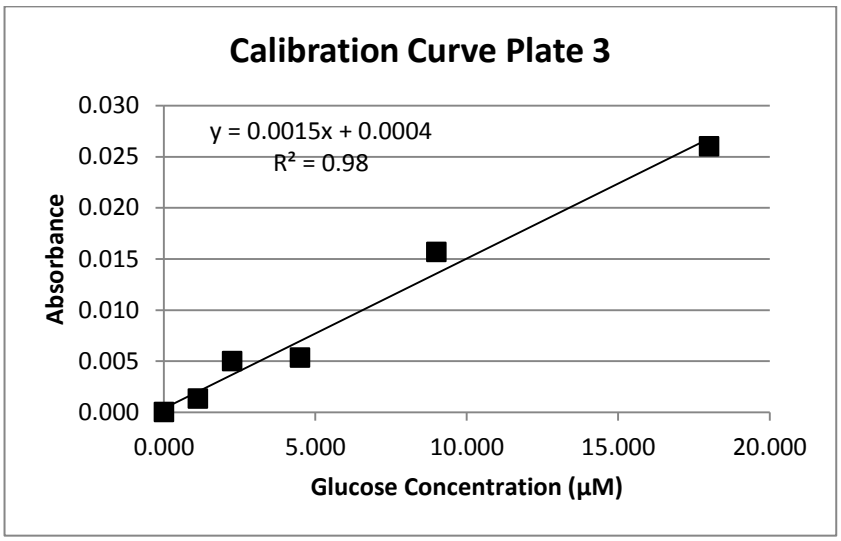

Figure 74: Calibration curve from plate 3 used in experiments of 30 and 60 minutes

The Third curve was used for the calibration of the experiment 3 of 30 ↔ min and all experiments in 30→ and 60 minutes of duration.

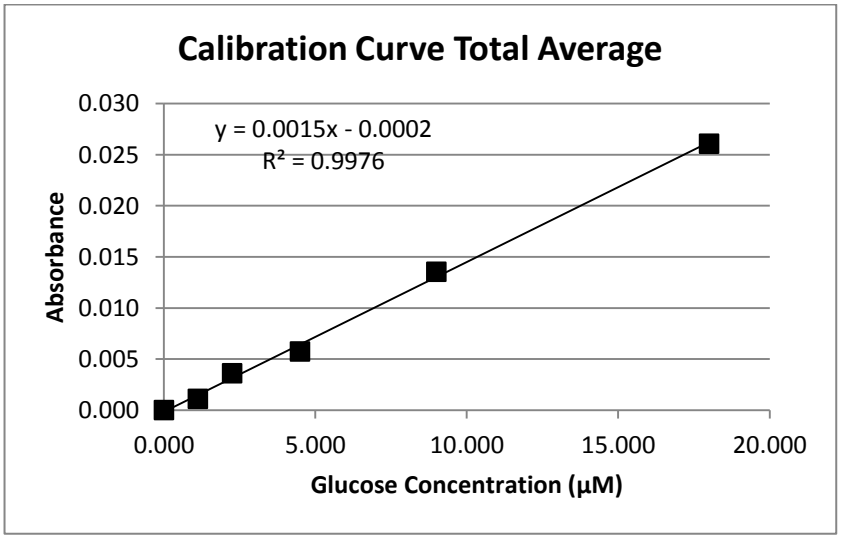

Figure 75: Calibration curve calculated from the average of the 3 calibration curves and used for experiments of 10, 15 and 30 minutes

And the last one is the average of all of them for samples in plate 2.

Appendix H. *In vitro* impedance bode plots

This appendix show the differences in impedance results for several situations: between electrodes, using the human interface 1294 switched on and off.

Comparison of impedance between pairs of electrodes before RI.

For each experiment carried out the impedance was measured for the 3 electrodes in pairs: between electrode 1 and 2 (E1,2), between electrode 1 and 3 (E1,3) and between electrode 2 and 3 (E2,3).

The following graphs show values for experiment 4 of 15 minutes of duration for the 3 pairs.

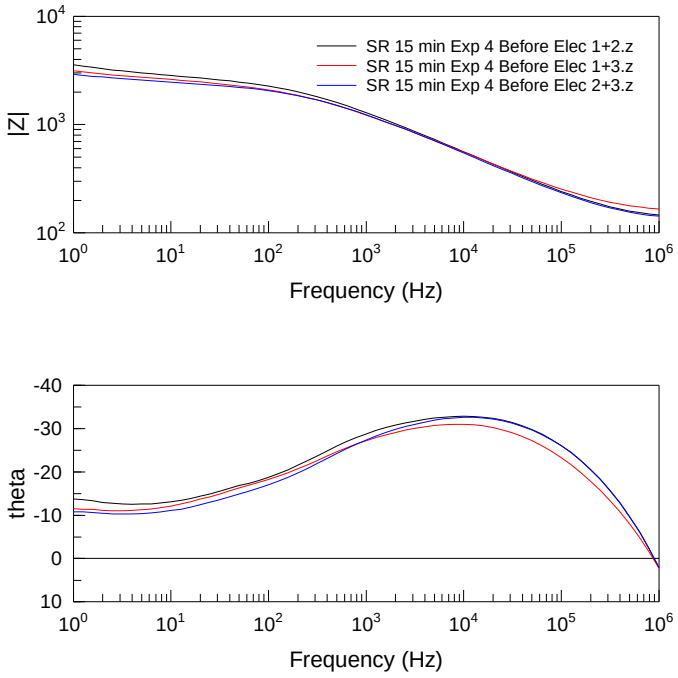

Figure 76: Bode plot showing impedance differences between the 3 pairs of electrodes in in vitro experiment 4 of 15 minutes of duration

	Magnitude (Ω)						
Freq. (Hz)	**1**	**10**	**100**	**1000**	**10000**	**100000**	**1000000**
E 1,2	3569	2844	2266	1292	562	241	146
E 1,3	3137	2610	2093	1226	556	254	166
E 2,3	2916	2475	2057	1234	546	235	143
Difference	653	369	209	58	16	6	3

Table 39: Magnitude values for the 3 pairs of electrodes in in vitro experiment 4 of 15 minutes before applying reverse iontophoresis

Looking at the magnitude graph all of the 3 signals are represented very close to each other. That little difference between them means they represent almost the same values. From the table with values that can be stated. The difference between the largest from the smallest is hardly 3 ohms at 1 MHz.

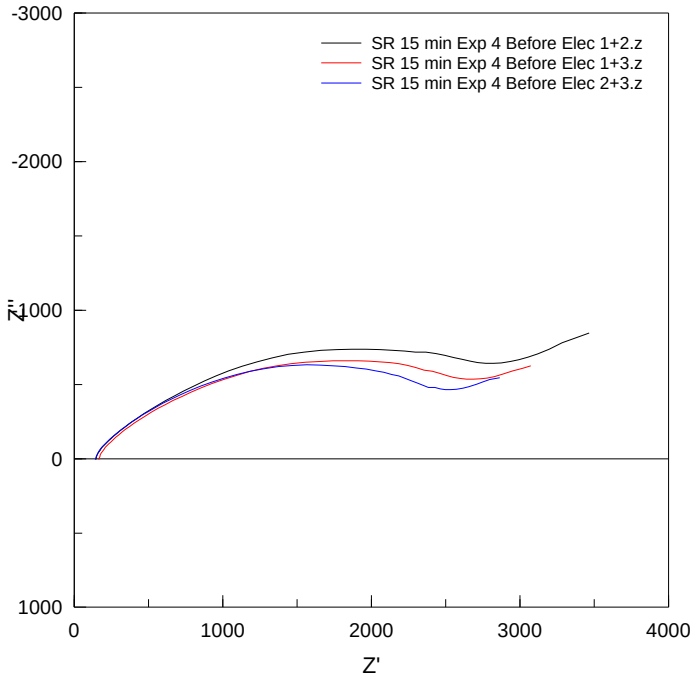

Figure 77: Complex plot showing impedance differences between the 3 pairs of electrodes in in vitro experiment 4 of 15 minutes of duration

The complex plot also shows that little variation between all 3 pairs of electrodes. That difference will be more appreciated when compared with the values after applying reverse iontophoresis.

Comparison of impedances using the human interface 1260 and using the analyser 1294 directly.

The following graphs show values for experiment 2 in which the human interface was used and experiment 4 in which the analyser was attached without the human interface. For both cases the signal between electrodes 1 and 2 is represented.

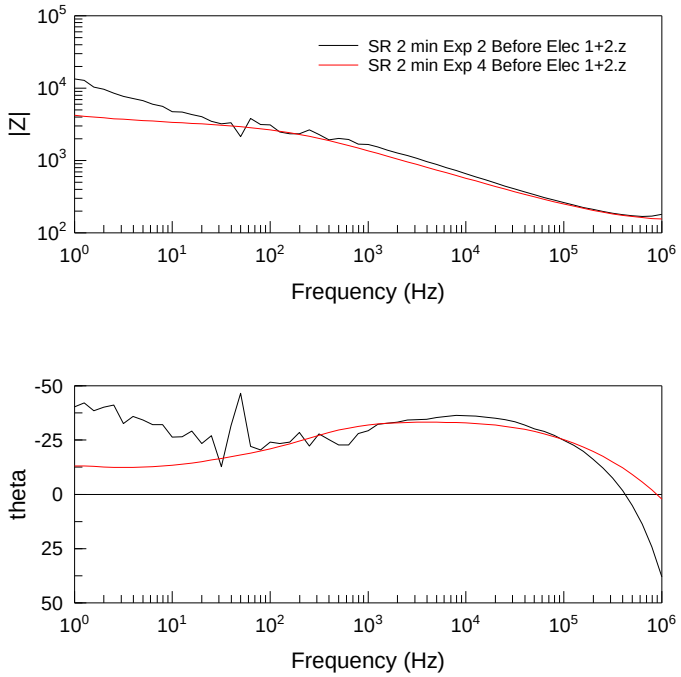

Figure 78: Bode plot showing impedance differences using the human interface 1260 and connecting the electrodes to the analyser 1294 directly in in vitro experiments 2 and 4 of 2 minutes of duration

	Magnitude (Ω)						
Freq. (Hz)	**1**	**10**	**1000**	**10000**	**100**	**100000**	**1000000**
Exp. 2	13411	4746	1662	660	3126	262	180
Exp. 4	4198	3389	1360	570	2649	250	155

Table 40: Magnitude values for the same pair of electrodes in in vitro experiments 2 and 4 of 2 minutes of duration

The graphs show the difference using the human interface and using the gain/phase analyser directly. Experiment 2 was performed with the human interface attached and experiment 4 was measured directly from the analyser. As it can be observed in both graphs there is a peak at a frequency of 50Hz that corresponds to the noise

introduced by the power lines. The human interface introduces extra noise as the range in which the precision is higher becomes narrower as it is shown in the procedure of the gain/phase interface.

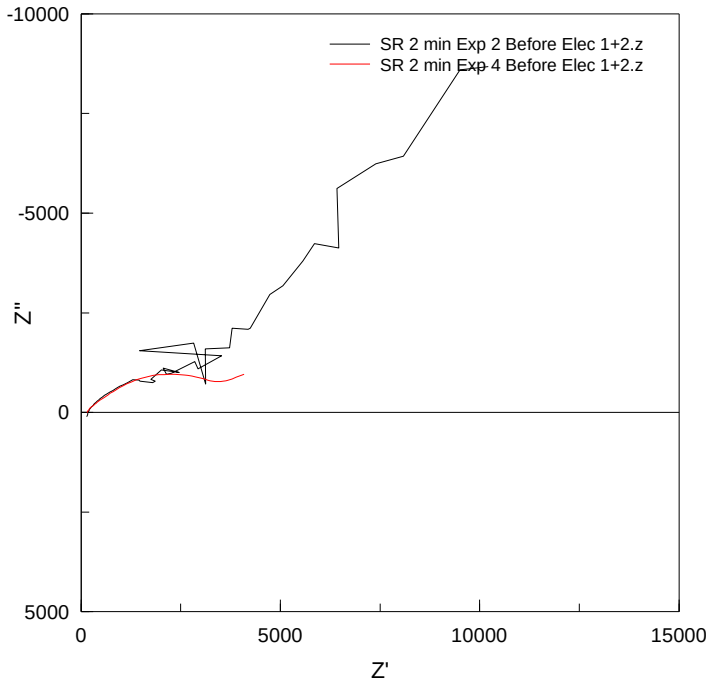

Figure 79: Complex plot showing impedance differences using the human interface 1260 and connecting the electrodes to the analyser 1294 directly in in vitro experiments 2 and 4 of 2 minutes of duration

The complex plot is difficult to read; nevertheless the difference between signals is quite clear.

Comparison of impedances with human interfaces switched on and off

The graphs below show signals for experiments 2 and 3 of 2 minutes of duration in which the human interface was switched on and switched off respectively.

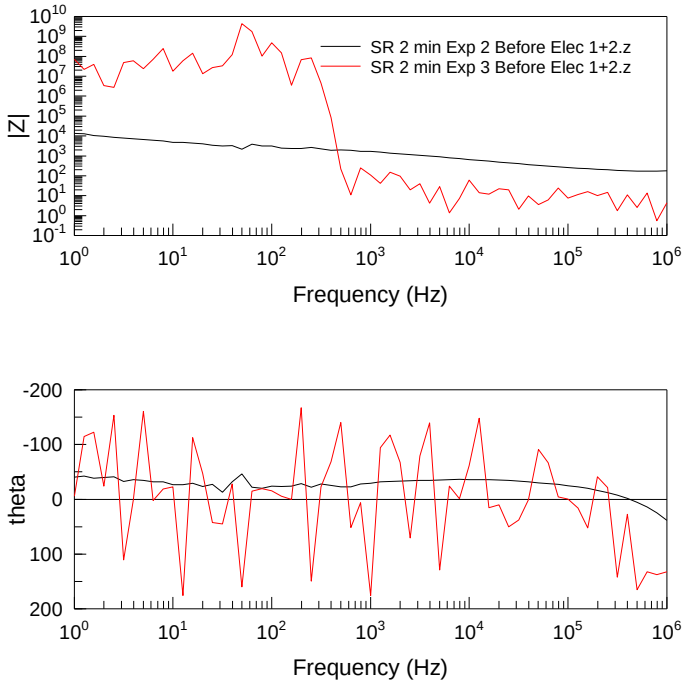

Figure 80: Bode plot showing the result of the correct switching of the interface in in vitro experiments 2 and 3 of 2 minutes of duration

	Magnitude (Ω)						
Freq. (Hz)	**1**	**10**	**100**	**1000**	**10000**	**100000**	**1000000**
Exp. 2	13411	4746	3126	1662	660	262	180
Exp. 3	70401000	16491000	465520000	110	29	8	3

Table 41: Magnitude values for the same pair of electrodes in in vitro experiments 2 and 3 of 2 minutes of duration with the human interface on and off

If using the human interface module it also needs to be switched on, otherwise the results are invalid as can be compared in the graphs. Experiment 2 was performed with the human interface switched on and experiment 3 with the module off. The numbers shown in the table also represent an impedance much higher than expected.

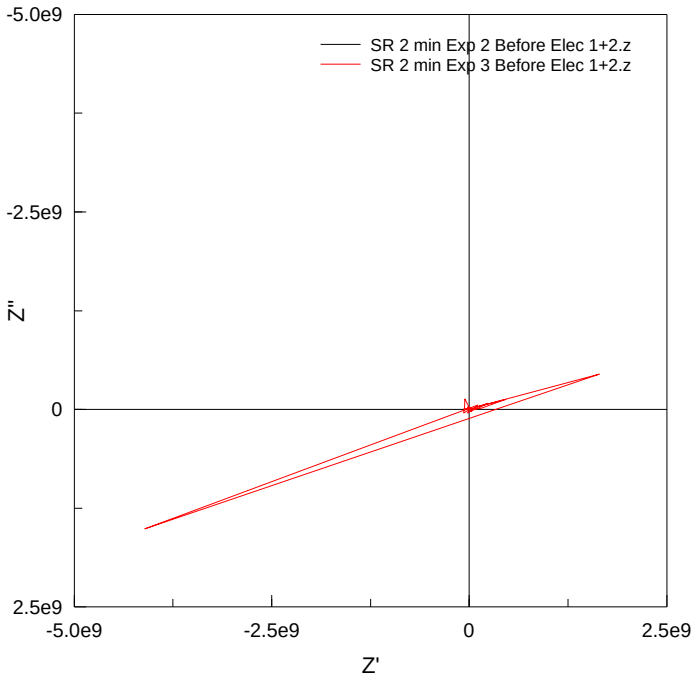

Figure 81: Complex plot showing the result of the correct switching of the interface in in vitro experiments 2 and 3 of 2 minutes of duration

Appendix I. *In vitro* experiments and their circumstances

Table 42 shows the circumstances in which each experiment was performed. They were performed either with the 1260 only, with both 1260 and 1294 switched on or switched off.

Duration	Exp.	Before/After	Circumstances
2 minutes	1	Before	Human interface 1294 used
		After	Not taken
	2	Before & After	Human interface 1294 used
	3	Before & After	Human interface switched off
	4	Before & After	Connected to analyser 1260
5 minutes	1	Before & After	Human interface 1294 used
	2	Before & After	Human interface 1294 used
	3	Before & After	Human interface switched off
	4	Before & After	Connected to analyser 1260
10 minutes	1	Before & After	Human interface 1294 used
	2	Before & After	Human interface 1294 used
	3	Before & After	Human interface 1294 used
	4	Before & After	Connected to analyser 1260
15 minutes	1	Before & After	Human interface 1294 used
	2	Before & After	Human interface 1294 used
	3	Before & After	Human interface 1294 used
	4	Before & After	Connected to analyser 1260
30 minutes	1	Before & After	Human interface 1294 used
	2	Before & After	Connected to analyser 1260
	3	Before & After	Connected to analyser 1260
30 minutes	1	Before & After	Connected to analyser 1260
	2	Before & After	Connected to analyser 1260
	3	Before & After	Connected to analyser 1260
60 minutes	1	Before & After	Connected to analyser 1260
	2	Before & After	Connected to analyser 1260
	3	Before & After	Connected to analyser 1260
	4	Before & After	Connected to analyser 1260

Table 42: Circumstances in which the impedance from the experiments was measured

Appendix J. *In vitro* impedance results – Detailed views

This appendix shows detailed views of the impedances measured in the in vitro experiments. First some examples of the real part are shown, then some others for the imaginary part and finally the magnitude is shown.

Real part of the impedance

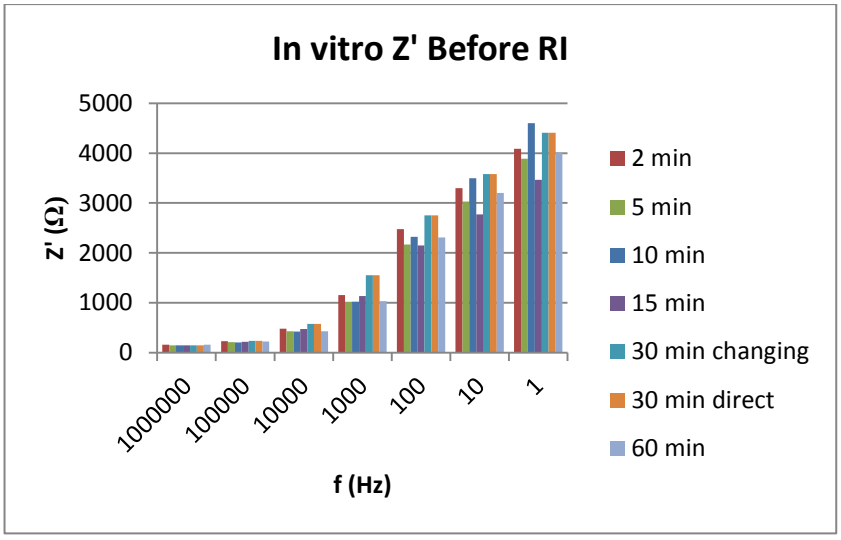

Figure 82: Z' before applying reverse iontophoresis for all experiments

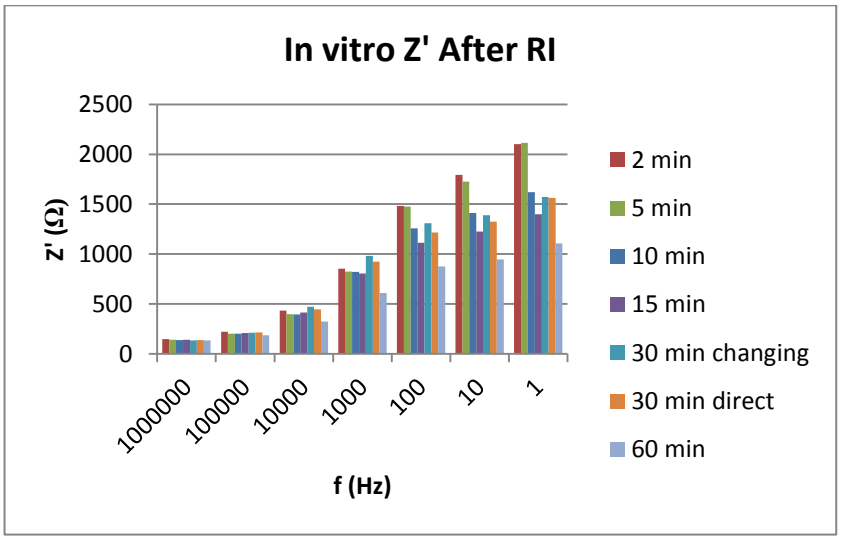

Figure 83: Z' after applying reverse iontophoresis for all experiments

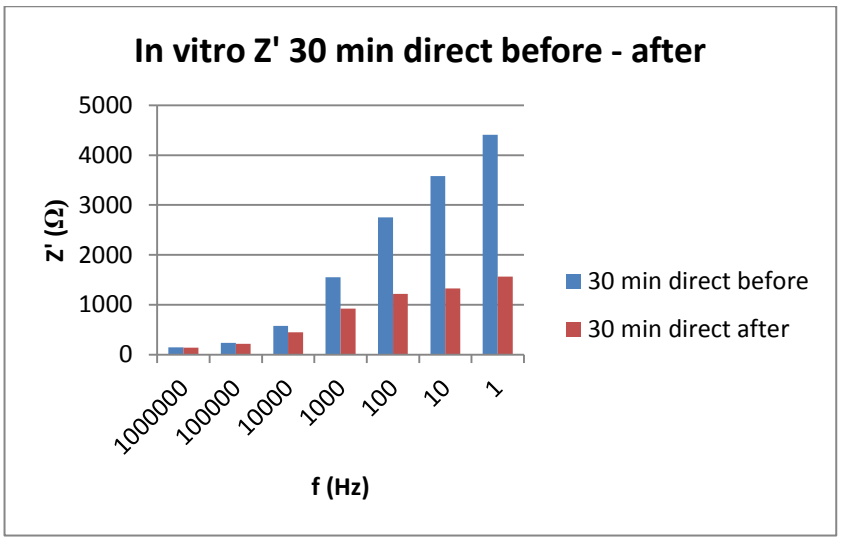

Figure 84: Comparison of Z' before and after applying reverse iontophoresis for 30 minutes experiment

Imaginary part of the impedance

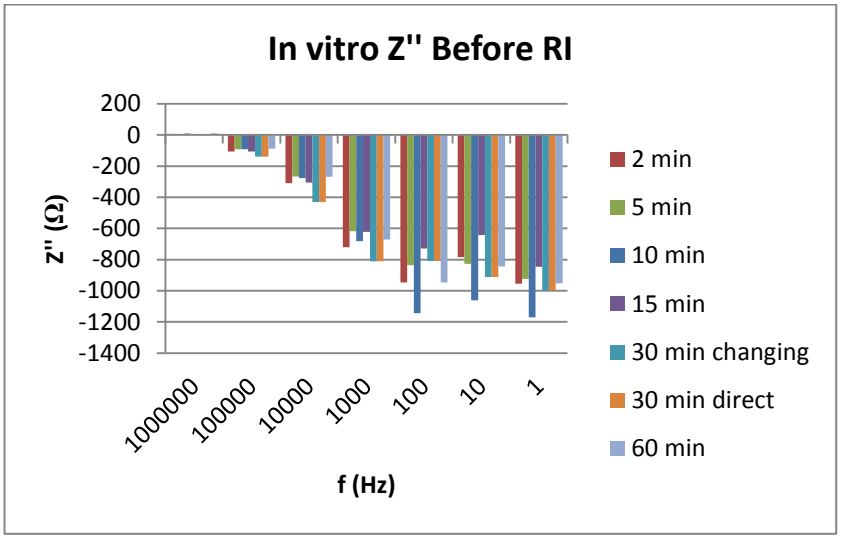

Figure 85: Z'' before applying reverse iontophoresis for all experiments

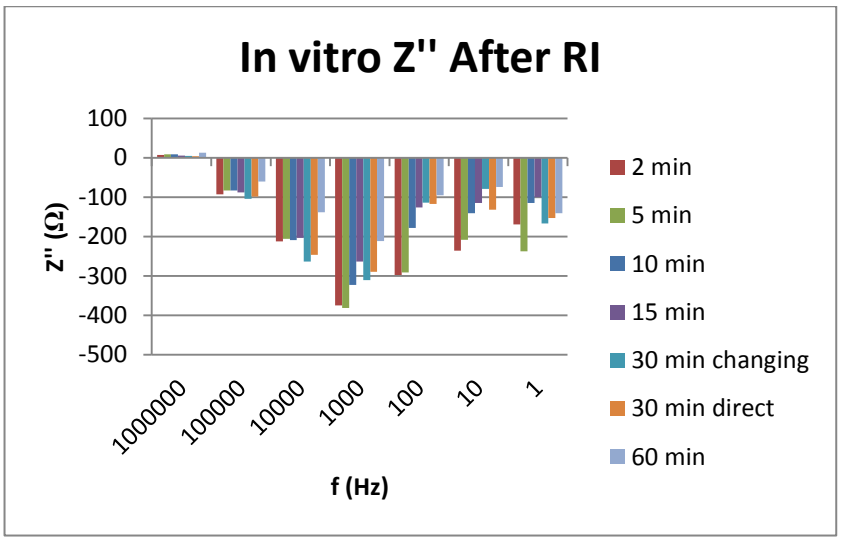

Figure 86: Z'' after applying reverse iontophoresis for all experiments

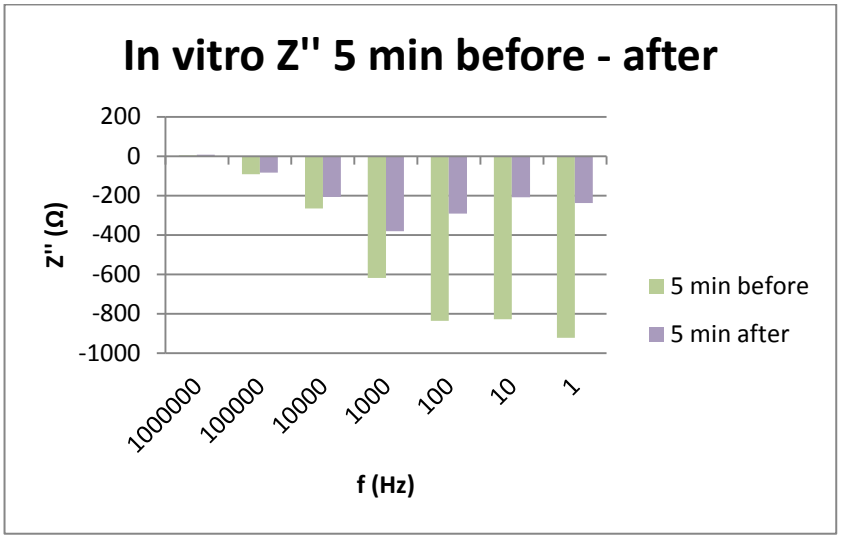

Figure 87: Comparison of Z'' before and after applying reverse iontophoresis for 5 minutes experiment

Modulus of the impedance

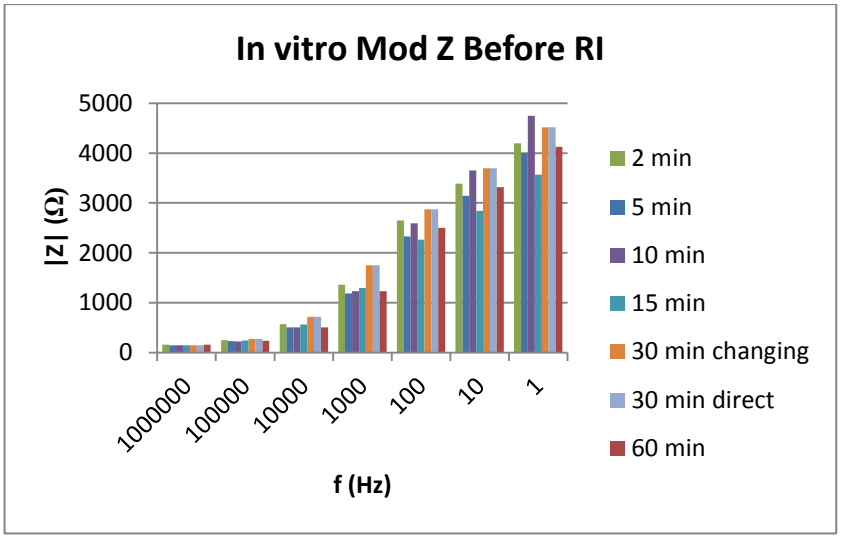

Figure 88: Magnitude of Z before applying reverse iontophoresis for all experiments

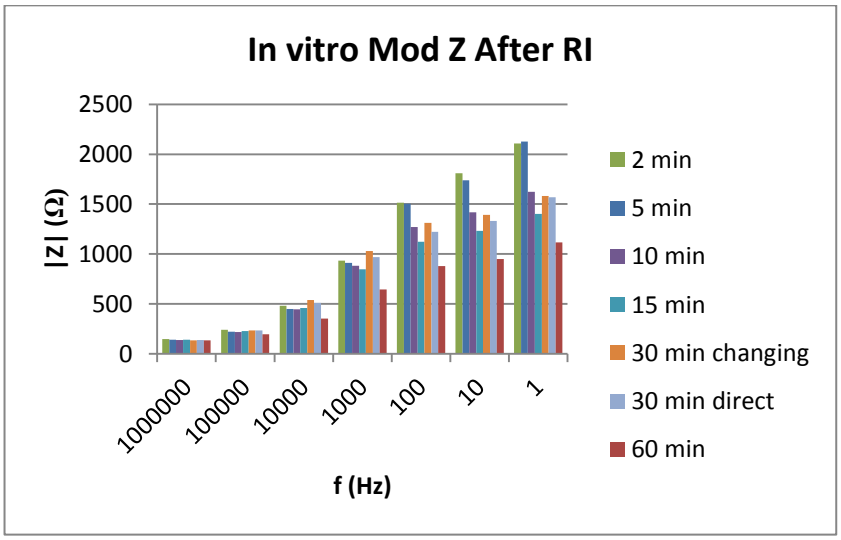

Figure 89: Magnitude of Z after applying reverse iontophoresis for all experiments

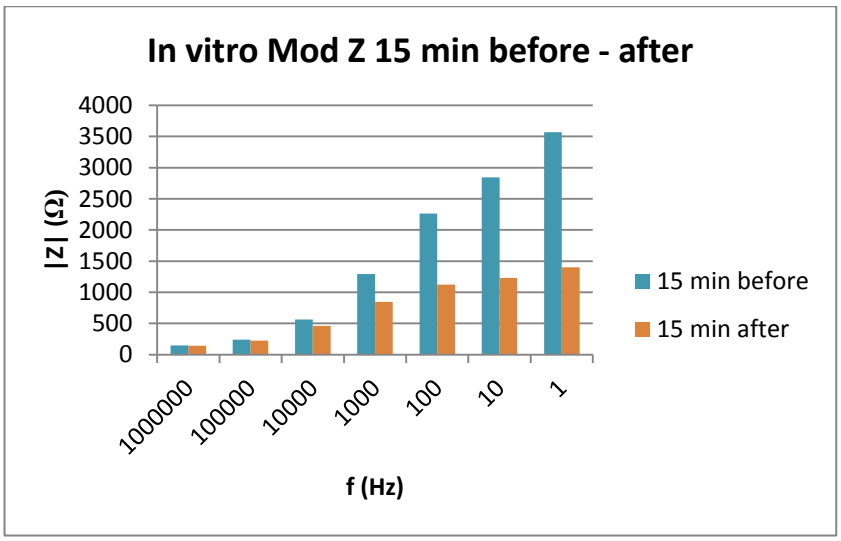

Figure 90: Comparison of magnitude of Z before and after applying reverse iontophoresis for 15 minutes experiment

Appendix K. *In vivo* potassium results – detailed views

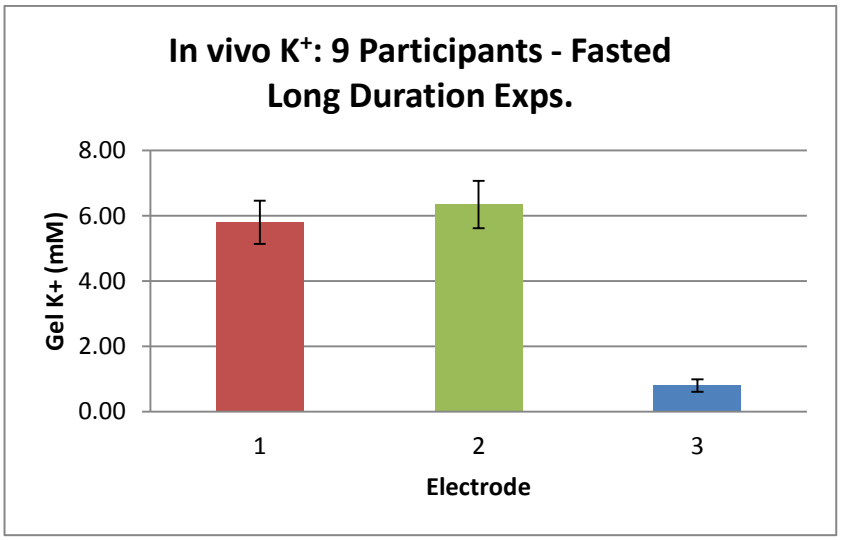

Figure 91: In vivo average values for electrodes 1, 2 and 3 for the 9 participants in fasted state. Experiments of 60 minutes.

Appendix L. *In vivo* glucose calibration curves

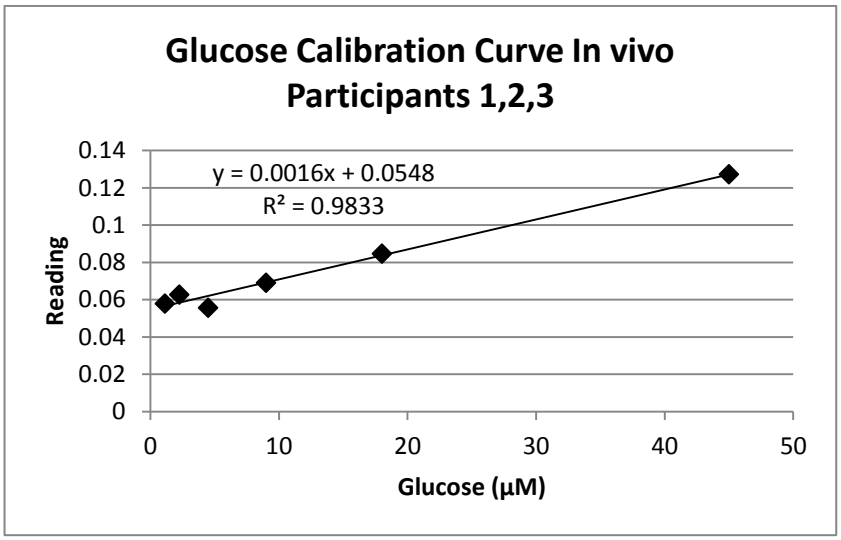

Figure 92: In vivo glucose calibration curve used for participants 1, 2 and 3

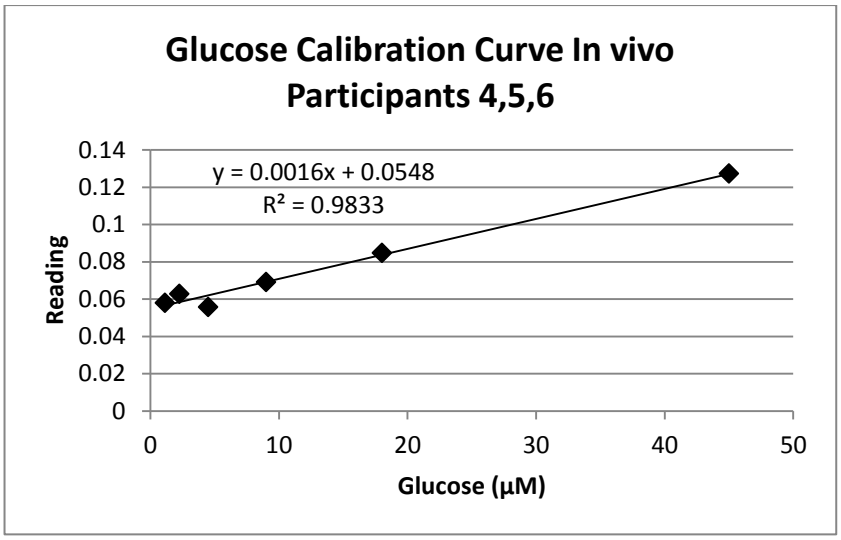

Figure 93: In vivo glucose calibration curve used for participants 4, 5 and 6

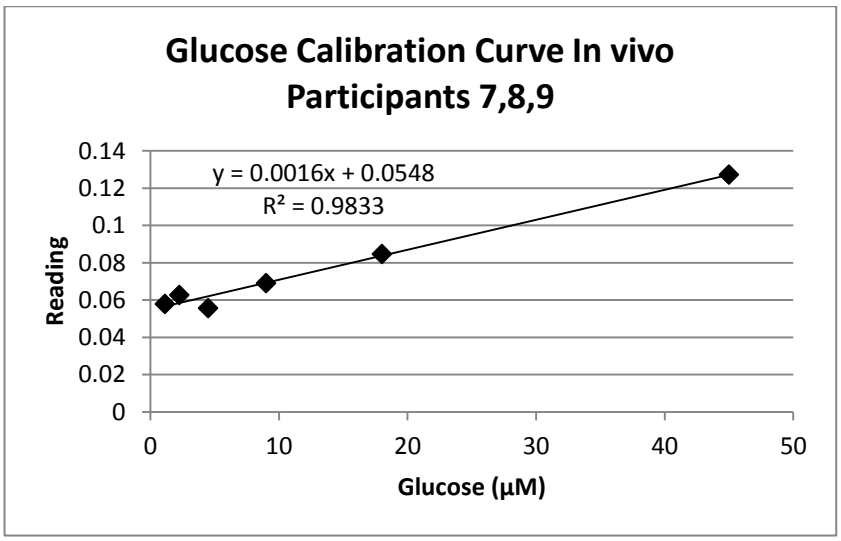

Figure 94: In vivo glucose calibration curve used for participants 7, 8 and 9

Appendix M. Proof of the simplification for the calculation of C

The second order equation for C is arranged as:

$$Z''\omega^2 R_p^2 C^2 + j\omega R_p^2 C + Z'' = 0$$

The general solution for the second order equation for C is:

$$C = \frac{-j\omega R_p^2 \pm \sqrt{\left(j\omega R_p^2\right)^2 - 4Z''^2\omega^2 R_p^2}}{2Z''\omega^2 R_p^2} =$$

First, brackets are developed:

$$= \frac{-j\omega R_p^2 \pm \sqrt{-\omega^2 R_p^4 - 4Z''^2\omega^2 R_p^2}}{2Z''\omega^2 R_p^2} =$$

Then common variables inside the square root are taken out together with the negative sign which is simply j (the imaginary number):

$$= \frac{-j\omega R_p^2 \pm j\omega R_p\sqrt{R_p^2 + 4Z''^2}}{2Z''\omega^2 R_p^2} =$$

Common variables are simplified in numerator and denominator:

$$= j\frac{-R_p \pm \sqrt{R_p^2 + 4Z''^2}}{2Z''\omega R_p^2} =$$

At this point it is considered that R_p is much greater than Z''. If $R_p >> Z''$ then Z'' can be ignored inside the square root:

$$= j\frac{-R_p \pm \sqrt{R_p^2}}{2Z''\omega R_p^2} =$$

Simplifying common variables in numerator and denominator:

$$= j\frac{-1 \pm 1}{2Z''\omega^2} =$$

Finally 2 solutions are possible. First considers the second part positive, which cancels the terms and the second one gives a valid result which is the one used for the calculations.

$$= \begin{cases} j\dfrac{-1+1}{2Z''\omega} = 0 \\ j\dfrac{-1-1}{2Z''\omega} = j\dfrac{-1}{Z''\omega} \end{cases}$$